COPPE
Instituto Alberto Luiz Coimbra de Pós-Graduação e Pesquisa de Engenharia
UFRJ

MODELLING OF REACTIVE ABSORPTION FOR NATURAL GAS TREATMENT

Carlos Henrique Ferreira Brasil de Souza

Dissertação de Mestrado apresentada ao Programa de Pós-graduação em Engenharia Química, COPPE, da Universidade Federal do Rio de Janeiro, como parte dos requisitos necessários à obtenção do título de Mestre em Engenharia Química.

Orientadores: Argimiro Resende Secchi
Letícia Cotia dos Santos

Rio de Janeiro
Dezembro de 2019

MODELLING OF REACTIVE ABSORPTION FOR NATURAL GAS TREATMENT

Carlos Henrique Ferreira Brasil de Souza

DISSERTAÇÃO SUBMETIDA AO CORPO DOCENTE DO INSTITUTO ALBERTO LUIZ COIMBRA DE PÓS-GRADUAÇÃO E PESQUISA DE ENGENHARIA (COPPE) DA UNIVERSIDADE FEDERAL DO RIO DE JANEIRO COMO PARTE DOS REQUISITOS NECESSÁRIOS PARA A OBTENÇÃO DO GRAU DE MESTRE EM CIÊNCIAS EM ENGENHARIA QUÍMICA.

Examinada por:

Prof. Argimiro Resende Secchi, D.Sc.

Eng. Letícia Cotia dos Santos, D.Sc.

Prof. Príamo Albuquerque Melo Jr., D.Sc.

Prof. Márcio Luis Lyra Paredes, D.Sc.

RIO DE JANEIRO, RJ – BRASIL
DEZEMBRO DE 2019

Souza, Carlos Henrique Ferreira Brasil de

Modelling of Reactive Absorption for Natural Gas treatment/Carlos Henrique Ferreira Brasil de Souza. – Rio de Janeiro: UFRJ/COPPE, 2019.

XVII, 108 p.: il.; 29, 7cm.

Orientadores: Argimiro Resende Secchi

Letícia Cotia dos Santos

Dissertação (mestrado) – UFRJ/COPPE/Programa de Engenharia Química, 2019.

Referências Bibliográficas: p. 98 – 106.

1. Absorção reativa. 2. Modelagem. 3. Remoção de CO2. I. Secchi, Argimiro Resende *et al.* II. Universidade Federal do Rio de Janeiro, COPPE, Programa de Engenharia Química. III. Título.

Acknowledgements

First I would like to thank both my advisers Argimiro and Letícia, for helping me through this whole process of learning and personal growth. I am also thankful to Petrobras, without whose support this would not be possible, and to the Federal University of Rio de Janeiro, who promotes science and spread knowledge to our society. Both institutions represent the Brazilian state, and this scientific production is an example of how vital is the state in supporting and sponsoring innovation and granting the development of the country. The continuity of such incentives rely on ourselves as a democratic society in making our voice heard.

I am also thankful to my family and friends, who helped me throughout this process in uncountable ways. Specially pointing out Camila who has been with me in all classes and meetings, and Pedro who has given me the unconditional support and love that this difficult time demands.

Resumo da Dissertação apresentada à COPPE/UFRJ como parte dos requisitos necessários para a obtenção do grau de Mestre em Ciências (M.Sc.)

MODELAGEM DA ABSORÇÃO REATIVA PARA TRATAMENTO DE GÁS NATURAL

Carlos Henrique Ferreira Brasil de Souza

Dezembro/2019

Orientadores: Argimiro Resende Secchi
Letícia Cotia dos Santos

Programa: Engenharia Química

O objetivo deste trabalho é desenvolver um modelo para simular a absorção de CO_2 utilizando uma solução de monoetanolamina. O CO_2 e um problema para o gás natural, uma vez que ele reduz seu poder calorífico, acelera a corrosão em dutos e ainda pode congelar durante os processos criogênicos nas unidades tradicionais de tratamento. A absorção reativa do CO_2 utilizando alcanolaminas é o método mais consolidado para remover este contaminante do gás natural. Por isso, um bom modelo é essencial para projeto, operação e otimização corretos dessa unidade. Um modelo rigoroso baseado em taxas de transferência de massa e utilizando a teorida do duplo filme foi proposto para realizar a modelagem da absorção do CO_2 utilizando monoetanolamina. Foi utilizada a discretização pelo método dos volumes finitos para resolver o sistema de equações diferenciais parciais. Três modelos foram propostos para resolver o sistema de equações algébrico-diferenciais, cada um com um número decrescente de simplificações, com objetivo de gerar estimativas iniciais para a solução final. O modelo foi validado utilizando dados de planta piloto disponíveis na literatura, e o parâmetro de área interfacial foi ajustado. Finalmente, alguns estudos de caso foram simulados para verificar a consistência do modelo.

Abstract of Dissertation presented to COPPE/UFRJ as a partial fulfillment of the requirements for the degree of Master of Science (M.Sc.)

MODELLING OF REACTIVE ABSORPTION FOR NATURAL GAS TREATMENT

Carlos Henrique Ferreira Brasil de Souza

December/2019

Advisors: Argimiro Resende Secchi
Letícia Cotia dos Santos

Department: Chemical Engineering

The objective of this work is to create a model to simulate the absorption of CO_2 using monoethanolamine solution. CO_2 is a problem for natural gas, since it reduces its calorific capacity, accelerates corrosion in ducts, and also may freeze cryogenic processing lines in a traditional gas treatment plant. Reactive absorption of CO_2 using alkanolamines is the most consolidated method of removing this contaminant from natural gas. Therefore, a good model of this unit is paramount for correct design, operation and optimization. A rigorous rate-based two-film model was proposed for modelling absorption of CO_2 using monoethanolamine. Discretization with finite volumes was performed to solve the resulting partial differential equation system. Three models were then proposed to solve the algebraic-differential equation system, each with decreasing number of simplifications in order to generate initial guesses for the final solution. The model was validaded using literature data from pilot plant, and the interfacial area parameter was adjusted. Finally, some case studies were simulated in order to verify its consistency.

Contents

List of Figures

List of Tables

List of Symbols

Latin symbols:

- A: Area
- a: Activity
- $\mathbf{B}$: Auxiliary matrix for Maxwell-Steffan fluxes calculation
- C: Molar concentration
- C_p: Molar calorific capacity
- D: Diffusion coefficient
- d: Density
- e: Electron's charge
- F: Molar flow
- f: Fugacity
- G: Gibbs free energy
- g: Specific Gibbs free energy
- H: Henry's law coefficient
- h: Specific enthalpy
- H: Enthalpy
- I: Ionic force
- J: Molar flux
- K: Equilibrium constant
- k: Reaction rate constant

- M: Total mole number
- N: Total number of components
- n: Number of mole
- P: Pressure
- q: Heat flux
- r: Reaction rate
- T: Absolute temperature
- t: Time
- V: Volume
- v: Molar volume
- X: Effective concentration for activity coefficient calculation
- x: Liquid-phase molar fraction
- y: Gas-phase molar fraction
- z: Electric charge

Greek symbols:

- α: Effective interfacial area parameter
- β: Exponential mesh parameter
- γ: Activity coefficient
- δ: Film length
- ϵ: Error of estimated parameter α
- η: Either gas or liquid film coordinate
- ϑ: Stoichiometric coefficient
- κ: Boltzmann constant
- Λ: Heat conductivity
- λ: Dielectric constant
- μ: Chemical potential

- ν: Cinematic viscosity
- ρ: Closest approach parameter for Pitzer's equation
- φ: Electric potential
- ϕ: Fugacity coefficient
- ω: Acentric factor

Special symbols:

- đ: Generalized driving force for Maxwell-Steffan equation
- Đ: Maxwell-Steffan diffusion coefficient
- $\mathfrak{F}$: Faraday constant
- $\mathcal{K}$: Tuning parameter for controller
- $\mathfrak{R}$: Universal gas constant

Symbols, when appear in superscript:

- 0: Referent to inlet condition
- b: Referent to bulk phase
- EQ: When in an equilibrium condition
- ex: Excess property
- I: Referent to the gas or liquid films
- P^0: At standard pressure

Symbols, when appear in subscript:

- c: In critical condition
- e: Reference to reactants of a chemical reaction
- for: In reference to the forward reaction
- i: i-th component
- j: j-th component
- L: Liquid
- p: Reference to the products of a chemical reaction

- r: Reduced condition
- for: In reference to the reverse reaction
- s: In reference to the solvent
- t: Total, referring to every component

List of Abbreviations

AMP	2-amino-2-methyl-propanol, p. 6
DEAB	4-diethylamino-2-butanol, p. 12
DEA	Diethanolamine, p. 5
DGA	Diglycolamine, p. 6
DIPA	Diisopropanolamine, p. 6
MDEA	Methyl-diethanolamine, p. 5
MEA	Monoethanolamine, p. 2
NRTL	Non-random two-liquid, p. 20
PZ	Piperazine, p. 6, 12
TEA	Triethanolamine, p. 5
e-NRTL	Electrolyte non-random two-liquid equation, p. 20

Chapter 1

Introduction

1.1 Motivation

Most of Brazilian's oil and gas reservoirs are located in maritimer locations, and its expansion is moving towards larger depths. In 2007 major discoveries were made in the so called pre-salt layer, which made Brazil's proven reservoirs to increase from 15 billion barrels in 2004 to 30 billion in 2009. Petrobras, Brazilian state oil company, has constantly succeeded in exploring those reservoirs, as from 2010 to 2016 oil production in this layer has increased from 41 thousand to 1 million barrels per day.

As a common attribute of pre-salt reservoirs, most have a high gas to oil ratio, and a high CO_2 content. Whereas in post-salt reservoirs CO_2 content usually stays lower than 5%, some pre-salt production fields have reached up to 40% of CO_2.

Carbon dioxide is a contaminant to natural gas due to three main factors:

- CO_2 has no calorific power, what would reduce the energy content of natural gas, limiting its utilization.
- CO_2 is corrosive to transport ducts, which gains extra importance given that pre-salt oil plataforms are often more than 200 km away from the coast, making it imperative to control corrosion.
- CO_2 has a high freezing point, what would render natural gas processing plants infeasible, since most of them operates under cryogenic temperature conditions.

In consonance with that, Brazilian law specifies that natural gas can only be sold with a CO_2 content up to 3% molar.

Commercially, two mature technologies compete for the removal of CO_2 from natural gas: membrane treatment and amine treatment. BAKER and LOKHANDWALA (2008)

showed the difference in application of each technology. While amine treatment are more indicated to high gas flows and low CO_2 concentration, membranes are more competitive with lower flows and higher concentration. High CO_2 concentration together with a high gas flow rate require combined solutions for treatment. The most common strategy is to reduce CO_2 offshore using membranes, and finish it onshore in gas treatment units with amine treatment.

Amine treatment is a chemical absorption - or reactive absorption - process, which consists of gas being absorbed by a liquid phase with combination of reaction and absorptive mass transfer (KORONAKI *et al.*, 2015). The liquid phase containing the absorbed component is then regenerated with increase of temperature and decrease of pressure.

The most mature and commercially applied amine is monoethanolamine (MEA) due to its high absorptive capacity (KORONAKI *et al.*, 2015).

Because of the importance of amine treatment in natural gas processing, given Brazil's scenario, in which pre-salt gas production with high CO_2 content is constantly increasing, the correct modelling of this process is fundamental for better design and operation of such units.

However, this system has some particular complexities in its modelling, which is best performed with rate-based approaches. As will be shown, this approach presents numerical difficulties to solve, and literature to convergence strategies is scarce. In this context this work presents itself.

1.2 Objectives

The main objective of this work is to develop a model to simulate the absorption of CO_2 using monoethanolamine.

Specific objectives are:

- To develop and implement a mathematical model based on the two-film theory in the open software EMSO for simulating an absorption column
- To propose a numeric strategy for solving the two-film model
- To validate the model with literature pilot plant data
- To verify model consistency by means of simulating case scenarios

1.3 Dissertation Structure

This work is divided into five chapters. The first gives a brief introduction, in which the motivation and objectives of this work are presented. The second chapter contains a literature review, focusing mainly on the modelling of reactive absorption processes and thermodynamics of the system here studied. Next, in the third chapter, the modelling methodology is presented, which include the equations used, and all assumptions and simplifications considered. Results are presented in Chapter 4, which includes model validation and case scenarios. Chapter 5 presents the conclusion of this work and suggestions for future works.

Chapter 2

Literature review

This chapter will approach some concepts and areas that are vital for the understanding of this work. First, an overall description of the amine treatment process will be made, followed by the modelling of reactive absorption processes. Finally, a review of the thermodynamics of the amine systems will be presented.

2.1 The Amine Treatment Process

Chemical absorption - or reactive absorption - processes with amine solutions are the most commonly used for removal of acid gases from natural gas (RUFFORD *et al.*, 2012). They rely on reactions of CO_2 with the absorbent to form weakly bonded intermediate compounds, and these reactions can be reversed by application of heat to release the CO_2 and regenerate the absorbent (OLAJIRE, 2010).

A typical chemical absorption process consists of an absorber and a stripper, in which absorbent is regenerated (YU *et al.*, 2012). Figure 2.1 shows a schematic of the process. Natural gas rich in CO_2 is fed in the bottom of the absorber, counter-current to the liquid, which is fed in the top. Mass transfer and chemical reactions occur with the contact between gas and liquid phases, and CO_2 is therefore transferred to the liquid phase. Clean natural gas - also referred as sweetened gas - exits the absorber in the top, whereas CO_2-rich amine, commonly referred as rich amine, leave the absorber from the bottom and continues to be regenerated in the stripper. Temperature is elevated and pressure is decreased in the stripper, what disfavours the chemical reactions and release the CO_2-rich acid gas in the top of the stripper. Regenerated amine - also called lean amine - is cooled and pressurized to return to the absorber (KUCKA *et al.*, 2003b).

Amines are organic compounds derived from ammonia, in which one or more

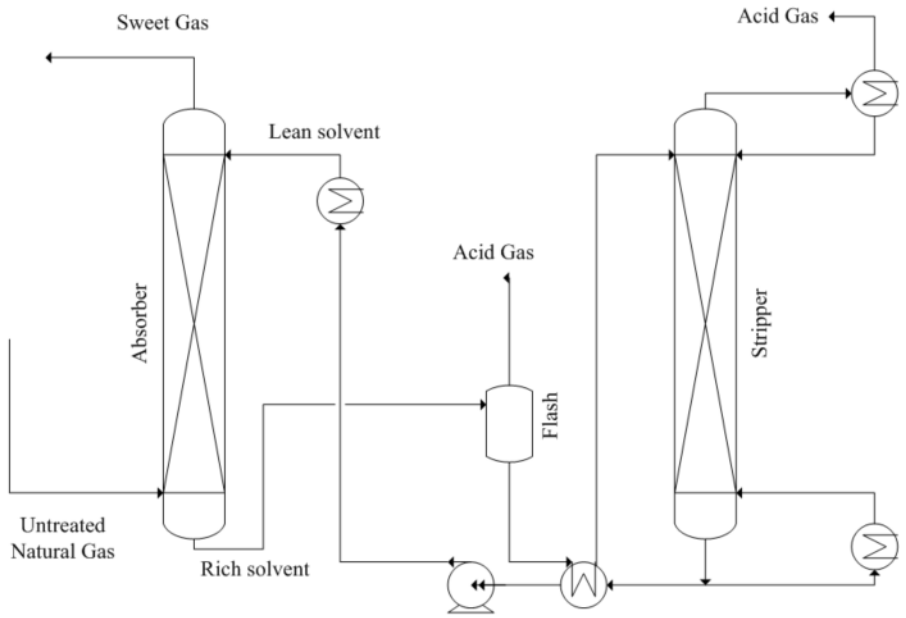

Figure 2.1: Simplified flow diagram of amine absorption unit.

hydrogen atoms have been substituted by an alkyl or aromatic group. According to the degree of substitution of the amine, it can be classified into primary, secondary or tertiary, being examples, respectively monoethanolamine (MEA), diethanolamine (DEA) and Methyl-diethanolamine (MDEA). Figure 2.2 shows the molecular structure of those amines. All of those examples are considered alkanolamines, since they contain at least on hydroxyl (OH) group in the substitutes. They are the most widely used solvent for CO_2 removal in chemical absorption processes (YU *et al.*, 2012).

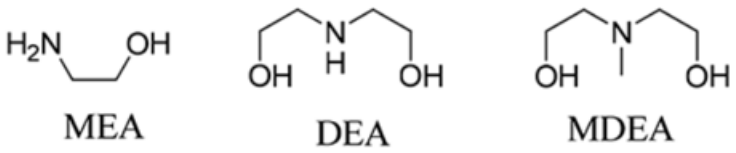

Figure 2.2: Structure of MEA, DEA and MDEA, illustrating respectively primary, secondary and tertiary alkanolamines

Primary amines are more reactive to CO_2 than secondary amines, which are more reactive than tertiary. For example, second order reaction constant between MEA and CO_2 was reported by SADA *et al.* (1976), being 8,400 $\mathrm{L/s/mol}$ at 25°C, value that reduces to 1,340 and 16.8 in respect to DEA and triethanolamine (TEA), respectively.

An important parameter to compare amine performances is the absorptions capacity - also named loading. It is the number of moles of CO_2 absorbed by the solution per each amine mole. Despite being more reactive, primary and secondary amines tend to have lower loadings when compared to tertiary amines. That is explained by the absorption mechanism. Primary and secondary amines - represented by R_1R_2NH - have at least one hydrogen bounded to the basic nitrogen and, therefore, are able to form the zwitterion ($R_1R_2N^+HCOO^-$) as shown in Equation 2.1 (VERSTEEG and VAN SWAAIJ, 1988). The acid hydrogen is then attacked by a base, which can be water, but most commonly is the amine itself, as shown in Equation 2.2. The overall equation, when the base considered is the amine, is shown in Equation 2.3. Loading is then 0.5 of mol CO_2 / mol of Amine.

$$CO_2 + R_1R_2NH \rightleftharpoons R_1R_2N^+HCOO^- \tag{2.1}$$

$$R_1R_2NH^+HCOO^- + B \rightleftharpoons R_1R_2NCOO^- + BH^+ \tag{2.2}$$

$$2\,R_1R_2NH + CO_2 \rightleftharpoons R_1R_2NCOO^- + {R_1R_2NH_2}^+ \tag{2.3}$$

Tertiary amines - represented as $R_1R_2R_3N$ - cannot directly react to CO_2, since they have no hydrogen bonded to the basic nitrogen. Therefore the reaction is the formation of bicarbonate through base catalysis of CO_2 hydration (BERNHARDSEN and KNUUTILA, 2017), shown in Equations 2.4 and 2.5 with Equation 2.6 being the net reaction (SADA *et al.*, 1976). It can be noted that, for tertiary amines, the bicarbonate formation gives a loading of 1.0 mol of CO_2 per mol of amine.

$$R_1R_2R_3N + H_2O \rightleftharpoons R_1R_2R_3NH^+ + OH^- \tag{2.4}$$

$$CO_2 + OH^- \rightleftharpoons {HCO_3}^- \tag{2.5}$$

$$R_1R_2R_3N + CO_2 + H_2O \rightleftharpoons R_1R_2R_3NH^+ + {HCO_3}^- \tag{2.6}$$

It is notable that the choice for the type of solvent to be used in an amine treatment plant is not trivial. Figure 2.3 shows various common amines and their abbreviations. MEA, however, is the most commonly used solvent, and in 1990 accounted for 40% of the CO_2 capture market (DEMONTIGNY *et al.*, 2001). With that in mind, MEA was chosen to be the solvent for this work, keeping in mind that the concept is representative of any reactive amine gas treating process.

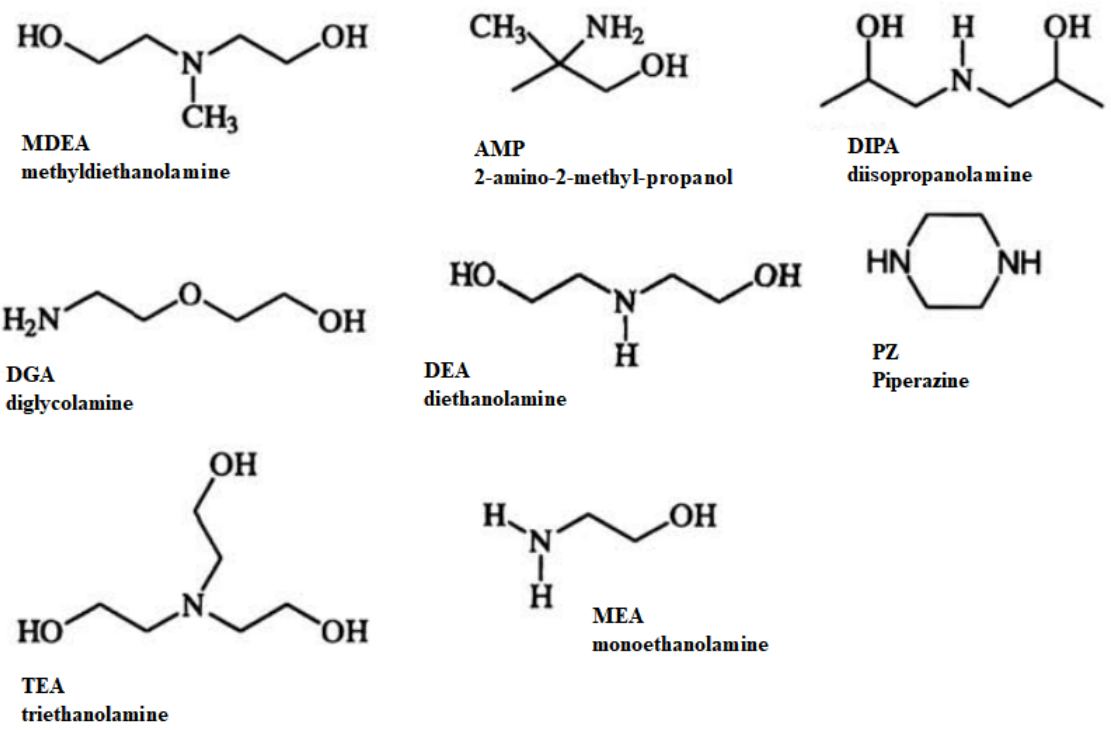

Figure 2.3: Structure of different amines, their names and common abbreviations

2.2 Reactive Absorption Modelling

2.2.1 Overview

Reactive or chemical absorption is the process in which one gas stream reacts with a liquid stream resulting in the absorption of one or more component from the gas phase to the liquid phase, in a combination of chemical reaction and mass transport. The contact between the two phases usually takes place in a column, in which gas is fed in the bottom, and the liquid phase is fed in the top.

The manufacture of nitric and sulphuric acid, soda ash and bleaches, as well as purification of natural gas, or synthesis gas involve the reaction between liquid and gas (KENIG *et al.*, 1999) are examples of reactive absorption applications.

An important characteristic of reactive absorption process is the combination of chemical reactions and/or equilibrium with mass transfer and also column hydrodynamics. Moreover, most processes are of a multicomponent nature, what make its modelling challenging. The ideal model has to be rigorous enough to encompass all complex aspects of the problem and manageable enough in order to enable easy implementation (KORONAKI *et al.*, 2015).

Concerning the mass transfer, NOERES *et al.* (2003) divided the modelling approaches into: equilibrium and non-equilibrium (or rate-based) models. The first assume an instantaneous mass transfer, or perfect mixing, and therefore, no mass transfer resistance. The latter is used when that simplification is not reasonable and mass transfer resistance must be taken into account.

Mass transfer at the gas/liquid interface can be described using different theoretical concepts: the two-film model (LEWIS and WHITMAN, 1924) or the penetration model (HIGBIE, 1935). Both of them need experimentally estimated model parameters, however the two-film model is advantageous since there is a broad spectrum of correlation available in literature.

The two film theory suggests that there are two thin areas (films) that are adjacent to the interface separating the two bulk phases, which are ideally mixed. It is assumed that the overall mass and heat transfer resistance is concentrated in these two films. The theory considers that the only mass transport mechanism through the films is stationary diffusion (KENIG *et al.*, 2002). A deeper discussion about the two film theory will be presented in the next section, since it was the approach chosen for this work.

In the gas/liquid interface occur the mass and heat transfers. These phenomena are often approached with enhancement factors (KORONAKI *et al.*, 2015). According to KENIG and SEFERLIS (2009), these factors represent the acceleration of mass transfer due to chemical reactions in the interfacial region and are either obtained by fitting experimental results or derived theoretically based on simplified model assumptions. However, the authors point out that it is not possible to derive the enhancement factors properly from data on binary experiments, and a theoretical description of reversible, parallel or consecutive reactions is based on rough simplifications.

An alternative to this approach is to directly calculate interfacial molar fluxes through Maxwell-Stefan equations. This approach is considered more rigorous and less dependent on experiments (KENIG *et al.*, 2002). Figure 2.4 summarizes the different mass transfer approaches to the modelling of reactive absorption.

Concerning chemical reactions, it is worth noting its distinctive velocity in each particular process, as it can vary from very slow to infinitely high (instantaneous). Chemical equilibrium is often considered when reaction rates are high, however, both equilibrium and rate-based models may consider reaction kinetics.

Liquid-gas process units are usually tray or packing columns. According to KENIG

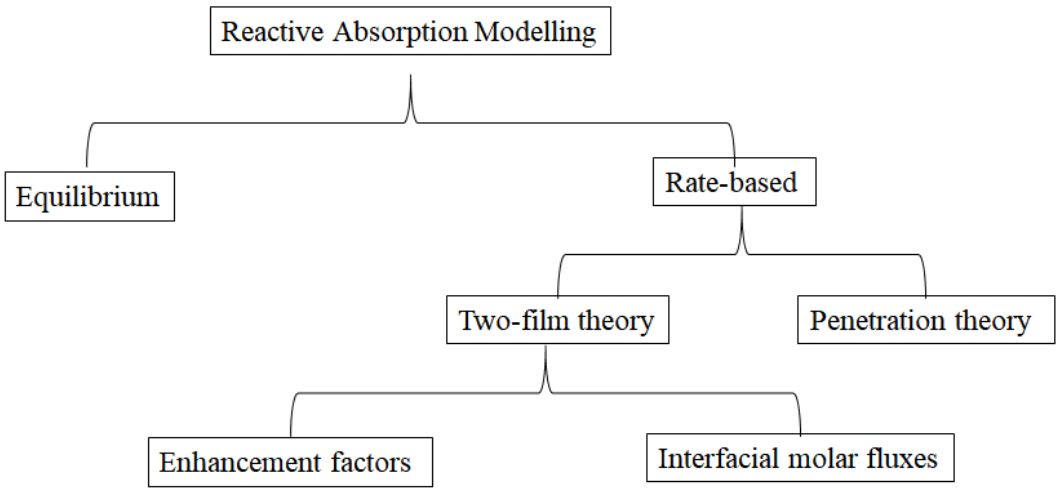

Figure 2.4: Mass transfer approaches to modelling reactive absorption.

et al. (2001), these columns are considered as a cascade of segments called stages, which relate to each other through mass and energy balances, as shown in Figure 2.5. The authors present the evolution in the way those stages can be designed in Figure 2.6. This figure is widely cited as it summarizes different model approaches in literature. The simplest model is the bottom left, in which chemical and physical equilibrium is assumed in each theoretical stage. The next is the bottom right, which adds reaction kinetics to the equilibrium stage - which is physically inconsistent, though widely applied (KORONAKI *et al.*, 2015). The upper models consider mass transfer rates, and gain complexity moving rightwards, adding factors such as reaction kinetics, electrolytes influence and film reactions. For future reference in this text, the model types were numbered from 1 to 5.

KORONAKI *et al.* (2015) made a review of different models published up to 2015. Here the main results are summarized in Table 2.1. It is notable that equilibrium models are not frequent in literature, as this kind of system consistently do not reach equilibrium conditions.

An important result concerning the choice of rate-based over equilibrium models in reactive absorption application was reported by KENIG *et al.* (2002). The system studied is coke gas purification, which consists of the selective absorption of H_2S and NH_3 over CO_2, using water as absorbing media. A pilot scale tower was simulated using both equilibrium and rate-based approaches - both considering reaction kinetics - and the axial bulk liquid concentration profiles were plotted together with experimental results. It was notable that equilibrium models yielded results inconsistent with the experimental studies, as the selectivity towards H_2S and HCN absorption could not be correctly predicted.

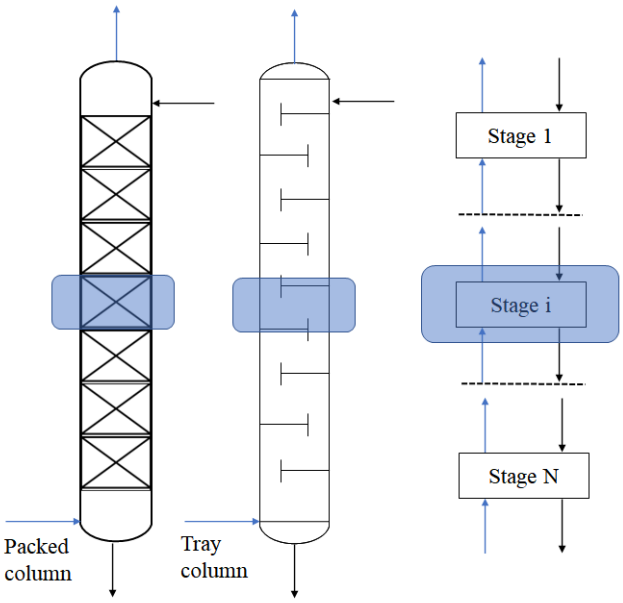

Figure 2.5: Column discretization scheme.

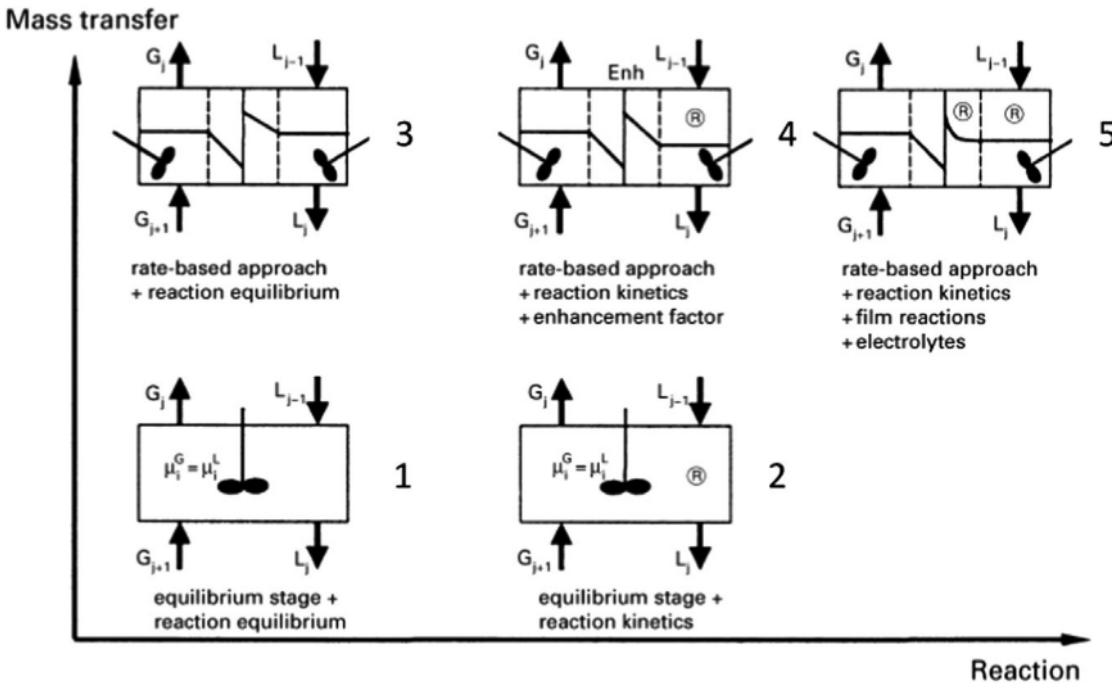

Figure 2.6: Model complexity evolution taken from KENIG *et al.* (2001) with authorization from Elsevier.

Table 2.1: Summarize of recent reactive absorption models for the removal of CO_2, expanded from KORONAKI *et al.* (2015). D stands for dynamic model, and SS for steady-state

Researcher	**Model type**	**Solvent**	**Simulated Equipment**	**Validation**
PINTOLA *et al.* (1993)	4 SS	MEA	Absorber	Pilot plant
KENIG *et al.* (1999)	5 D	Aqueous ammonia	Absorber	Coke Pilot Plant
AL-BAGHLI *et al.* (2001)	4 SS	MEA and DEA	Absorber	Not available
KUCKA *et al.* (2003b)	5 SS	Amines	Absorber	Pilot Plant (TONTIWACHWUTHIKUL *et al.*, 1992) and Industrial Plant (PINTOLA *et al.*, 1993)
BOLHÀR-NORDENKAMPF *et al.* (2004)	4 SS	MDEA	Absorber and Desorber	Commercially operated MDEA plant
ABOUDHEIR *et al.* (2006)	4 SS	AMP	Absorber	Two pilot plants
GABRIELSEN *et al.* (2006)	4 SS	AMP	Absorber	Pilot Plant (TONTIWACHWUTHIKUL *et al.*, 1992)
KVAMSDAL *et al.* (2009)	4 D	MEA	Absorber	Pilot Plant at University of Texas
GHAEMI *et al.* (2009)	4 D	Partially carbonated ammonia	Absorber	Pilot plant
LAWAL *et al.* (2010)	5 D	MEA	Absorber and Desorber	Pilot Plant at University of Texas
MORES *et al.* (2011)	2 SS	MEA	Absorber and Desorber	Pilot Plant at University of Texas

Continued on next page

Table 2.1 – Summarize of recent reactive absorption models for the removal of CO_2, expanded from KORONAKI *et al.* (2015). D stands for dynamic model, and SS for steady-state(*Continued from previous page*)

Researcher	**Model type**	**Solvent**	**Simulated Equipment**	**Validation**
KHAN *et al.* (2011)	4 SS	MEA	Absorber	Pilot Plant (TONTIWACHWUTHIKUL *et al.*, 1992) and Industrial Plant (PINTOLA *et al.*, 1993)
PUXTY *et al.* (2011)	5 SS	Amines and ammonia mixtures	Absorber	Wetted wall apparatus
HARUN *et al.* (2011)	4 D	MEA	Absorber and Desorber	Simulation from Aspen Plus
DUGAS and ROCHELLE (2011)	5 SS	MEA and PZ	Absorber	Pilot plant
GASPAR and CORMOS (2012)	4 D	Alkanolamines	Absorber	Pilot plants (AROONWILAS *et al.*, 2003) and (TOBIESEN *et al.*, 2008) and (TONTIWACHWUTHIKUL *et al.*, 1992)
SEMA *et al.* (2012)	4 SS	DEAB	Absorber	Pilot plant (SHI *et al.*, 2012)
JAYARATHNA *et al.* (2013)	4 D	MEA	Absorber	Pilot Plant at University of Texas
SAIMPERT *et al.* (2013)	4 SS	MEA	Absorber and Desorber	Pilot plant
MAC DOWELL *et al.* (2013)	5 D	MEA	Absorber	Pilot plant for steady-state validation (TONTIWACHWUTHIKUL *et al.*, 1992)
NITTAYA *et al.* (2014)	4 D	MEA	Absorber and Desorber	Pilot plant
MOIOLI *et al.* (2014)	5 SS	PZ	Absorber	Pilot plant (PLAZA, 2012)

2.2.2 Rate-based approach

As previously described, rate-based approach is most commonly used when modelling reactive absorption of CO_2 with amine solutions, since thermodynamic equilibrium is hardly archived under operating conditions (KENIG *et al.*, 2002). Additionally, for multicomponent mixtures - which are almost always the industrial case - diffusion interactions between several components result into unusual phenomena like osmotic or reverse diffusion and mass transfer barrier (NOERES *et al.*, 2003).

In order to directly calculate the heat and mass flows between the liquid and the gas, the two-film model is widely used. It assumes that all the resistance to mass transfer is concentrated in thin films adjacent to the phase interface and that transfer occurs within these films by molecular diffusion only (NOERES *et al.*, 2003). Outside the films there are the liquid and gas bulk phases, in which no composition gradient is present and, therefore, perfect mixing is assumed. That means that in the film region, there is only one-dimension diffusion transport (KENIG *et al.*, 2002). Figure 2.7 shows an schematic representation of the two-film model, in which one component is transferred from the gas phase to the liquid phase. The interface is the only point of the model, in which thermodynamic equilibrium is assumed.

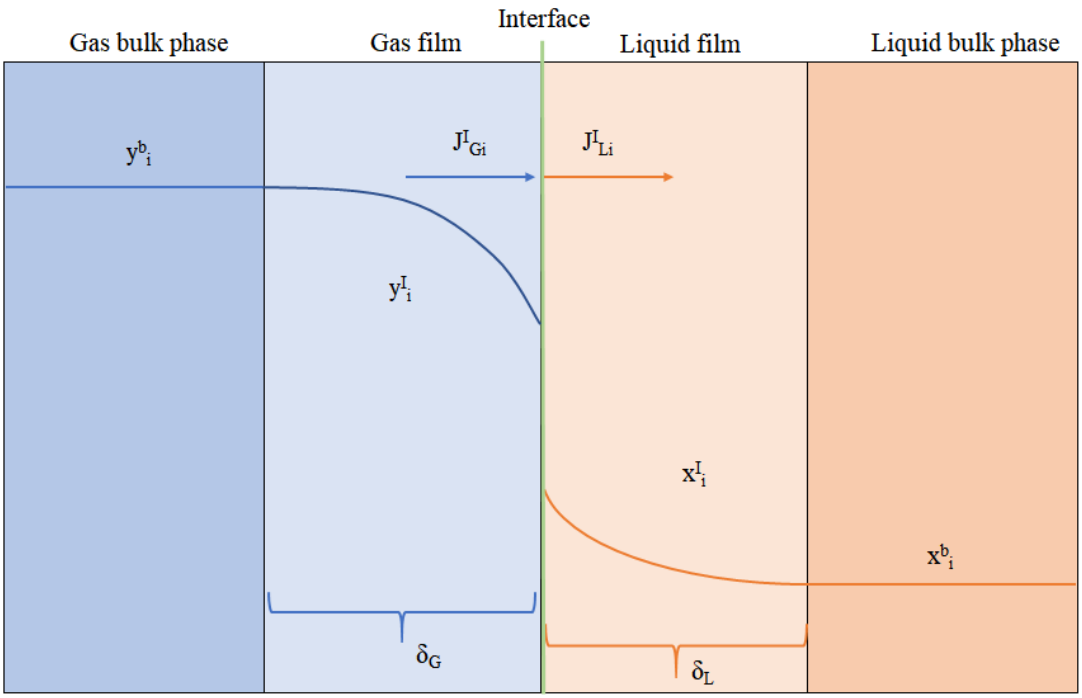

Figure 2.7: Two-film model representation

In the film normal direction, molecular unidimensional diffusion occurs according to the Maxwell-Stefan equation, which correlates the component molar flow with the

gradient of its chemical potential in the generalized form shown in Equations 2.7 and 2.8 (TAYLOR and KRISHNA, 1993).

$$đ_i = \sum_{j=1}^{n} \frac{x_i^I J_{Lj} - x_j^I J_{Li}}{C_{Lt} Đ_{ij}} \tag{2.7}$$

$$đ_i = \frac{x_i}{\Re T} \frac{d\mu_i}{d\eta} \tag{2.8}$$

In these equations, J_{Li} are the mass fluxes, C_{Li} is the concentration and $đ_i$ is the Maxwell-Stefan diffusion coefficient. $\Re$ is the universal gas constant, μ_i is chemical potential and η denotes the film direction. The superscript I denotes that the variable is in either gas or liquid films. The term d_i is the generalized driving force and when dealing with electrolytes, it must also account the gradient of the electrical potential φ, as shown in Equation 2.9 (TAYLOR and KRISHNA, 1993), in which $\mathfrak{F}$ is the Faraday constant.

$$đ = \frac{x_i}{\Re T} \frac{d\mu_i}{d\eta} + x_i z_i \frac{\mathfrak{F}}{\Re T} \frac{1}{\delta_L} \frac{d\varphi}{d\eta} \tag{2.9}$$

However, TAYLOR and KRISHNA (1993) suggested that for dilute electrolyte solutions, the molar flow equations can be reduced to the Nernst-Planck equation (Equation 2.10) and experiments conducted by KENIG *et al.* (2001) showed that this reduction is possible with no significant loss of complexity. In this approximation, chemical potential is approximated to $RT \ln x_i$ and Maxwell-Stefan coefficient sums are condensed in a effective coefficient, $D_{Li,\text{eff}}$. In equation 2.10, J_{Ln} refers to the solvent's flux.

$$J_{Li} = -\frac{C_{Lt} D_{Li,\text{eff}}}{\delta_L} \left(\frac{dx_i}{d\eta} + x_i z_i \frac{\mathfrak{F}}{\Re T} \frac{d\varphi}{d\eta} \right) + x_i J_{Ln} \tag{2.10}$$

At the exact point of the gas/liquid interface, equilibrium is assumed, so that molecular

species distribute themselves among gas and liquid phase. Henry's constants usually represent the reference state for molecular solutes as CO_2 as shown in Equation 2.11 (AUSTGEN *et al.*, 1989).

$$y_i^I \hat{\phi}_i P = x_i^I \gamma_i^* H_i^{P^o} \exp\left(\frac{\bar{v_i^\infty}\,(P - P^o)}{\Re T}\right) \tag{2.11}$$

In this equation, $\hat{\phi}_i$ is the $i-th$ component fugacity coefficient, P is the absolute pressure, H_i is the Henry's equilibrium constant for the component i, P^o is the reference pressure, γ is the liquid phase activity coefficient and $\bar{v_i^\infty}$ is the liquid molar volume.

It is notable that, in the two films, the transport equations form a second order differential equation, whose boundary conditions are the concentration in the bulk phase, and the concentration determined by thermodynamic equilibrium in the gas/liquid interface. This equation must be solved simultaneously with balance equations in the bulk phases.

Altogether with common balance equations, rate-based model connect specific models for all the following aspects:

- Thermodynamics for gas phase
- Thermodynamics for liquid phase
- Reaction kinetics and/or chemical equilibrium
- Column hydrodynamics
- Physical properties estimation

2.3 Thermodynamics of CO_2-Alkanolamine systems

The absorption of CO_2 in aqueous solutions of alkanolamines is described with a series of chemical reactions which greatly favours acid gas solubility (KONTOGEORGIS and FOLAS, 2010).

Irrespective of the alkanolamine present, - here represented by $R_1R_2R_3N$ - the following reactions must be accounted for (KONTOGEORGIS and FOLAS, 2010):

- Ionization of water:

  $2\,H_2O \rightleftharpoons H_3O^+ + OH^-$

- Hydrolysis and ionization of dissolved CO_2:

  $CO_2 + 2\,H_2O \rightleftharpoons H_3O^+ + HCO_3^-$

- Dissociation of bicarbonate:

  $HCO_3^- + H_2O \rightleftharpoons H_3O^+ + CO_3^{2-}$

- Dissociation of a protonated alkanolamine:

  $R_1R_2R_3NH^+ + H_2O \rightleftharpoons H_3O^+ + R_1R_2R_3N$

For secondary and tertiary amines - R_1R_2NH - carbamate formation is also possible:

$$R_1R_2NH + H_2O \rightleftharpoons R_1R_2NCOO^- + H_3O^+$$

In order to fully describe the absorption of gaseous CO_2 by alkanolamine solution, a thermodynamic model must consider gas and liquid phases fugacity, and most of them must consider ionic therms for the liquid phase.

According to KONTOGEORGIS and FOLAS (2010), the most simple thermodynamic model applied to these systems is the Kent-Eisenberg approach (KENT and EISENBERG, 1976). According to which, all activity coefficients and vapour phase fugacity coefficients are assumed equal to one, i.e, both ideal gas and liquid are assumed and two chemical equilibrium constants are fitted to experimental data. This approach has been applied to MEA, DEA and MDEA but not to mixed alkanolamines.

More complexes models include activity coefficient models and equations of state, and most of the suitable for electrolytes are used for CO_2–water– alkanolamines and several important approaches are summarized in Tables 2.2 and 2.3. e-NRTL and e-UNIQUAC are typically combined with a cubic equation of state like SRK for the vapour phase. Except for the SAFT model of BUTTON and GUBBINS (1999), where chemical reactions are not considered, all the others are electrolyte models.

Since coulombic forces are very long range, most electrolyte models combine the Debye-Hückel theory for the electrostatic interactions with an equation to represent short-term interaction. The most well-known activity coefficient models for electrolyte solutions are those of Pitzer, e-NRTL and e-UNIQUAC. Only the last has ion-specific parameters. All three models have been applied to numerous aqueous and mixed solvent salt solutions, and various properties have been considered (activity coefficients, solid–liquid equilibria, critical micelles concentration of aqueous ionic surfactants). The models are not predictive in any way and a large number of parameters are required,

typically fitted to all available data (KONTOGEORGIS and FOLAS, 2010).

Table 2.2: Activity coefficient models applied to CO_2–water–alkanolamines. Expanded from KONTOGEORGIS and FOLAS (2010)

Model	Reference	Application	Comments
Pitzer	SILKENBA *et al.* (1998)	AMP, MDEA, AMP/MDEA blend	Satisfactory results for mixed alkanolamines based on results for single alkanolamines
	KAMPS *et al.* (2001)	MDEA (also H_2S)	-
e-NRTL	CHEN *et al.* (2001)	Various organic electrolytes	-
	CHEN and EVANS (1986)	Ammonia	-
	POSEY and ROCHELLE (1997)	MDEA (also H_2S)	-
	CULLINANE and ROCHELLE (2005)	PZ	-
	AUSTGEN *et al.* (1989)	MEA, DEA	Validated to temperatures of 25–120°C
	AUSTGEN *et al.* (1991)	MDEA/MEA, MDEA/MEA MDEA/DEA PZ/MDEA MEA, DEA, MDEA, AMP, PZ, MEA/MDEA, PZ/MDEA, AMP/MDEA	Loading from 0–1 and concentration of 30% for mixed amines
	LIU *et al.* (1999)	MEA	-
	BISHNOI and ROCHELLE (2002)	MDEA	-
		PZ/MDEA	Composition of up to 30% in PZ
	AROUA *et al.* (2002)	AMP, MDEA and blends	-

Continued on next page

Table 2.2 – *Continued from previous page*

Model	Reference	Application	Comments and accuracy
	ADDICKS *et al.* (2002)	MDEA	25–200°C and loadings up to 8M
	BARREAU *et al.* (2006)	DEA	310–394K and loadings up to 1.2
e-UNIQUAC	KAEWSICHAN *et al.* (2001)	MEA, MDEA, MEA/MDEA blend (also H2S)	25–120°C
	ADDICKS *et al.* (2002)	MDEA	25–200°C and loadings up to 8M
	THOMSEN and RASMUSSEN (1999)	Ammonia–water	20°C, concentration of 0.1–2M
	THOMSEN (2005)	Ammonia-water	-
	GARCÍA *et al.* (2006)	CO_2–water	-
	FARAMARZI *et al.* (2009)	MDEA, MEA and MEA/ MDEA blends	-

The performance of many electrolytic equations of state is very good, but it largely depends on the focus given, e.g, not all models have been developed for a large number of salts or applied to mixed salts. But there are positive features and it appears that they require fewer parameters than the electrolyte activity coefficient models. Moreover, several of these parameters, e.g, ionic diameters and segment energies, have well-defined meanings and their values, which are estimated from experimental data, can be tested independently. Several ways have been developed for reducing the number of adjustable parameters by utilizing semi-theoretical correlations or trends using the Pauling or Stokes ionic diameters (KONTOGEORGIS and FOLAS, 2010).

In this work, due to availability of parameters, the e-NRTL model will be used and further described in detail.

2.3.1 The e-NRTL equation

The e-NRTL is a model developed by Chen, Britt, Boston and Evans (CHEN *et al.*, 1982) and was designed to represent the properties of all kinds of electrolyte systems, in a vast range of concentrations and ionic forces.

Table 2.3: Equation of State models applied to CO_2–water–alkanolamines. Adapted from KONTOGEORGIS and FOLAS (2010)

Model	Reference	Application	Comments
Fürst and Renon, Wong-Sandler mixing rules (+NRTL)	VALLÉE *et al.* (1999)	DEA (also for H_2S)	37–107°C, concentration of 0.5–3.5 M, and loading up to 2.34
	CHUNXI and FÜRST (2000)	MDEA (also H_2S)	25–120°C and loadings up to 2. Observed 10–40% deviation
Based on SEK using Huron-Vidal mixing rules and three ionic terms	SOLBRAA (2002)	MDEA	10% error in pressure
	HUTTENHUIS *et al.* (2008)	MDEA	-
Linear combination of the Vidal and Michelsen mixing rules coupled with the original UNIFAC (LCVM)	VRACHNOS *et al.* (2004)	MDEA	298–393K
	VRACHNOS *et al.* (2006)	MEA, MDEA and MDEA/MEA	Loading up to 1.4
SAFT	BUTTON and GUBBINS (1999)	MEA, DEA	No electrolyte term is used. 40% deviation in CO_2 loading
	MAC DOWELL *et al.* (2013)	MEA	-

It is considered that in electrolyte solutions different types of interaction may be found: ion-ion, molecule-molecule and ion-molecule (CHEN *et al.*, 1982). From those, only the first interaction is considered long-range, meaning that the other two are short-range interactions.

Therefore, the excess Gibbs energy of electrolyte systems can be considered as the sum of two terms, one related to long-range forces between ions and the other to short-range forces between all the species (CHEN *et al.*, 1982).

The long-range interaction contribution is modelled with the extended form of the Debye-Hückel equation proposed by PITZER (1980).

$$\frac{G^{ex*}_{PDH}}{\Re T} = \left(-\sum_{k=1}^{N} n_k\right)\left(\frac{4A_\phi I_x}{\rho}\right)\ln\left(1+\rho I_x^{1/2}\right) \tag{2.12}$$

In this equation, G^{ex*}_{PDH} is the Pitzer-Debye-Hückel excess Gibbs energy contribution, n_k in the number of moles of k species, ρ is the closest approach parameter. A_ϕ is a factor calculated with equation 2.13 and I_x is the ionic force calculated with equation 2.14.

$$A_\phi = \left(\frac{1}{3}\right)\left(\frac{2\pi N_0 d_s}{M_S}\right)\left(\frac{e^2}{\lambda\kappa T}\right)^{3/2} \tag{2.13}$$

M_S is the molecular weight of the solvent, N_0 is the Avogadro's number, d_S is solvent's density, e is the electron's charge, λ is the dielectric constant and κ is the Boltzmann constant.

$$I_x = \frac{1}{2}\sum_{i}^{N} z_i^2 x_i \tag{2.14}$$

z_i is the charge of specie i, and x_i is its molar fraction.

The short-range forces between molecules are represented using the non-random two-liquid (NRTL) equation (RENON and PRUASNITZ, 1968) approach. The reasons for this choice were enumerated by CHEN *et al.* (1982):

- Electrolyte systems have large heats of mixing, which makes the entropy of mixing

negligible

- The model is algebraically simple, and require only binary parameters
- It does not require specific volume or area data, such as that required by UNIQUAC local composition model

The model considers two fundamental assumptions:

1. The like-ion repulsion assumption states that the local composition of cations around cations is zero (and likewise for anions around anions). This is the same as stating that the repulsive forces between ions of like charge are relatively large.
2. The local electroneutrality assumption states that the distribution of cations and anions around a central molecule is such that the net local ionic charge is zero.

Some important definitions of the model are shown in Equations 2.15 to 2.17, in which X_i is the effective mole fraction, g_{ji} and g_{ii} are energies of interaction between $j-i$ and $i-i$ species, respectively. α is called nonrandomness factor. G_{ij} is defined in Equation 2.16.

$$\begin{aligned} &X_i = x_i C_i \text{ , where:} \\ &C_i = Z_i \text{ , for electrolytes} \\ &C_i = 1 \text{ , for molecular species} \end{aligned} \tag{2.15}$$

$$G_{ij} = \exp\left(-\alpha_{ij}\tau_{ij}\right) \tag{2.16}$$

$$\tau_{cm} = \frac{g_{ij} - g_{ii}}{\mathfrak{R}T} \tag{2.17}$$

For a multicomponent system, the model is reproduced in Equation 2.18 , in which the subscripts c, a and m denote, respectively, cations, anions and molecules.

$$\frac{g^{ex}_{NRTL}}{\Re T} = \sum_m X_m \frac{\sum_j X_j G_{jm} \tau_{jm}}{\sum_k X_k G_{km}} + \sum_c X_c \sum_{a'} \frac{X_{a'}}{\sum_{a"} X_{a"}} \frac{\sum_j X_j G_{jc,a'c} \tau_{jc,a'c}}{\sum_k X_k G_{kc,a'c}} + \sum_a X_a \sum_{c'} \frac{X'_c}{\sum_{c"} X_{c"}} \frac{\sum_j X_j}{\sum_k X_k} \tag{2.18}$$

In Equation 2.18, the following relations are valid (CHEN and EVANS, 1986)

$$G_{jc,a'c} = \exp\left(-\alpha_{jc,a'c} \tau_{jc,a'c}\right) \tag{2.19}$$

$$G_{ja,c'a} = \exp\left(-\alpha_{ja,c'a} \tau_{ja,c'a}\right) \tag{2.20}$$

$$G_{ca,m} = \exp\left(-\alpha_{ca,m} \tau_{ca,m}\right) \tag{2.21}$$

$$G_{cm} = \frac{\sum_a X_a G_{ca,m}}{\sum_{a'} X_{a'}} \tag{2.22}$$

$$G_{am} = \frac{\sum_c X_c G_{ca,m}}{\sum_{c'} X_{c'}} \tag{2.23}$$

$$\alpha_{cm} = \frac{\sum_a X_a \alpha_{ca,m}}{\sum_{a'} X_{a'}} \tag{2.24}$$

$$\alpha_{am} = \frac{\sum_c X_c \alpha_{ca,m}}{\sum_{c'} X_{c'}} \tag{2.25}$$

$$\tau_{ma,ca} = \tau_{am} - \tau_{ca,m} + \tau_{m,ca} \tag{2.26}$$

$$\tau_{mc,ac} = \tau_{cm} - \tau_{ca,m} + \tau_{m,ca} \tag{2.27}$$

$$\tau_{ca,ca'} = -\tau_{ca',ca} \tag{2.28}$$

$$\alpha_{mc,ac} = \alpha_{cm} \tag{2.29}$$

$$\alpha_{ma,ca} = \alpha_{am} \tag{2.30}$$

With these relations, the only needed parameter for the model are the binary interaction parameters: $\tau_{mm'}$, $\tau_{m'm}$, $\tau_{ca,m}$, $\tau_{m,ca}$, $\tau_{ca,ca'}$, $\tau_{ca',ca}$, $\tau_{ca,c'a}$, $\tau_{c'a,ca}$, and the correspondent nonrandomness factors.

In Equation 2.18, the pure component state is adopted as the reference state for the reference Gibbs energy of molecules, and the hypothetical homogeneously mixed, completely dissociated liquid electrolyte mixture is adopted as the reference state for electrolytes (CHEN and EVANS, 1986).

Since the most common reference state for electrolytes is the infinite dilution aqueous state, the equation must be normalized as shown in Equation 2.31.

$$\frac{g^{ex*}_{NRTL}}{\Re T} = \frac{g^{ex}_{NRTL}}{\Re T} - \sum_{m \neq w} x_m \ln \gamma^{\infty}_m - \sum_{c} x_c \ln \gamma^{\infty}_c - \sum_{a} x_a \ln \gamma^{\infty}_a \tag{2.31}$$

A model for the vapor-liquid equilibria for aqueous acid-gas/alkanolamine systems was developed by AUSTGEN *et al.* (1989). It followed the model already presented by CHEN *et al.* (1982) with a modification on the long-range term to account for the excess Gibbs energy of transfer from infinite dilution in the mixed solvent to infinite dilution in the aqueous phase - called the Born therm - as shown in Equation 2.32.

$$\frac{g^{ex*}_{BORN}}{\mathfrak{R}T} = \left(\frac{e^2}{2kT}\right)\left(\frac{1}{D_s} - \frac{1}{D_w}\right)\left(\sum_i \frac{x_i z_i^2}{r_i}\right) \tag{2.32}$$

The specific Gibbs excess energy is therefore calculated with Equation 2.33.

$$g^{ex*} = g^{ex*}_{PDH} + g^{ex*}_{BORN} + g^{ex*}_{NRTL} \tag{2.33}$$

2.4 Final Considerations

Literature review for modelling chemical absorption of CO_2 showed that complex models which consider a rate-based approach and two-film theory are more accepted. However, information about the numerical method of solution, i.e. convergence method, of the complex equation system that this rigorous approach generates is scarce. Because of that, it is still difficult to implement open-source simulators for this system, and in that context this work presents itself, as it proposes a numerical step-by-step solution method. Chemical absorption of CO_2 with MEA was chosen, keeping in mind that the solution methodology for other compounds would be absolutely analogue.

Chapter 3

Methodology

This chapter first present the system which is being modelled, as well as all the equations that were employed in its description. Then, the methodologies utilized to calculate physical properties are also presented, as well as transport properties, which here are understood as those properties correlated to the mass transfer inside packed columns. Subsequently, it is shown the methods employed to solve the resulting system of equations. In the end of this chapter, it is described how the model parameter was estimated.

3.1 Mathematical modelling

The main objective of this work is to simulate an absorption column for CO_2 removal of natural gas utilizing monoethanolamine as a solvent. In order to do that the following premisses and simplifications were adopted:

- Gas feed will be a mixture of CO_2 and CH_4
- Aqueous solution of monoethanolamine will be used as solvent
- Stage discretization will be used for column modelling
- Two-film theory will describe the mass transfer between gas and liquid phases
- All physical properties will be temperature and composition dependent when applicable
- Column pressure drop will be neglected
- Column operates adiabatically

In order to simulate an absorption column, a classical equilibrium-stage discretization was used, meaning that either a tray or packing column will be divided into equilibrium

stages, in which individual balances will be performed, as shown in the schematic Figure 3.1, adapted from KENIG and SEFERLIS (2009). The relation between one equilibrium stage and the packing height is usually determined via empirical correlations. However, if one does not want to resort on such correlations, this approach is also convenient, since each equilibrium stage can be so small as one might want, in order to rigorously simulate a long packing segment.

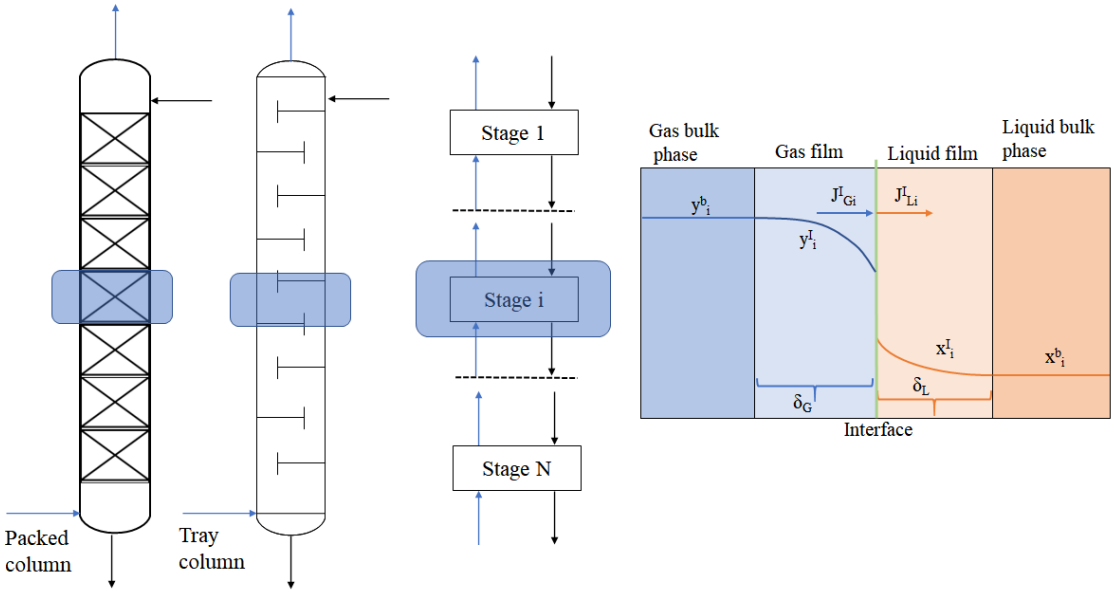

Figure 3.1: Column discretization scheme.

Stage i, as identified in Figure 3.1, is object of the balance equations that will be described. In each stage, a gas and a liquid phase are in contact and, between them, there are two films, which contain all mass and heat transfer resistances between both phases. This is the two-film theory, already described in Chapter 2.

In order to present the equations to describe this system, the following additional assumptions were made:

- Column operates in plug flow
- Stages have constant gas and liquid volume
- Reactions occur only in liquid phase

In this work, only steady-state operation condition is relevant, though the balances will be equated considering transitory terms. The reason for that will be cleared subsequently when convergence strategies will be presented.

Figure 3.2 shows the the regions where the balances are considered in the two-film model, as well as inlet and outlet molar fluxes and a schematic concentration gradient. Region A represents the bulk gas phase, region B the gas film, region C the liquid film, and region D the bulk liquid.

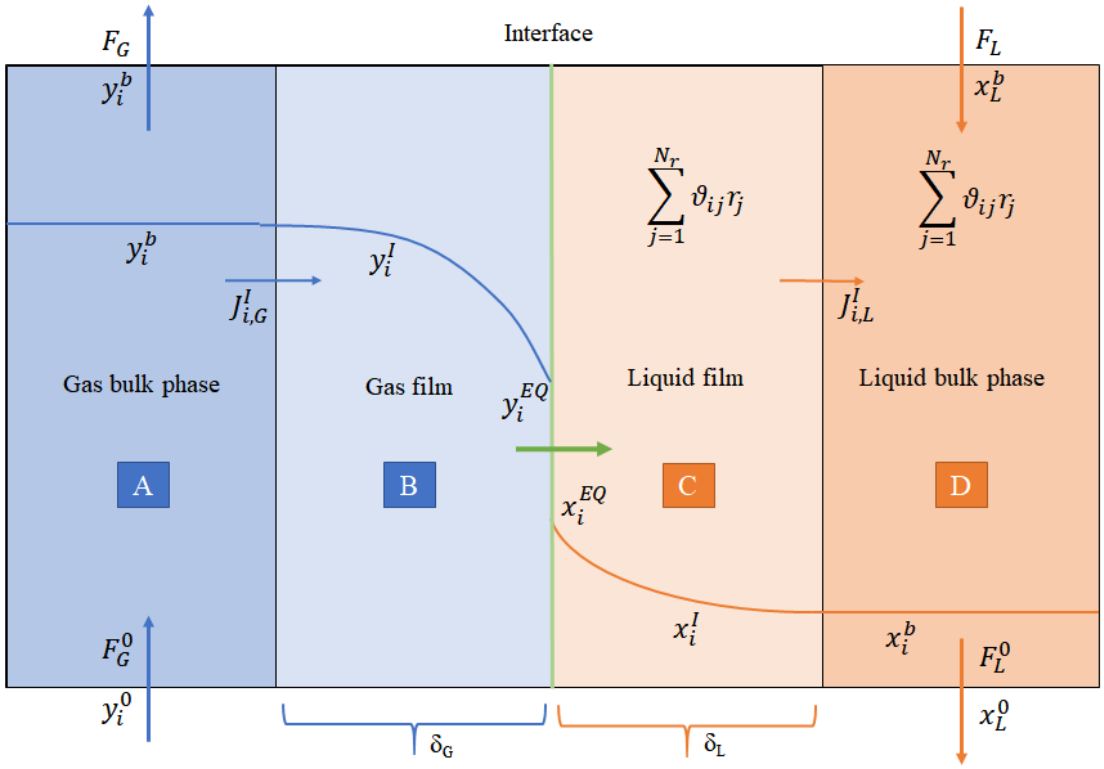

Figure 3.2: Representation of the two-film model with indication of regions for mass balance equations and molar fluxes.

- Region A mass balance:

  Gas bulk phase mole balance for the $i-th$ component:

$$\frac{\partial \left(y_i^b M_G^b\right)}{\partial t} = F_G^0 y_i^0 - F_G y_i^b + A^I J_{i,G}^I|_{\eta=\delta_G} \tag{3.1}$$

  In this equation, M_G^b represent the total moles number in the stage volume V_G, F is the molar flow and y_i is the molar fraction of the component i. Superscript 0 denotes that it refers to the inlet condition and b to the bulk phase. A_I is the interface area and J^I is the mass flux. The relation between M_G and V_G is:

$$M_G^b = V_G / v_G \tag{3.2}$$

In this equation, v_G is calculated using the gas-phase state equation.

Complementing the system of equations, pressure in the stage is equal to the inlet pressure, as shown in Equation 3.3. Also there is the constraint in molar fractions, shown in Equation 3.4.

$$P_G = P_G^0 \tag{3.3}$$

$$\sum_{i=1}^{N} y_i^b = 1 \tag{3.4}$$

- Region B mass balance:

  In the gas film, only one-dimensional molecular diffusion occur, according to the Maxwell-Stefan equations, along the film coordinate η. Mass balance in the film for the $i-th$ component:

$$\frac{\partial C_{i,G}^I}{\partial t} = -\frac{1}{\delta_G}\frac{\partial J_{i,G}^I}{\partial \eta} \tag{3.5}$$

  The Maxwell-Stefan equation is employed to calculate the molar fluxes J_i^I:

$$đ_i = \sum_{j=1}^{N} \frac{y_i^I J_{j,G}^I - y_j^I J_{i,G}^I}{C_{t,G}^I \text{Đ}_{ij}} \tag{3.6}$$

  and the driving force $đ_i$ is given by:

$$đ_i = \frac{y_i^I}{\Re T}\frac{1}{\delta_G}\frac{\partial \mu_{i,G}^I}{\partial \eta} \tag{3.7}$$

  This generates a second order partial differential equation system, which must be submitted to boundary conditions. In this case, in the bulk-phase / film boundary, there must be equality of molar concentration. In the gas / liquid interface, concentration is given by thermodynamic equilibrium:

$$
\begin{aligned}
y_i^I|_{\eta=\delta_G} &= y_i^b \\
y_i^I|_{\eta=0} &= y_i^{EQ}
\end{aligned}
\tag{3.8}
$$

The superscript EQ denote a property in thermodynamic equilibrium, which may only be calculated accounting for both gas and liquid phases fugacity as shown in Equation 3.9.

$$
\hat{f}_{i,G}^{EQ} = \hat{f}_{i,L}^{EQ} \tag{3.9}
$$

Procedure for calculation of such equilibrium will be described later in this chapter.

If the system has n components, only $n-1$ fluxes are independent, therefore, the last component flux must be calculated so that no pressure gradient is observed in the gas film:

$$
P_G^I = P_G \tag{3.10}
$$

The matrix form of the Maxwell-Stefan equation was used to calculate the $n-1$ independent molar fluxes (TAYLOR and KRISHNA, 1993):

$$
C_{t,G}^I \mathbf{đ} = -\mathbf{B} \times \mathbf{J_G^I} \tag{3.11}
$$

In this equation:

$$
\mathbf{đ} = \begin{pmatrix} đ_1 \\ đ_2 \\ \vdots \\ đ_{n-1} \end{pmatrix}_{n-1\times 1} \tag{3.12}
$$

$$\mathbf{J_G^I} = \begin{pmatrix} J_{1,G}^I \\ J_{2,G}^I \\ \vdots \\ J_{n-1,G}^I \end{pmatrix}_{n-1\times 1} \tag{3.13}$$

$$\mathbf{B} = \begin{pmatrix} B_{1,1} & B_{1,2} & \dots & B_{1,n-1} \\ B_{2,1} & B_{2,2} & \dots & B_{2,n-1} \\ \vdots & & & \vdots \\ B_{n-1,1} & B_{n-1,2} & \dots & B_{n-1,n-1} \end{pmatrix}_{n-1\times n-1} \tag{3.14}$$

With the elements of $\mathbf{B}$ being given by:

$$B_{i,i} = \frac{y_i}{\mathbf{Đ}_{in}} + \sum_{\substack{k=1 \\ i\neq k}}^{n} \frac{y_k}{\mathbf{Đ}_{i,k}} \tag{3.15}$$

$$B_{i,j} = -y_i \left(\frac{1}{\mathbf{Đ}_{i,j}} - \frac{1}{\mathbf{Đ}_{i,n}} \right) \tag{3.16}$$

- Region C mass balance:

  The liquid film mass balance is analogue to the gas film, with the addition of chemical reaction terms, represented by the stoichiometric coefficient of the j reaction for i component ϑ_{ij}, and the reaction rate r_j:

$$\frac{\partial C_{i,L}^I}{\partial t} = -\frac{1}{\delta_L}\frac{\partial J_{i,L}^I}{\partial \eta} + \sum_{j=1}^{N_r} \vartheta_{ij} r_j \tag{3.17}$$

  Fluxes are calculated through the Nernst-Planck equation:

$$J_{i,L}^I = -\frac{C_{t,L}^I D_{Li,\text{eff}}}{\delta_L}\left(\frac{\partial x_i^I}{\partial \eta} + x_i^I z_i \frac{\mathfrak{F}}{\mathfrak{R}T}\frac{\partial \varphi}{\partial \eta} \right) + x_i^I J_{n,L}^I \tag{3.18}$$

  and boundary conditions are also analogous to the gas. However, since the equilibrium boundary condition was already used in the gas film balance, another condition

must be used for consistency, i.e., guarantee the continuity through the interface. In that case, equality of molar fluxes was considered, what physically means that all molar flux that leaves the gas phase must enter the liquid phase - what explains the negative sign.

$$\begin{aligned} -J^I_{i,L}|_{\eta=0} &= J^I_{i,G}|_{\eta=0} \\ x^I_i|_{\eta=\delta_L} &= x^b_i \end{aligned} \tag{3.19}$$

- Region D mass balance:

  Liquid bulk phase mole balance is analogue, though with addition of chemical reaction term, which will account for N_r chemical reactions:

$$\frac{\partial\left(x^b_i M^b_L\right)}{\partial t} = F^0_L x^0_i - F_L x^b_i + A^I J^I_{i,L}|_{\eta=\delta_L} + V_L \sum_{j=1}^{N_r} \vartheta_{ij} r_j \tag{3.20}$$

  Similarly to the gas phase, the relation between M_L and M_L is given by the molar volume v_L, which is calculated with a empirical equation, which will be shown later.

$$M^b_L = V_L / v_L \tag{3.21}$$

  Also complemented by the constraint in the molar fractions:

$$\sum_{i=1}^{N} x^b_i = 1 \tag{3.22}$$

Next, energy balances must be performed. Figure 3.3 shows the two-film model with representations for energy fluxes, temperature concentration and the same balance regions used before.

- Region A energy balance:

  In gas bulk phase, energy balance is:

$$M^b_G C^b_{p,G} \frac{\partial T^b_G}{\partial t} = F^0_G h^0_G - F_G h^b_G + A_I q^I_G|_{\eta=\delta_G} \tag{3.23}$$

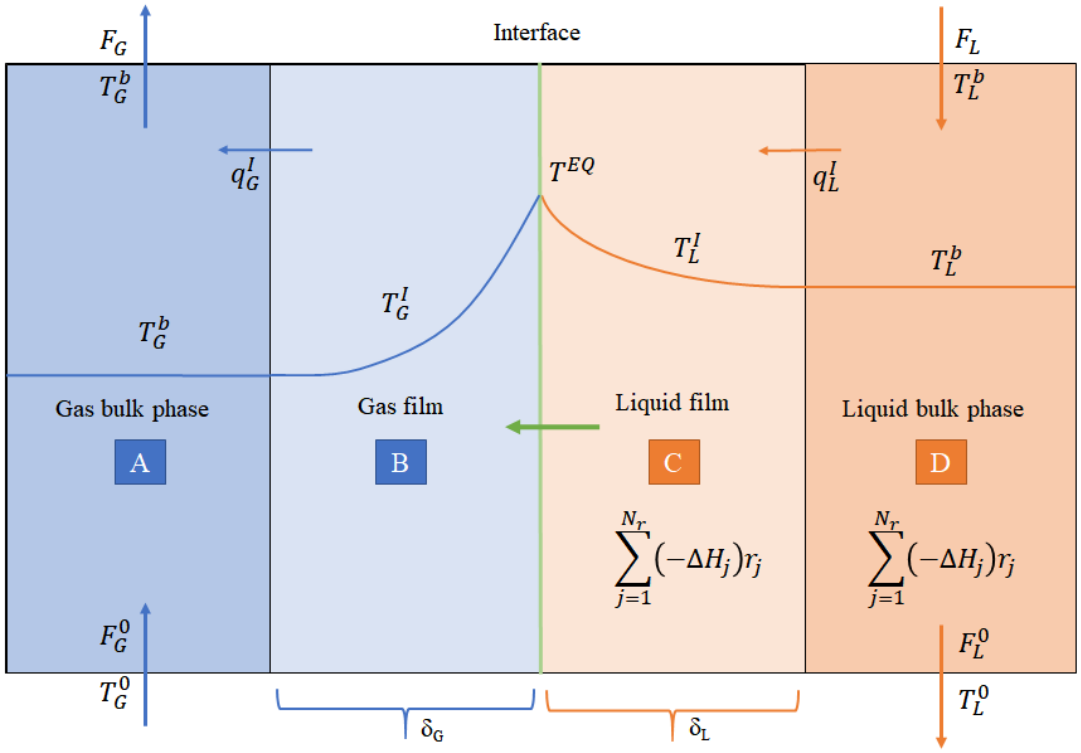

Figure 3.3: Representation of the two-film model with indication of the regions for energy balance equations and energy fluxes

- Region B energy balance:

  In gas film, there is one-dimensional heat conduction happening together with the mass transfer. Therefore energy balance in this region is:

$$\frac{\partial T_G^I}{\partial t} = -\frac{1}{C_{t,G} C_{p,G}^I \delta_G} \frac{\partial q_G^I}{\partial \eta} \tag{3.24}$$

  and the heat flux q_G^I is given by:

$$q_G^I = -\frac{\Lambda_G}{\delta_G} \frac{\partial T_G^I}{\partial \eta} + h_G^I J_{t,G}^I \tag{3.25}$$

  In this equation h is the specific enthalpy and Λ is the heat conductivity.

  Analogously to the mass balance, heat balance also yields a second order partial differential equation, which needs boundary conditions to be completed. In the bulk gas/film interface, temperature in the boundary is equal to that of the bulk. In the gas/liquid interface, temperature in both films must be equal, as in this point there

is thermodynamic equilibrium. Boundary conditions are therefore:

$$\begin{aligned} T_G^I|_{\eta=\delta_G} &= T_G^b \\ T_G^I|_{\eta=0} &= T^{EQ} = T_L^I|_{\eta=0} \end{aligned} \tag{3.26}$$

- Region C energy balance:

  The liquid film energy balance is similar to the gas film, with the addition of the heat generated by the chemical reactions:

$$\frac{\partial T_L^I}{\partial t} = -\frac{1}{C_{t,L} C_{p,L}^I \delta_L} \left(\frac{\partial q_L^I}{\partial \eta} + \delta_L \sum_{j=1}^{N_r} (-\Delta H_j)\, r_j^I \right) \tag{3.27}$$

  and the heat flux q_L^I is given by:

$$q_L^I = -\frac{\Lambda_L}{\delta_L} \frac{\partial T_L^I}{\partial \eta} + h_L^I J_{t,L}^I \tag{3.28}$$

  Boundary conditions are analogous as in mass balance. In the gas/liquid interface there is equality of heat fluxes, and in the bulk liquid / liquid film interface there is equality of temperatures.

$$\begin{aligned} -q_G^I|_{\eta=0} &= q_L^I|_{\eta=0} \\ T_L^I|_{\eta=\delta_L} &= T_L^b \end{aligned} \tag{3.29}$$

- Region D energy balance:

  Bulk liquid energy balance is given by:

$$M_L^b C_{p,L}^b \frac{\partial T_L^b}{\partial t} = F_L^0 h_L^0 - F_L h_L^b + A_I q_L^I|_{\eta=\delta_L} + V_L \sum_{j=1}^{N_r} (-\Delta H_j)\, r_j \tag{3.30}$$

The outputs of those balance equations are the composition, temperature and molar flow of each exit stream that leaves the stage. These streams will be used as inlets for the other adjacent stages balance equations.

3.1.1 Process Thermodynamics

Equation 3.9 states that the boundary condition for the gas/liquid interface is fugacity equalities. Therefore, gas and liquid fugacities must be accounted for. This section will describe the models used in that calculation, as well as how they were numerically implemented.

Since liquid phase is very complex, with ionic components and parallel chemical equations, a gamma-phi approach was used, which means that each phase was described by a different equation, as shown in Equation 2.11, which is repeated here:

$$y_i^I \hat{\phi}_i P = x_i^I \gamma_i^* H_i^{P^o} \exp\left(\frac{\bar{v_i^\infty}\left(P - P^o\right)}{\mathfrak{R}T}\right) \tag{3.31}$$

Gas phase

For gas phase, the well-known Soave-Redlich-Kwong equation of state - Equation 3.32 - was applied, and all thermodynamic properties are derived therefrom.

$$P = \frac{\mathfrak{R}T}{v - b} - \frac{a}{v\left(v + b\right) + v\left(v - b\right)} \tag{3.32}$$

In which:

$$a = \frac{0.45724\mathfrak{R}^2 T_c^2}{P_c}\left[1 + m\left(1 - \sqrt{T_r}\right)\right]^2 \tag{3.33}$$

$$m = 0.37464 + 1.5422\omega - 0.26992\omega^2 \tag{3.34}$$

$$b = \frac{0.0778\mathfrak{R}T_c}{P_c} \tag{3.35}$$

Fugacity coefficient can be, therefore, determined using the Equation of State as shown in Equation 3.36.

$$\ln \phi_{i,G} = \int_0^P \left(\frac{v_{i,G}}{\Re T} - \frac{1}{P} \right) dP \tag{3.36}$$

Liquid phase

The MEA-CO_2-Water system may be described by the set of Equations 3.37 to 3.41. Expressions for calculation of this chemical equilibrium constant as a function of temperature were taken from AUSTGEN *et al.* (1989), and are shown in Table 3.1.

$$2\,H_2O \rightleftharpoons H_3O^+ + OH^- \tag{3.37}$$

$$CO_2 + 2\,H_2O \rightleftharpoons H_3O^+ + HCO_3^- \tag{3.38}$$

$$HCO_3^- + H_2O \rightleftharpoons H_3O^+ + CO_3^{2-} \tag{3.39}$$

$$MEAH_2^+ + H_2O \rightleftharpoons H_3O^+ + MEAH \tag{3.40}$$

$$MEACOO^- + H_2O \rightleftharpoons HCO_3^- + MEAH \tag{3.41}$$

Table 3.1: Temperature dependence of equilibrium constants for reactions, $\ln K = C_1 + C_2/T + C_3 \ln T + C_4 T$ (AUSTGEN *et al.*, 1989)

Reaction	C_1	C_2(K)	C_3	C_4(K^{-1})
3.37	132.899	-13445.9	-22.4773	0
3.38	231.465	-12092.1	-36.7816	0
3.39	216.049	-12.431.7	-35.4819	0
3.40	2.1211	-8189.38	0	-0.007484
3.41	2.8898	-3635.09	0	0

The system has, therefore, nine reactive species, of which three are molecular, four are anionic and two are cationic. The system, however, is not at the chemical equilibrium. According to KUCKA *et al.* (2003b) reaction represented by Equation 3.42 is kinetically controlled.

$$CO_2 + MEAH + H_2O \rightleftharpoons MEACOO^- + H_3O^+ \tag{3.42}$$

Equations 3.37 to 3.41 were modified to fully describe the system considering the kinetically controlled reaction and also provide better numeric stability, and are shown in the following equations:

$$HCO_3^- \rightleftharpoons CO_2 + OH^- \tag{3.43}$$

$$HCO_3^- + H_2O \rightleftharpoons H_3O^+ + CO_3^{2-} \tag{3.44}$$

$$MEAH_2^+ + H_2O \rightleftharpoons MEAH + H_3O^+ \tag{3.45}$$

$$HCO_3^- + MEAH \rightleftharpoons MEACOO^- + H_2O \tag{3.46}$$

In order to certify if the reactions in Equations 3.42 to 3.46 fully describe this system, the corresponding stoichiometric coefficients were organized in a matrix, which was reduced to its echelon form to verify if all lines are linearly independent. Results are shown in Equation 3.47.

$$\boldsymbol{\vartheta} = \begin{bmatrix} -1 & -1 & -1 & 0 & 1 & 0 & 0 & 1 & 0 \\ 1 & 0 & 0 & 1 & 0 & -1 & 0 & 0 & 0 \\ 0 & -1 & 0 & 0 & 0 & -1 & 1 & 1 & 0 \\ 0 & -1 & 1 & 0 & 0 & 0 & 0 & 1 & -1 \\ 0 & 1 & -1 & 0 & 1 & -1 & 0 & 0 & 0 \end{bmatrix}$$

$$\rightarrow \boldsymbol{\vartheta} = \begin{bmatrix} -1 & -1 & -1 & 0 & 1 & 0 & 0 & 1 & 0 \\ 0 & -1 & -1 & 1 & 1 & -1 & 0 & 1 & 0 \\ 0 & 0 & 2 & -1 & -1 & 1 & 0 & 0 & 1 \\ 0 & 0 & 0 & -0.5 & -0.5 & -0.5 & 1 & 0 & 0.5 \\ 0 & 0 & 0 & 0 & 1 & -1 & 0 & 1 & -1 \end{bmatrix} \tag{3.47}$$

The linearly independent reactions were named as shown in Table 3.2.

Table 3.2: Chemical reactions considered in the aqueous CO_2/MEA system

Name	**Reaction**	**Type**
R1	$CO_2 + MEAH + H_2O \rightleftharpoons MEACOO^- + H_3O^+$	Kinetically controlled
R2	$HCO_3^- \rightleftharpoons CO_2 + OH^-$	Instantaneous
R3	$HCO_3^- + H_2O \rightleftharpoons H_3O^+ + CO_3^{2-}$	Instantaneous
R4	$MEAH_2^+ + H_2O \rightleftharpoons MEAH + H_3O^+$	Instantaneous
R5	$HCO_3^- + MEAH \rightleftharpoons MEACOO^- + H_2O$	Instantaneous

Since all reactions are reversible, an equilibrium constant is considered for each reac-

tion, based on activities:

$$\begin{aligned} K_j &= \prod_i a_i^{\vartheta_{ij}} \\ a_i &= x_i \gamma_i \end{aligned} \tag{3.48}$$

Kinetically controlled reaction R1 must consider forward and reverse reaction rates directly. The forward constants were experimentally determined in a concentration base by KUCKA *et al.* (2003a) and is shown in Equation 3.49.

$$k^c_{R1,for} = 4.495 \times 10^{11} \exp\left(\frac{-44940}{\Re T}\frac{\text{kJ}}{\text{kmol}}\right)\frac{\text{m}^3}{\text{kmol s}} \tag{3.49}$$

Reverse reaction rate is then calculated using Equation 3.50. However, since both forward constants were experimentally determined in a concentration base, they must be converted to an activity base before calculation of the reverse constant, as shown in Equation 3.51, in which the index e represent only the reactants of the reaction.

$$K_j = \frac{k_{j,rev}}{k_{j,for}} \tag{3.50}$$

$$k_{j,for} = k^c_{j,for}\frac{C_t^{\sum_e \vartheta_{e,j}}}{\prod_e \gamma_e^{\vartheta_{e,j}}} \tag{3.51}$$

Finally, with both forward and reverse reaction constants, reaction rate - r_j - can be directly calculated and incorporated to a component mass balance, according to Equation 3.52, in which e denotes reactants and p products.

$$r_j = k_{j,for}\prod_e (x_e\gamma_e)^{\vartheta_{e,j}} - k_{j,rev}\prod_p (x_p\gamma_p)^{\vartheta_{p,j}} \tag{3.52}$$

To account for chemical reactions that are instantaneous, i.e. in equilibrium, a new variable is defined, the reaction degree of advancement - ξ - which is expressed in mol/s. It is an extensive independent variable that denotes the extension with which reactants have turned into products. This variables must be incorporated to each component mass balance and solved so that equilibrium relation represented by Equation 3.48 are satisfied. As an example, bulk liquid mole balance equation, whose simplified form was shown in previous section in Equation 3.20, becomes:

$$\frac{\partial\left(x_i^b M_L^b\right)}{\partial t} = F_L^0 x_i^0 - F_L x_i^b + A^I J_{i,L}^I|_{\eta=\delta_L} + V_L \sum_{j=1}^{N_r} \vartheta_{ij} r_j + \sum_{j=1}^{N_{req}} \vartheta_{ij} \xi_j \tag{3.53}$$

In liquid bulk phase, as well as each discrete liquid film volume, mass balance must be complimented with both reaction terms and solved together, so that equilibrium relations are regarded.

Detailed procedure for the calculation of activity coefficients will be given in the next section.

Activity coefficient Calculation

The activity coefficient can be obtained by the derivative of the excess Gibbs energy with respect to the mole number, as shown in Equation 3.54.

$$\ln \gamma_i = \left[\frac{\partial\left(n_t g^{ex*}/\Re T\right)}{\partial n_i}\right]_{T,P,n_{j\neq i}} \tag{3.54}$$

Since the excess Gibbs energy is a sum of three contributions, as shown in Equation 2.33, the activity coefficient will be the sum of the derivatives of each contribution: the Pitzer Debye-Hückel long-range ion-ion contribution, the Born contribution and the NRTL short-range contribution. Therefore, taking the derivative in Equation 2.33, yields:

$$\begin{aligned} \ln \gamma_i &= \left[\frac{\partial\left(n_t g^{ex*}/\Re T\right)}{\partial n_i}\right] \\ &= \left[\frac{\partial\left(n_t g_{PDH}^{ex*}/\Re T\right)}{\partial n_i}\right] + \left[\frac{\partial\left(n_t g_{BORN}^{ex*}/\Re T\right)}{\partial n_i}\right] + \left[\frac{\partial\left(n_t g_{NRTL}^{ex*}/\Re T\right)}{\partial n_i}\right] \\ &= \ln \gamma_{i,PDH} + \ln \gamma_{i,BORN} + \ln \gamma_{i,NRTL} \end{aligned} \tag{3.55}$$

The first term, the Pitzer Debye-Hückel contribution, is obtained by derivation from Equation 2.12 and the result is shown in Equation 3.56.

$$\ln\left(\gamma_{i,PDH}\right) = -A_\phi \left\{ \left(\frac{2Z_i^2}{\rho}\right) \ln\left(1+\rho I_x^{1/2}\right) + \left(\frac{z_i^2 I_x^{1/2} - 2I_x^{3/2}}{1+\rho I_x^{1/2}}\right) \right\} \tag{3.56}$$

The parameter ρ is called distance of closest approach, A_ϕ is the Debye-Hückel constant for osmotic coefficient and I_x is the ionic strength in mole fraction scale.

The distance of closest approach was fixed at 14.9 suggested by PITZER (1980) and followed by AUSTGEN *et al.* (1989). The mixed solvent dielectric constant was calculated using a simple mass fraction average mixing rule (AUSTGEN *et al.*, 1989). Values for the dielectric constant for pure MEA was taken from published work of IKADA *et al.* (1969), and for water was taken from ARCHER and WANG (1989). Both were considered temperature dependent.

The second term, the Born contribution, is obtained by derivation of Equation 2.32, and is shown in Equation 3.57. The subscripts w and s refer, respectively, to water and the mixed solvent.

$$\ln \gamma_{i,BORN} = \left(\frac{e^2}{2\kappa T}\right)\left(\frac{1}{\lambda_s} - \frac{1}{\lambda_w}\right)\left(\frac{z_i^2}{r_i}\right) \tag{3.57}$$

The last term, the NRTL contribution, will be distinct depending on the nature of the component - whether it is molecular, cation or anion. The result of derivation of Equation 2.18 is reproduced from CHEN and EVANS (1986) in Equation 3.58 for molecular species, Equation 3.59 for anions and Equation 3.60 for cations.

$$\begin{aligned}
\ln \gamma_{m,NRTL} = & \frac{\sum_j X_j G_{jm}\tau_{jm}}{\sum_k X_k G_{km}} \\
& + \sum_{m'} \frac{X_{m'} G_{mm'}}{\sum_k G_{km'}} \left(\tau_{mm'} - \frac{\sum_k X_k G_{km'}\tau_{km'}}{\sum_k X_k G_{km'}}\right) \\
& + \sum_c X_c \sum_{a'} \frac{X_{a'}}{\sum_{a"} X_{a"}} \frac{G_{mc,a'c}}{\sum_k X_k G_{kc,a'c}} \left(\tau_{mc,a'c} - \frac{\sum_k X_k G_{kc,a'c}\tau_{kc,a'c}}{\sum_k X_k G_{kc,a'c}}\right) \\
& + \sum_a X_a \sum_{c'} \frac{X_{c'}}{\sum_{c"} X_{c"}} \frac{G_{ma,c'a}}{\sum_k X_k G_{ka,c'a}} \left(\tau_{ma,c'a} - \frac{\sum_k X_k G_{ka,c'a}\tau_{ka,c'a}}{\sum_k X_k G_{ka,c'a}}\right)
\end{aligned} \tag{3.58}$$

$$\begin{aligned}
\ln \gamma_{a,NRTL} = & \sum_{c'} \frac{X_{c'}}{\sum_{c"} X_{c"}} \frac{\sum_k X_k G_{ka,c'a}\tau_{ka,c'a}}{\sum_k X_k G_{ka,c'a}} \\
& + \sum_m \frac{X_m G_{am}}{\sum_k X_k G_{km}} \left(\tau_{am} - \frac{\sum_k X_k G_{km}\tau_{km}}{\sum_k X_k G_{km}}\right) \\
& + \sum_c X_c \sum_{a'} \frac{X_{a'}}{\sum_{a"} X_{a"}} \frac{G_{ac,a'c}}{\sum_k X_k G_{kc,a'c}} \left(\tau_{ac,a'c} - \frac{\sum_k X_k G_{kc,a'c}\tau_{kc,a'c}}{\sum_k X_k G_{kc,a'c}}\right)
\end{aligned} \tag{3.59}$$

$$\frac{1}{Z_c}\ln\gamma_{c,NRTL} = \sum_{a'}\frac{X_{a'}}{\sum_{a"}X_{a"}}\frac{\sum_k X_k G_{kc,a'c}\tau_{kc,a'c}}{\sum_k X_k G_{kc,a'c}} + \sum_m \frac{X_m G_{cm}}{\sum_k X_k G_{km}}\left(\tau_{cm} - \frac{\sum_k X_k G_{km}\tau_{km}}{\sum_k X_k G_{km}}\right) + \sum_a X_a \sum_{c'}\frac{X_{c'}}{\sum_{c"}X_{c"}}\frac{G_{ca,c'a}}{\sum_k X_k G_{ka,c'a}}\left(\tau_{ca,c'a} - \frac{\sum_k X_k G_{ka,c'a}\tau_{ka,c'a}}{\sum_k X_k G_{ka,c'a}}\right) \tag{3.60}$$

The nonrandomness factors were fixed at values recommended for water (CHEN and EVANS, 1986) and alkanolamine (MOCK *et al.*, 1986). Therefore, the only adjustable parameters of the e-NRTL model are the short-range binary interaction parameters.

The work AUSTGEN *et al.* (1989) used a number of experimental VLE data to fit the main parameters needed. However, not all parameters have statistical significance when fitted to experimental data, and were, therefore, set to default values. Table 3.3 summarizes the values used in the model. The parameters were temperature dependent according to Equation 3.61.

$$\tau = a + \frac{b}{T} \tag{3.61}$$

Besides, in the values shown in Table 3.3, the authors set to zero all ion pair-ion pair interaction parameters.

The nonrandomness factor was fixed at 0.2 for molecule-molecule interactions, and for water-ion pair, ion pair-water interactions. For alkanolamine-ion pair and acid gas-ion pair interactions, this value was fixed at 0.1, following the work of AUSTGEN *et al.* (1989).

At last, the activity coefficient found with the previous equations must be normalized in order to refer to the proper infinitely diluted reference state, as already shown in Equation 2.31. The unsymmetrical activity coefficient is, therefore, given by Equation 3.62.

$$\gamma^*_{i,NRTL} = \frac{\gamma_{i,NRTL}}{\gamma_i^\infty},\ i = \text{solute} \tag{3.62}$$

The infinitely diluted activity coefficient are calculated by taking the proper limits from

Table 3.3: Energy parameters fitted by AUSTGEN *et al.* (1989). The values with * indicate that non-statistical significance was observed and, therefore, default value was used. When applied, T is given in Kelvin.

$\tau_{mm'}$

	CO_2	H_2O	MEAH
CO_2	0	$10.064 - 3268.14/T$	0*
H_2O	$10.064 - 3268,14/T$	0	1.674
MEAH	0*	$0 - 649.75/T$	0

$\tau_{ca,m}$

	CO_2	H_2O	MEAH
H_3O^+,OH^-	−8*	−4*	−8*
H_3O^+,$MEACOO^-$	−8*	−4*	−8*
H_3O^+,HCO_3^-	−8*	−4*	−8*
H_3O^+,CO_3^{2-}	−8*	−4*	−8*
$MEAH_2^+$,OH^-	−8*	−4*	−8*
$MEAH_2^+$,$MEACOO^-$	−8*	−5.098	−8*
$MEAH_2^+$,HCO_3^-	−8*	−4.088	−8*
$MEAH_2^+$,CO_3^{2-}	−8*	−4*	−8*

$\tau_{m,ca}$

	CO_2	H_2O	MEAH
H_3O^+,OH^-	15*	8*	15*
H_3O^+,$MEACOO^-$	15*	8*	15*
H_3O^+,HCO_3^-	15*	8*	15*
H_3O^+,CO_3^{2-}	15*	8*	15*
$MEAH_2^+$,OH^-	15*	8*	15*
$MEAH_2^+$,$MEACOO^-$	15*	10.268	15*
$MEAH_2^+$,HCO_3^-	15*	$4.55 + 1218.19/T$	15*
$MEAH_2^+$,CO_3^{2-}	15*	8*	15*

Equations 3.58, 3.59 and 3.60, yielding the results shown in Equation 3.63.

$$\begin{aligned}
\ln \gamma^{\infty}_{m,NRTL} &= \tau_{wm} \\
\ln \gamma^{\infty}_{c,NRTL} &= \sum_{a} \frac{X_a \tau_{wc,ac}}{\sum_{a'} X_a} + G_{cw}\tau_{cw} \\
\ln \gamma^{\infty}_{a,NRTL} &= \sum_{c} \frac{X_c \tau_{wa,ca}}{\sum_{c'} X_c} + G_{aw}\tau_{aw}
\end{aligned} \tag{3.63}$$

The implementation of the previous equations was made in a matrix form. Therefore, the following vectors, matrices and tensors were defined.

$$\boldsymbol{X_M} = \begin{pmatrix} X_{M_1} \\ \vdots \\ X_{M_m} \end{pmatrix}_{m\times 1} \tag{3.64}$$

$$\boldsymbol{X_A} = \begin{pmatrix} X_{A_1} \\ \vdots \\ X_{A_a} \end{pmatrix}_{a\times 1} \tag{3.65}$$

$$\boldsymbol{X_C} = \begin{pmatrix} X_{C_1} \\ \vdots \\ X_{C_c} \end{pmatrix}_{c\times 1} \tag{3.66}$$

$$\boldsymbol{T_{MM'}} = \begin{pmatrix} \tau_{M_1M_1} & \cdots & \tau_{M_1M_m} \\ \vdots & \ddots & \vdots \\ \tau_{M_mM_1} & \cdots & \tau_{M_mM_m} \end{pmatrix}_{m\times m} \tag{3.67}$$

$$\boldsymbol{A_{MM'}} = \begin{pmatrix} \alpha_{M_1M_1} & \cdots & \alpha_{M_1M_m} \\ \vdots & \ddots & \vdots \\ \alpha_{M_mM_1} & \cdots & \alpha_{M_mM_m} \end{pmatrix}_{m\times m} \tag{3.68}$$

$$\boldsymbol{T_{CA,M}} = \begin{pmatrix} \tau_{C_1A_1,M_*} & \cdots & \tau_{C_1A_a,M_*} \\ \vdots & \ddots & \vdots \\ \tau_{C_cA_1,M_*} & \cdots & \tau_{C_cA_a,M_*} \end{pmatrix}_{c\times a\times m} \quad M_* = M_1, \cdots, M_m \tag{3.69}$$

$$\boldsymbol{A_{CA,M}} = \begin{pmatrix} \alpha_{C_1A_1,M_*} & \cdots & \alpha_{C_1A_a,M_*} \\ \vdots & \ddots & \vdots \\ \alpha_{C_cA_1,M_*} & \cdots & \alpha_{C_cA_a,M_*} \end{pmatrix}_{c\times a\times m} \quad M_* = M_1, \cdots, M_m \tag{3.70}$$

$$\boldsymbol{T_{M,CA}} = \begin{pmatrix} \tau_{M_*,C_1A_1} & \cdots & \tau_{M_*,C_1A_a} \\ \vdots & \ddots & \vdots \\ \tau_{M_*,C_cA_1} & \cdots & \tau_{M_*,C_cA_a} \end{pmatrix}_{c\times a\times m} \quad M_* = M_1, \cdots, M_m \tag{3.71}$$

$$\boldsymbol{T_{CA,C'A}} = \begin{pmatrix} \tau_{C_1A_1,C'_*A_1} & \cdots & \tau_{C_1A_a,C'_*A_a} \\ \vdots & \ddots & \vdots \\ \tau_{C_cA_1,C'_*A_1} & \cdots & \tau_{C_cA_a,C'_*A_a} \end{pmatrix}_{c\times a\times c} \quad C_* = C_1, \cdots, C_c \tag{3.72}$$

$$\boldsymbol{A_{CA,C'A}} = \begin{pmatrix} \alpha_{C_1A_1,C'_*A_1} & \cdots & \alpha_{C_1A_a,C'_*A_a} \\ \vdots & \ddots & \vdots \\ \alpha_{C_cA_1,C'_*A_1} & \cdots & \alpha_{C_cA_a,C'_*A_a} \end{pmatrix}_{c\times a\times c} \quad C_* = C_1, \cdots, C_c \tag{3.73}$$

$$\boldsymbol{T_{AC,A'C}} = \begin{pmatrix} \tau_{A_1C_1,A'_*C_1} & \cdots & \tau_{A_1C_c,A'_*C_c} \\ \vdots & \ddots & \vdots \\ \tau_{A_aC_1,A'_*C_1} & \cdots & \tau_{A_aC_c,A'_*C_c} \end{pmatrix}_{c\times a\times c} \quad A_* = A_1, \cdots, A_a \tag{3.74}$$

$$\boldsymbol{A_{AC,A'C}} = \begin{pmatrix} \alpha_{A_1C_1,A'_*C_1} & \cdots & \alpha_{A_1C_c,A'_*C_c} \\ \vdots & \ddots & \vdots \\ \alpha_{A_aC_1,A'_*C_1} & \cdots & \alpha_{A_aC_c,A'_*C_c} \end{pmatrix}_{c\times a\times c} \quad A_* = A_1, \cdots, A_a \tag{3.75}$$

The previous variables contain all the adjustable e-NRTL model parameters, as previously stated. Therefore, the next variables are obtained with relations shown in Equations 2.19 to 2.30.

$$\boldsymbol{G_{MM'}} = \begin{pmatrix} \exp\left(-\alpha_{M_1M_1}\tau_{M_1M_1}\right) & \cdots & \exp\left(-\alpha_{M_1M_m}\tau_{M_1M_m}\right) \\ \vdots & \ddots & \vdots \\ \exp\left(-\alpha_{M_mM_1}\tau_{M_mM_1}\right) & \cdots & \exp\left(-\alpha_{M_mM_m}\tau_{M_mM_m}\right) \end{pmatrix}_{m\times m} \tag{3.76}$$

The operation made in Equation 3.76 will henceforth be written as shown in Equation 3.77, in which the operator $\odot$ was created for sake of simplification.

$$\boldsymbol{G_{MM'}} = \exp\left(-\boldsymbol{A_{MM'}} \odot \boldsymbol{T_{MM'}}\right) \tag{3.77}$$

$$\boldsymbol{G_{CA,M}} = \exp\left(-\boldsymbol{A_{CA,M}} \odot \boldsymbol{T_{CA,M}}\right)_{c\times a\times m} \tag{3.78}$$

$$\boldsymbol{G_{C^*M}} = \left(\frac{\boldsymbol{X'_A} \times \boldsymbol{G_{C^*A,M}}}{\sum_{i=1}^{a}\left(X_{A_i}\right)}\right)_{c\times m} C^* = C_1, \cdots, C_c \tag{3.79}$$

$$\boldsymbol{G_{A^*M}} = \left(\frac{\boldsymbol{X'_C} \times \boldsymbol{G_{CA^*,M}}}{\sum_{i=1}^{c}\left(X_{C_i}\right)}\right)_{a\times m} \tag{3.80}$$

$$\boldsymbol{A_{C^*M}} = \left(\frac{\boldsymbol{X_A^T} \times \boldsymbol{A_{C^*A,M}}}{\sum_{i=1}^{a}\left(X_{A_i}\right)}\right)_{c\times m} \tag{3.81}$$

$$\boldsymbol{A_{A^*M}} = \left(\frac{\boldsymbol{X_C^T} \times \boldsymbol{A_{CA^*,M}}}{\sum_{i=1}^{c}\left(X_{C_i}\right)}\right)_{a\times m} \tag{3.82}$$

$$\boldsymbol{G_{CM}} = \exp\left(-\boldsymbol{A_{CM}} \odot \boldsymbol{T_{CM}}\right)_{c\times m} \text{ used to find } \boldsymbol{T_{CM}} \tag{3.83}$$

$$\boldsymbol{G_{AM}} = \exp\left(-\boldsymbol{A_{AM}} \odot \boldsymbol{T_{AM}}\right)_{a\times m} \text{ used to find } \boldsymbol{T_{AM}} \tag{3.84}$$

$$\boldsymbol{T_{MA,C^*A}} = (\boldsymbol{T_{AM}} - \boldsymbol{T_{C^*A,M}} + \boldsymbol{T_{M,C^*A}})_{m\times a\times c} \tag{3.85}$$

$$\boldsymbol{T_{MC,A^*C}} = (\boldsymbol{T_{CM}} - \boldsymbol{T_{CA^*,M}} + \boldsymbol{T_{M,CA^*}})_{m\times c\times a} \tag{3.86}$$

$$\boldsymbol{G_{CA,C'A}} = \exp\left(-\boldsymbol{A_{CA,C'A}} \odot \boldsymbol{T_{CA,C'A}}\right)_{c\times a\times c} \tag{3.87}$$

$$\boldsymbol{G_{AC,A'C}} = \exp\left(-\boldsymbol{A_{AC,A'C}} \odot \boldsymbol{T_{AC,A'C}}\right)_{a\times c\times a} \tag{3.88}$$

$$\boldsymbol{G_{MA,CA}} = \exp\left(-\boldsymbol{A_{MA,CA}} \odot \boldsymbol{T_{MA,CA}}\right)_{m\times a\times c} \tag{3.89}$$

$$\boldsymbol{G_{MC,AC}} = \exp\left(-\boldsymbol{A_{MC,AC}} \odot \boldsymbol{T_{MC,AC}}\right)_{m\times a\times c} \tag{3.90}$$

$$\boldsymbol{A_{MA,C^*A}} = \left(\boldsymbol{A_{AM}^T}\right)_{m\times a\times c} C^* = C_1, \cdots, C_c \tag{3.91}$$

$$\boldsymbol{A_{MC,A^*C}} = \left(\boldsymbol{A_{CM}^T}\right)_{m\times c\times a} A^* = A_1, \cdots, A_a \tag{3.92}$$

Equations 3.58, 3.59 and 3.60 can be rewritten in terms of the previously defined matrices, as shown in Equations 3.93, 3.94 and 3.95

$$
\begin{aligned}
&\ln \gamma_{M_i,NRTL} = \\
&\left\{ \frac{\boldsymbol{H^T_{MM'_i}} \times \boldsymbol{X_M} + \boldsymbol{H^T_{AM_i}} \times \boldsymbol{X_A} + \boldsymbol{H^T_{CM_i}} \times \boldsymbol{X_C}}{\boldsymbol{G^T_{MM'_i}} \times \boldsymbol{X_M} + \boldsymbol{G^T_{AM_i}} \times \boldsymbol{X_A} + \boldsymbol{G^T_{CM_i}} \times \boldsymbol{X_C}} \right\} \\
&+ \left\{ \left[\frac{\boldsymbol{G_{M_iM'}}}{\left(\boldsymbol{G^T_{MM'}} \times \boldsymbol{X_M} + \boldsymbol{G^T_{AM}} \times \boldsymbol{X_A} + \boldsymbol{G^T_{CM}} \times \boldsymbol{X_C}\right)^T} \right] \right. \\
&\left. * \left[\boldsymbol{T_{M_iM'}} - \frac{\left(\boldsymbol{H^T_{MM'}} \times \boldsymbol{X_M} + \boldsymbol{H^T_{AM}} \times \boldsymbol{X_A} + \boldsymbol{H^T_{CM}} \times \boldsymbol{X_C}\right)^T}{\left(\boldsymbol{G^T_{MM'}} \times \boldsymbol{X_M} + \boldsymbol{G^T_{AM}} \times \boldsymbol{X_A} + \boldsymbol{G^T_{CM}} \times \boldsymbol{X_C}\right)^T} \right] \right\} \\
&\qquad \times \boldsymbol{X_M} \\
&+ \left\{ \left[\frac{\boldsymbol{G_{M_iC,AC}}}{\left(\boldsymbol{G^T_{MC,AC}} \times \boldsymbol{X_M} + \boldsymbol{G^T_{AC,A'C}} \times \boldsymbol{X_A} + \boldsymbol{G^T_{C'C,AC}} \times \boldsymbol{X_C}\right)^T} \right] \right. \\
&\left. * \left[\boldsymbol{T_{M_iC,AC}} - \frac{\left(\boldsymbol{H^T_{MC,AC}} \times \boldsymbol{X_M} + \boldsymbol{H^T_{AC,A'C}} \times \boldsymbol{X_A} + \boldsymbol{H^T_{C'C,AC}} \times \boldsymbol{X_C}\right)^T}{\left(\boldsymbol{G^T_{MC,AC}} \times \boldsymbol{X_M} + \boldsymbol{G^T_{AC,A'C}} \times \boldsymbol{X_A} + \boldsymbol{G^T_{C'C,AC}} \times \boldsymbol{X_C}\right)^T} \right] \right\} \\
&\qquad \times \frac{\boldsymbol{X_A}}{sum\boldsymbol{X_A}} \times \boldsymbol{X_C} \\
&+ \left\{ \left[\frac{\boldsymbol{G_{M_iA,CA}}}{\left(\boldsymbol{G^T_{MA,CA}} \times \boldsymbol{X_M} + \boldsymbol{G^T_{A'A,CA}} \times \boldsymbol{X_A} + \boldsymbol{G^T_{CA,C'A}} \times \boldsymbol{X_C}\right)^T} \right] \right. \\
&\left. * \left[\boldsymbol{T_{M_iA,CA}} - \frac{\left(\boldsymbol{H^T_{MA,CA}} \times \boldsymbol{X_M} + \boldsymbol{H^T_{A'A,CA}} \times \boldsymbol{X_A} + \boldsymbol{H^T_{CA,C'A}} \times \boldsymbol{X_C}\right)^T}{\left(\boldsymbol{G^T_{MA,CA}} \times \boldsymbol{X_M} + \boldsymbol{G^T_{A'A,CA}} \times \boldsymbol{X_A} + \boldsymbol{G^T_{CA,C'A}} \times \boldsymbol{X_C}\right)^T} \right] \right\} \\
&\qquad \times \frac{\boldsymbol{X_C}}{\sum_{j=1}^{c} X_{C_j}} \times \boldsymbol{X_A}
\end{aligned}
\tag{3.93}
$$

$$\frac{1}{Z_{A_i}} \ln \gamma_{A_i,NRTL} =$$

$$\left\{ \frac{\boldsymbol{H^T_{MA'_i,CA_i}} \times \boldsymbol{X_M} + \boldsymbol{H^T_{A'A_i,CA_i}} \times \boldsymbol{X_A} + \boldsymbol{H^T_{CA_i,C'A_i}} \times \boldsymbol{X_C}}{\boldsymbol{G^T_{MA'_i,CA_i}} \times \boldsymbol{X_M} + \boldsymbol{G^T_{A'A_i,CA_i}} \times \boldsymbol{X_A} + \boldsymbol{G^T_{CA_i,C'A_i}} \times \boldsymbol{X_C}} \right\} \times \frac{\boldsymbol{X_C}}{\sum_{j=1}^{c} X_{C_j}}$$

$$+ \left\{ \left[\frac{\boldsymbol{G_{A_iM}}}{\left(\boldsymbol{G^T_{MM'}} \times \boldsymbol{X_M} + \boldsymbol{G^T_{AM}} \times \boldsymbol{X_A} + \boldsymbol{G^T_{CM}} \times \boldsymbol{X_C}\right)^T} \right] * \left[\boldsymbol{T_{A_iM}} - \frac{\left(\boldsymbol{H^T_{MM'}} \times \boldsymbol{X_M} + \boldsymbol{H^T_{AM}} \times \boldsymbol{X_A} + \boldsymbol{H^T_{CM}} \times \boldsymbol{X_C}\right)^T}{\left(\boldsymbol{G^T_{MM'}} \times \boldsymbol{X_M} + \boldsymbol{G^T_{AM}} \times \boldsymbol{X_A} + \boldsymbol{G^T_{CM}} \times \boldsymbol{X_C}\right)^T} \right] \right\} \times \boldsymbol{X_M}$$

$$+ \left\{ \left[\frac{\boldsymbol{G_{A_iC,A'C}}}{\left(\boldsymbol{G^T_{MC,AC}} \times \boldsymbol{X_M} + \boldsymbol{G^T_{AC,A'C}} \times \boldsymbol{X_A} + \boldsymbol{G^T_{C'C,AC}} \times \boldsymbol{X_C}\right)^T} \right] * \left[\boldsymbol{T_{A_iC,A'C}} - \frac{\left(\boldsymbol{H^T_{MC,AC}} \times \boldsymbol{X_M} + \boldsymbol{H^T_{AC,A'C}} \times \boldsymbol{X_A} + \boldsymbol{H^T_{C'C,AC}} \times \boldsymbol{X_C}\right)^T}{\left(\boldsymbol{G^T_{MC,AC}} \times \boldsymbol{X_M} + \boldsymbol{G^T_{AC,A'C}} \times \boldsymbol{X_A} + \boldsymbol{G^T_{C'C,AC}} \times \boldsymbol{X_C}\right)^T} \right] \right\} \times \frac{\boldsymbol{X_A}}{\sum_{j=1}^{a} X_{A_j}} \times \boldsymbol{X_C}$$

(3.94)

$$
\begin{aligned}
&\frac{1}{Z_{C_i}} \ln \gamma_{C_i,NRTL} = \\
&\left\{ \frac{\boldsymbol{H^T_{MC_i,AC_i}} \times \boldsymbol{X_M} + \boldsymbol{H^T_{AC_i,A'C_i}} \times \boldsymbol{X_A} + \boldsymbol{H^T_{C'C_i,AC_i}} \times \boldsymbol{X_C}}{\boldsymbol{G^T_{MC_i,AC_i}} \times \boldsymbol{X_M} + \boldsymbol{G^T_{AC_i,A'C_i}} \times \boldsymbol{X_A} + \boldsymbol{G^T_{C'C_i,AC}} \times \boldsymbol{X_C}} \right\} \\
&\qquad \times \frac{\boldsymbol{X_A}}{\sum_{j=1}^{a} X_{A_j}} \\
&+ \left\{ \left[\frac{\boldsymbol{G_{C_iM}}}{\left(\boldsymbol{G^T_{MM'}} \times \boldsymbol{X_M} + \boldsymbol{G^T_{AM}} \times \boldsymbol{X_A} + \boldsymbol{G^T_{CM}} \times \boldsymbol{X_C}\right)^T} \right] \right. \\
&* \left. \left[\boldsymbol{T_{C_iM}} - \frac{\left(\boldsymbol{H^T_{MM'}} \times \boldsymbol{X_M} + \boldsymbol{H^T_{AM}} \times \boldsymbol{X_A} + \boldsymbol{H^T_{CM}} \times \boldsymbol{X_C}\right)^T}{\left(\boldsymbol{G^T_{MM'}} \times \boldsymbol{X_M} + \boldsymbol{G^T_{AM}} \times \boldsymbol{X_A} + \boldsymbol{G^T_{CM}} \times \boldsymbol{X_C}\right)^T} \right] \right\} \\
&\qquad \times \boldsymbol{X_M} \\
&+ \left\{ \left[\frac{\boldsymbol{G_{C_iA,C'A}}}{\left(\boldsymbol{G^T_{MA,CA}} \times \boldsymbol{X_M} + \boldsymbol{G^T_{A'A,CA}} \times \boldsymbol{X_A} + \boldsymbol{G^T_{CA,C'A}} \times \boldsymbol{X_C}\right)^T} \right] \right. \\
&* \left. \left[\boldsymbol{T_{C_iA,C'A}} - \frac{\left(\boldsymbol{H^T_{MA,CA}} \times \boldsymbol{X_M} + \boldsymbol{H^T_{A'A,CA}} \times \boldsymbol{X_A} + \boldsymbol{H^T_{CA,C'A}} \times \boldsymbol{X_C}\right)^T}{\left(\boldsymbol{G^T_{MA,CA}} \times \boldsymbol{X_M} + \boldsymbol{G^T_{A'A,CA}} \times \boldsymbol{X_A} + \boldsymbol{G^T_{CA,C'A}} \times \boldsymbol{X_C}\right)^T} \right] \right\} \\
&\qquad \times \frac{\boldsymbol{X_C}}{\sum_{j=1}^{c} X_{C_j}} \times \boldsymbol{X_A}
\end{aligned}
\tag{3.95}
$$

The term $\boldsymbol{H}$ is defined in Equation 3.96.

$$
\boldsymbol{H_{I,J}} = (\boldsymbol{G_{I,J}} \odot \boldsymbol{T_{I,J}}) \tag{3.96}
$$

In the CO_2-MEAH-water system, the components are shown in Table 3.4.

The matrices containing specific data adjusted by AUSTGEN *et al.* (1989) are presented from Equation 3.97 to 3.112.

$$
\boldsymbol{T_{MM'}} = \begin{pmatrix} 0 & 10.064 - 3268.14/T & 0 \\ 10.064 - 3268.14/T & 0 & 1.674 \\ 0 & -649.75/T & 0 \end{pmatrix} \tag{3.97}
$$

Table 3.4: Components considered in the MEAH-CO_2-H_2O system

Symbol	Component
M_1	CO_2
M_2	H_2O
M_3	MEAH
A_1	OH^-
A_2	$MEACOO^-$
A_3	HCO_3^-
A_4	CO_3^{2-}
C_1	H_3O^+
C_2	$MEAH_2^+$

$$\boldsymbol{A_{MM'}} = \begin{pmatrix} 0.2 & 0.2 & 0.2 \\ 0.2 & 0.2 & 0.2 \\ 0.2 & 0.2 & 0.2 \end{pmatrix} \tag{3.98}$$

$$\boldsymbol{T_{CA,M_1}} = \begin{pmatrix} -8 & -8 & -8 & -8 \\ -8 & -8 & -8 & -8 \end{pmatrix} \tag{3.99}$$

$$\boldsymbol{T_{CA,M_2}} = \begin{pmatrix} -4 & -4 & -4 & -4 \\ -4 & -5.098 & -4.088 & -4 \end{pmatrix} \tag{3.100}$$

$$\boldsymbol{T_{CA,M_3}} = \begin{pmatrix} -8 & -8 & -8 & -8 \\ -8 & -8 & -8 & -8 \end{pmatrix} \tag{3.101}$$

$$\boldsymbol{A_{CA,M_1}} = \begin{pmatrix} 0.1 & 0.1 & 0.1 & 0.1 \\ 0.1 & 0.1 & 0.1 & 0.1 \end{pmatrix} \tag{3.102}$$

$$\boldsymbol{A_{CA,M_2}} = \begin{pmatrix} 0.2 & 0.2 & 0.2 & 0.2 \\ 0.2 & 0.2 & 0.2 & 0.2 \end{pmatrix} \tag{3.103}$$

$$\boldsymbol{A_{CA,M_3}} = \begin{pmatrix} 0.1 & 0.1 & 0.1 & 0.1 \\ 0.1 & 0.1 & 0.1 & 0.1 \end{pmatrix} \tag{3.104}$$

$$\boldsymbol{T_{M_1,CA}} = \begin{pmatrix} 15 & 15 & 15 & 15 \\ 15 & 15 & 15 & 15 \end{pmatrix} \tag{3.105}$$

$$\boldsymbol{T_{M_2,CA}} = \begin{pmatrix} 8 & 8 & 8 & 8 \\ 8 & 10.268 & 4.55 + 1218.19/T & 8 \end{pmatrix} \tag{3.106}$$

$$\boldsymbol{T_{M_3,CA}} = \begin{pmatrix} 15 & 15 & 15 & 15 \\ 15 & 15 & 15 & 15 \end{pmatrix} \tag{3.107}$$

$$\boldsymbol{T_{CA,C'A}} = \begin{pmatrix} 0 & 0 & 0 & 0 \\ 0 & 0 & 0 & 0 \end{pmatrix} \text{ for } C' = 1, 2 \tag{3.108}$$

$$\boldsymbol{A_{CA,C'A}} = \begin{pmatrix} 0 & 0 & 0 & 0 \\ 0 & 0 & 0 & 0 \end{pmatrix} \text{ for } C' = 1, 2 \tag{3.109}$$

$$\boldsymbol{T_{AC,A'C}} = \begin{pmatrix} 0 & 0 \\ 0 & 0 \\ 0 & 0 \\ 0 & 0 \end{pmatrix} \text{ for } A' = 1, \cdots 4 \tag{3.110}$$

$$\boldsymbol{A_{AC,A'C}} = \begin{pmatrix} 0 & 0 \\ 0 & 0 \\ 0 & 0 \\ 0 & 0 \end{pmatrix} \text{ for } A' = 1, \cdots 4 \tag{3.111}$$

$$G_{CC,AC} = G_{AA,CA} = 0 \tag{3.112}$$

3.1.2 Physical Properties

A number of physical properties appear in the aforementioned equations. Some of them, specially in the gas phase, may be calculated directly from the state equation. However, in the liquid phase, due to its higher complexity - with ions and simultaneous chemical reactions - empirical correlations were preferred.

Molar volume

Gas phase molar volume is directly calculated form the SRK equation of state.

An equation for calculation of the liquid phase molar volume was developed by AMUNDSEN *et al.* (2009). In this model, molar volume of MEA-CO_2-H_2O solution is temperature and composition dependent as shown in Equation 3.113.

$$v_L = x_3 v_3 + (1 - x_3) v_2 + x_3(1 - x_3) \sum_{k=0}^{3} A_k (2x_3 - 1)^k \tag{3.113}$$

The coefficients A_k ($\mathrm{cm}^3/\mathrm{mol}$) are a function of temperature and are shown in Table 3.5. For each coefficient, a third degree polynomial was used to fit the data into an equation. The complete polynomials are shown in Appendix A.

Table 3.5: Values of parameters A_k ($\mathrm{cm}^3/\mathrm{mol}$) as a function of temperature, described by AMUNDSEN *et al.* (2009)

Temperature in °C	A_0	A_1	A_2	A_3
25	-2.5263	0.7404	0.5698	-1.6062
40	-2.4787	0.6135	0.6018	-1.2561
50	-2.4630	0.5338	0.6420	-0.9870
70	-2.4541	0.4324	0.7030	-0.6392
80	-2.4070	0.4664	0.5390	-0.7186

Viscosity

Dynamic viscosity of MEA and water was also determined by AMUNDSEN *et al.* (2009), as shown in Table 3.6. Data from this table was fitted into an exponential equation to be used in the model. Complete equations are shown in Appendix A.

Table 3.6: Dynamic viscosity of MEA and water as a function of temperature, reported by AMUNDSEN *et al.* (2009)

Temperature	Water dynamic viscosity	MEA dynamic viscosity
°C	mPa s	mPa s
25	0.890	17.9
40	0.653	9.6
50	0.546	6.7
70	0.404	3.7
80	0.354	2.8

Enthalpy and heat capacity

In the gas phase, derivations of the state equations were used to calculate enthalpy and heat capacity. The reference state was ideal gas at the temperature of 300K. Therefore, enthalpy and specific heat of gas phase was calculated using Equations 3.114 and 3.115.

$$H = H^{ig} + \int_{\infty}^{V} \left[T \left(\frac{\partial P}{\partial T} \right)_{V,N_j} + V \left(\frac{\partial P}{\partial V} \right)_{T,N_j} \right] dV \tag{3.114}$$

$$C_p = C_p^{ig} + T \int_{\infty}^{V} \left(\frac{\partial^2 P}{\partial T^2} \right)_V dV - \frac{T \left(\frac{\partial P}{\partial T} \right)_V^2}{\left(\frac{\partial P}{\partial V} \right)_V} - \Re \tag{3.115}$$

The solution heat capacity was measured by CHIU and LI (1999), who also developed a model to that property as shown in Equations 3.116 to 3.118.

$$C_{p,L} = x_3 C_{p,3} + (1 - x_3) C_{p,2} + C_{p,L}^E \tag{3.116}$$

$$C_{p,L}^{E} = x_3(1-x_3)\sum_{k=1}^{2} A_k(2x_3-1)^{k-1} \tag{3.117}$$

$$A_k = a_{k,0} + a_{k,1}(T/\mathrm{K}) \tag{3.118}$$

Parameters $a_{k,0}$ and $a_{k,1}$ were determined for the MEA-water system still by CHIU and LI (1999) and are shown in Table 3.7.

Table 3.7: Parameters for excess heat capacity calculation, determined by CHIU and LI (1999)

Parameter	**Value** $(\mathrm{J/molK})$
$a_{1,0}$	-148.90
$a_{1,1}$	0.492 08
$a_{2,0}$	28.033
$a_{2,1}$	-0.096 90

Enthalpy of the liquid phase was then directly integrated from the C_p equation, using a reference state of pure components at 25°C.

$$h_L(T) = h_L(T_0) + \int_{T'=T_0}^{T} C_{p,L}dT' \tag{3.119}$$

Diffusivity

Diffusivity is an important property that is used in the transport equations, namely, Maxwell-Stefan for gas phase and Nernst-Planck for liquid phase.

Gas phase diffusivity for each pair of components was determined using a correlation proposed by EDWARD FULLER *et al.* (1969) and recommended by POLING *et al.* (2001), shown in Equation 3.120.

$$D_{AB} = \frac{0.00143T^{1.75}}{PM_{AB}^{1/2}\left[(\sum_\nu)_A^{1/3} + (\sum_\nu)_B^{1/3}\right]^2} \tag{3.120}$$

In that equation, the term M_{AB} is the harmonic mean of the molecular weights of species A and B:

$$M_{AB} = 2\left(\frac{1}{M_A} + \frac{1}{M_B}\right)^{-1} \tag{3.121}$$

The term $\sum_\nu$ is the sum of each component atomic diffusion volume, which are tabled values for each atom in the molecular structure. In this work, these values were taken from POLING *et al.* (2001).

For the liquid phase, the correlation proposed by HAYDUK and MINHAS (1982) for aqueous solutions was used, as also recommended by POLING *et al.* (2001).

$$D_{AB} = 1.25 \times 10^{-8}\left(V_A^{-0.19} - 0.292\right) T^{1.52} \mu_L^{9.58/V_A - 1.12} \tag{3.122}$$

In this equation V_A is the molar volume of the solute in normal boiling point, and μ_L is the viscosity of the mixed solvent: water+MEA.

3.1.3 Transport Properties

Transport properties are those properties and parameters that have to do with constructive aspects of the absorption column, and its packings.

In the previously shown equations, the following parameters were presented, whose calculation will be further developed:

- δ_G: Gas film thickness;
- δ_L: Liquid film thickness;
- h_L: Liquid holdup;
- A_I: Gas/liquid interfacial area

The film thickness were estimated with a very simple relation proposed by KOLEV (1976), in which cinematic viscosity is determinant.

$$\delta_G = \left(\frac{\nu_G}{g}\right)^{1/3} \qquad \delta_L = \left(\frac{\nu_L}{g}\right)^{1/3} \tag{3.123}$$

Liquid holdup, proposed by BILLET and SCHULTES (1999), is shown in Equation 3.124. In that equation, u_L is the liquid velocity with respect to the column internal area, and a is a characteristic area, specific of the column packing.

$$h_L = \left(12\frac{1}{g}\frac{\mu_L}{\rho_L}u_L a^2\right)^{1/3} \tag{3.124}$$

The interfacial area can also be calculated with an empirical correlation proposed by BILLET and SCHULTES (1999), shown in Equation 3.125.

$$A_I = 1.5Va\left(ad_h\right)^{-0.5}\left(\frac{u_L d_h}{\nu_L}\right)^{-0.2}\left(\frac{u_L^2\rho_L d_h}{\sigma_L}\right)^{0.75}\left(\frac{u_L^2}{gd_h}\right)^{-0.45} \tag{3.125}$$

However, to account for a number of uncertainties inherent of empirical correlations, this model proposes that the interfacial area is to be adjusted by a parameter. This parameter would transform the estimated interfacial area to the actual interfacial area used in mass transfer, also called effective interfacial area - $A_{I,\text{eff}}$ as shown in Equation 3.126.

$$A_{I,\text{eff}} = \frac{A_I}{\alpha} \tag{3.126}$$

Details of how this parameter was adjusted is given in Section 3.3.

3.2 Solution methodology

The first step to solve this partial differential equation system was to perform a discretization procedure in order to transform it into a differential-algebraic equation system. This procedure will be described in Section 3.2.1.

The resulting differential-algebraic equation system was implemented in the software EMSO, which stands for Environment for Modelling, Simulation and Optimization (SECCHI, 2003) and solved by the numerical integrator DASSLC (SECCHI, 2012). It is a complete graphical environment where the user can model complex dynamic or steady-state processes by simply selecting and connecting model blocks. In addition, the user can develop new models using the EMSO modelling language or using those already made from the EMSO Model Library (EML). EML is an open source library of models written in the EMSO modelling language. The EMSO modelling language is an object-oriented language for modelling general dynamic or steady-state processes. In this work, no previous model was used.

EMSO also allows access of external routines inside the simulation environment. One of these routines is the VRTherm, which is a software capable of predicting physical and thermodynamic properties of mixtures using extensive data bases. In this work, VRTherm subroutine was used to calculate physical and thermodynamic properties of the gas phase using Soave-Redlich-Kwong equation of state. VRTherm does not support the liquid phase model (e-NRTL), and, therefore, it had to be directly implemented on EMSO.

3.2.1 Finite Volume discretization

To solve the non-linear partial differential system of equations, it was performed a discretization of the film coordinate η utilizing the finite-volume approach. This approach has the advantage of respect conservation laws within each discrete volume and was chosen over other common discretization methodologies after some experimenting. Finite differences and polynomial approximation were also considered and tested, however finite volume showed the best numerical stability and resolution time. Gas film was divided into k_G volumes and liquid film into k_L volumes as shown in Figure 3.4. In this figure, F.V. stands for *finite volume* and convention adopted was that first volume is that closer to the gas-liquid interface. The last volumes (k_G and k_L) are those in the boundary between film and bulk phases.

As can be shown in Figure 3.4, mole flux between any volume k and its neighbour $k-1$ has the same superscript as k. In boundary conditions, mole flux between bulk

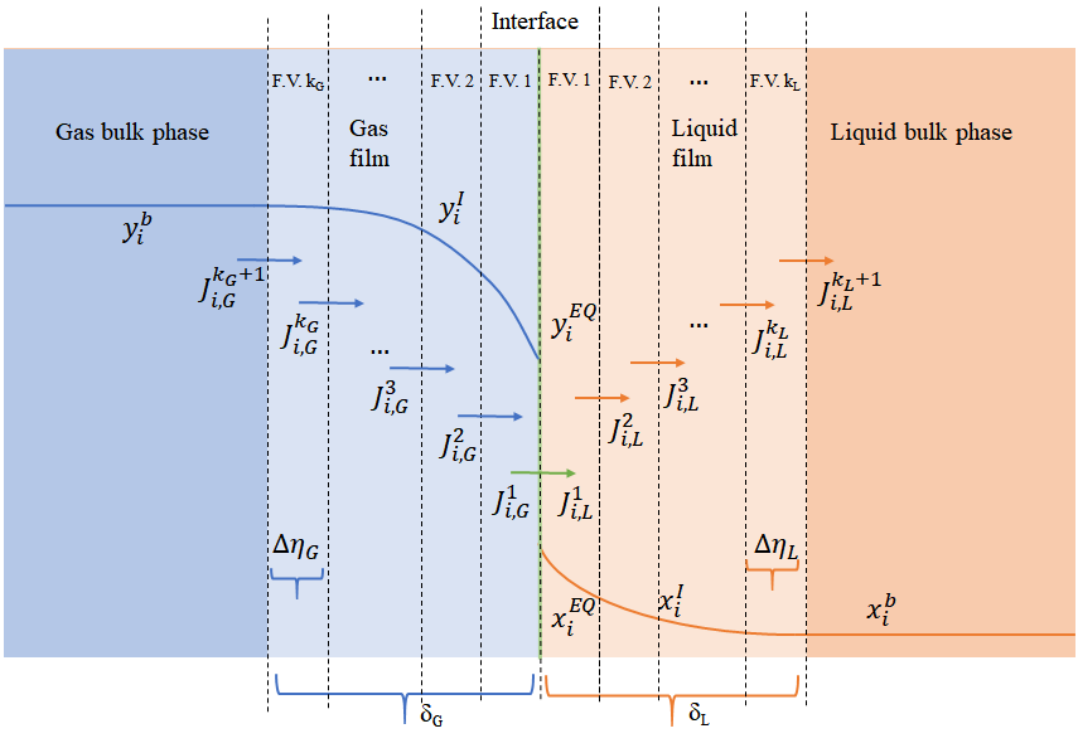

Figure 3.4: Representation of the two-film model with indication of finite volume discretization.

phase and film has superscript $k_G + 1$ or $k_L + 1$, and in the gas/liquid interface superscript is 1.

With those considerations, mass and energy balances for the films are replaced by a set of balances for each finite volume.

- Bulk gas mass balance

  Mass balance in bulk phase persists, with modification only in the flux to film, which now refer to the inlet of the last discrete volume, as shown in Figure 3.4.

$$\frac{\partial \left(y_i^b M_G^b\right)}{\partial t} = F_G^0 y_i^0 - F_G y_i^b + A^I J_{i,G}^{k_G+1} \tag{3.127}$$

- Discrete gas film mass balance

  For any discrete volume k, mass balance is given by:

$$\frac{dC_{i,G}^k}{dt} = \frac{J_{i,G}^k - J_{i,G}^{k+1}}{\Delta\eta_G} \tag{3.128}$$

In gas film, mole flux $J_{i,G}^k$ is given by Maxwell-Stefan equations, which, in the discrete form approximate the chemical potential gradient:

$$\sum_{j=1}^{N} \frac{y_i^k J_{j,G}^k - y_j^k J_{i,G}^k}{C_{t,G}^k \text{Đ}_{ij}} = \frac{y_i^k}{RT_G^k} \frac{\mu_{i,G}^k - \mu_{i,G}^{k-1}}{\Delta\eta_G} \tag{3.129}$$

This equation is valid for all internal fluxes, or $k = 2, ..., k_G$. Boundary conditions are treated separately.

To complement these equations, total concentration in the discrete volume is given by:

$$C_{t,G}^k = 1/v_G^k \tag{3.130}$$

Again, the gas molar volume is calculated using the gas state equation. And the component mole fraction $y_{i,G}^I$ is given by:

$$y_{i,G}^k = \frac{C_{i,G}^k}{C_{t,G}^k} \tag{3.131}$$

- Bulk liquid mass balance

  Equivalently to bulk gas balance, bulk liquid mass balance is given by:

$$\frac{d\left(x_i^b M_L^b\right)}{dt} = N_L^0 x_i^0 - N_L x_i^b + A^I J_{i,L}^{k_L+1} + V_L \sum_{j=1}^{N_r} \vartheta_{ij} r_j^b + \sum_{j=1}^{N_{req}} \vartheta_{ij} \xi_j^b \tag{3.132}$$

  In respect to the reactions which are in chemical equilibrium - the ξ_j term - the chemical equilibrium equation must also be respected:

$$K_j^b = \prod_i \left(x_i^b \gamma_i^b\right)^{\vartheta_{ij}} \tag{3.133}$$

- Discrete liquid film mass balance

  For any discrete volume k, mass balance is given by:

$$\frac{dC_{i,L}^k}{dt} = \frac{J_{i,L}^k - J_{i,L}^{k+1}}{\Delta\eta_L} + \sum_{j=1}^{N_r} \vartheta_{ij} r_j^k + \frac{1}{A_I \Delta\eta_L} \sum_{j=1}^{N_{req}} \vartheta_{ij} \xi_j^k \tag{3.134}$$

In liquid film, mole flux $J_{i,L}^k$ is given by Nernst-Planck equation, which, in the discrete form, approximates concentration and electrical potential gradients:

$$J_{i,L}^k = -C_{t,L}^k D_{Li,\text{eff}}^k \left(\frac{x_i^k - x_i^{k-1}}{\Delta\eta_L} + x_i^k z_i \frac{\mathfrak{F}}{\Re T_L^k} \frac{\varphi^k - \varphi^{k-1}}{\Delta\eta_L} \right) + x_i^k J_{n,L}^k \tag{3.135}$$

and, similarly to the bulk phase, equilibrium conditions must be satisfied:

$$K_j^k = \prod_i \left(x_i^k \gamma_i^k \right)^{\vartheta_{ij}} \tag{3.136}$$

As in gas phase, this equation is valid for all internal fluxes, or $k = 2, ..., k_L$. Boundary conditions are treated separately.

- Bulk gas energy balance

  Energy balance, as molar balance, only differs from the original with substitution of the heat flux from bulk to film:

$$M_G^b C_{p,G}^b \frac{\partial T_G^b}{\partial t} = F_G^0 h_G^0 - F_G h_G^b + A_I q_G^{k_G+1} \tag{3.137}$$

- Bulk liquid energy balance

  Equivalently to bulk gas energy balance, bulk liquid is given by:

$$M_L^b C_{p,L}^b \frac{\partial T_L^b}{\partial t} = F_L^0 h_L^0 - F_L h_L^b + A_I q_L^{k_L+1} + V_L \sum_{j=1}^{N_r} \left(-\Delta H_j \right) r_j \tag{3.138}$$

- Discrete gas film energy balance

$$\frac{dT_G^k}{dt} = \frac{1}{C_{p,G}^k C_{t,G}^k} \frac{q_G^k - q_G^{k+1}}{\Delta\eta_G} \tag{3.139}$$

The heat flux q_G^k is given by:

$$q_G^k = -k_G \frac{T_G^k - T_G^{k-1}}{\Delta\eta_G} + \bar{h_G^k} J_{T,G}^k \tag{3.140}$$

With average enthalpy ($\bar{h_G^k}$) being calculated as:

$$\bar{h_G^k} = \frac{h_G^k + h_G^{k-1}}{2} \tag{3.141}$$

- Discrete liquid film energy balance

$$\frac{dT_L^k}{dt} = \frac{1}{C_{p,L}^k C_{t,L}^k} \left(\frac{q_L^k - q_L^{k+1}}{\Delta\eta_L} + \sum_{j=1}^{N_r} \left(-\Delta H_j\right) r_j^I \right) \tag{3.142}$$

The heat flux q_L^k is given by:

$$q_L^k = -k_L \frac{T_L^k - T_L^{k-1}}{\Delta\eta_L} + \bar{h_L^k} J_{T,L}^k \tag{3.143}$$

As can be observed by previously shown equations, the finite volume approach creates second-order approximation of the derivatives from the original continuous problem. For example, if Equations 3.139 and 3.140 are combined, derivative of temperature in volume k is dependent on temperature in both adjacent volumes: $k+1$ and $k-1$.

$$\frac{dT_G^k}{dt} = -\frac{k_G}{C_{p,G}^k C_{t,G}^k} \left(\frac{T_G^{k+1} - 2T_G^k + T_G^{k-1}}{\Delta\eta_G^2} + \frac{\bar{h_G^{k+1}} J_{T.G}^{k+1} - \bar{h_G^k} J_{T.G}^k}{\Delta\eta_G} \right) \tag{3.144}$$

In order to preserve this second order approximation also in the boundary conditions, parabolic interpolation was proposed in all boundary conditions of the problem. Figure 3.5 shows an schematic of the parabolic interpolation used to calculate boundary condition of gas-liquid interface. The figure shows a concentration profile, though for the temperature profile the method is completely analogous. Using three concentrations points next to the interface, it is possible to define a second degree polynomial, with which the boundary condition is interpolated.

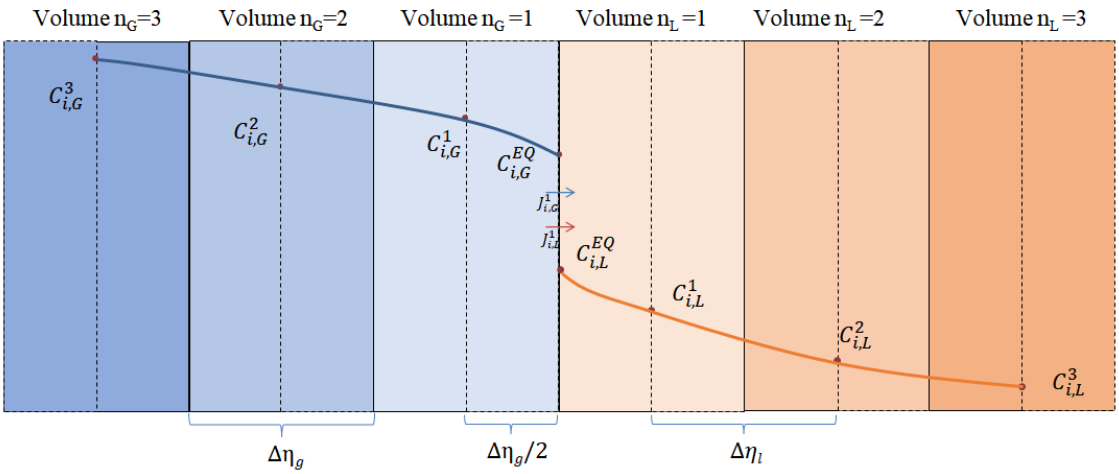

Figure 3.5: Representation of the parabolic interpolation used to calculate boundary conditions between gas and liquid films in the two-film model.

For the bulk-phase/film boundary condition, a second degree polynomial was also defined, as shown in Figure 3.6. With bulk-phase and the last two finite-volume concentrations, it is possible to define a parable, whose derivative originates the gradients needed for both mass and energy balances.

Both figures show second order polynomials that are defined for concentrations, though any property can be interpolated in the same way - such as temperature and chemical potential - in order to obtain the gradients needed for transport equations in boundary conditions. The second order polynomial that interpolates concentration in gas phase is called $P_2(C_{i,G})$, and the same logic is applied to other properties, such as temperature ($P_2(T_G)$) or chemical potential ($P_2(\mu_{i,G})$). Boundary conditions are the following:

- Gas/Liquid boundary condition

  For mass balance, thermodynamic equilibrium defines the relation between $C^{EQ}_{i,G}$ and $C^{EQ}_{i,L}$, expressed with fugacity equality:

$$\hat{f}^{EQ}_{i,G} = \hat{f}^{EQ}_{i,L} \tag{3.145}$$

  Details of fugacity calculation are described in the next section. Complementary to that, both molar fluxes in the interface must be equal:

$$J^1_{i,G} = -J^1_{i,L} \tag{3.146}$$

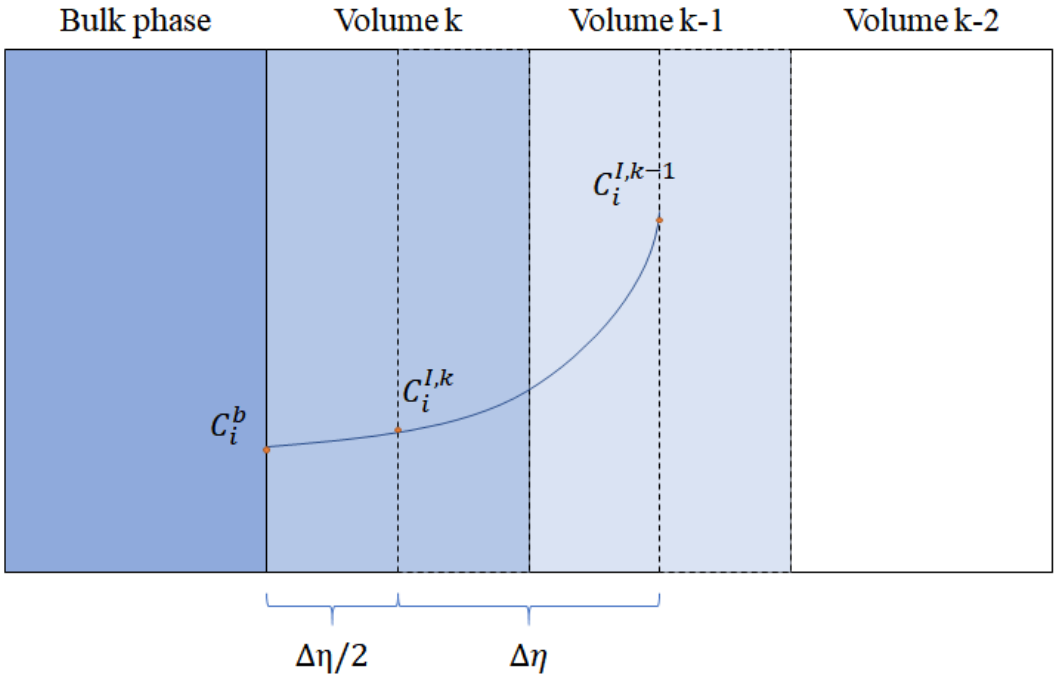

Figure 3.6: Representation of the parabolic interpolation used to calculate boundary conditions between bulk phase and film in the two-film model

Minus sign appear only because of reference adopted. It is notable that there is no explicit equation for molar fluxes $J_{i,G}^1$ and $J_{i,L}^1$, they are implicitly calculated in order to satisfy the equilibrium boundary condition. This issue is more explored later in this text, as this is an example of algebraic equation that causes the system structural differential index to be 2, which may be a problem.

For energy balance, equilibrium temperature from both phases, as well as the heat flux must be equal:

$$T_G^{EQ} = T_L^{EQ} \tag{3.147}$$

$$q_G^1 = -q_L^1 \tag{3.148}$$

- Bulk phase/film boundary condition

  In boundary between bulk phases and films, as already exposed, an second order polynomial was defined with properties from the bulk phase and the last two finite volumes of the discretization procedure. Therefore, mole and energy fluxes in

boundary will be calculated using gradients provided by this polynomial derivative.

For gas bulk/film boundary mole flux:

$$\sum_{j=1}^{N} \frac{y_i^k J_{j,G}^{k_G+1} - y_j^k J_{i,G}^{k_G+1}}{C_{t,G}^{k_G+1} \mathbf{Đ}_{ij}} = \frac{y_i^{k_G+1}}{RT_G^b} \frac{dP_2(\mu_{i,G})}{d\eta} \tag{3.149}$$

and energy flux:

$$q_G^{k_G+1} = -k_G \frac{dP_2(T_G)}{d\eta_G} + \bar{h_G^b} J_{T,G}^{k_G+1} \tag{3.150}$$

For liquid bulk/film boundary mole flux:

$$J_{i,L}^{k_L+1} = -C_{t,L}^{k_L+1} D_{Li,eff}^{k_L+1} \left(\frac{dP_2(x_I)}{d\eta_L} + x_i^k z_i \frac{F}{RT_L^k} \frac{dP_2(\varphi)}{d\eta_L} \right) + x_i^{k_L+1} J_{n,L}^{k_L+1} \tag{3.151}$$

and energy flux:

$$q_L^{k_L+1} = -k_L \frac{dP_2(T_L)}{d\eta_L} + \bar{h_L^b} J_{T,L}^{k_L+1} \tag{3.152}$$

The complete model for one stage of equilibrium after discretization with finite volumes is summarized in Table 3.8. Next sections describe details of the implementation of some of those equations.

Finally, the whole discretization procedure was shown for simplification reason, as if all finite volumes were equal in size. However, as the procedure was implemented, it was clear that the region close to the gas/liquid interface had more complex phenomena and, therefore, needed more points to be well described. In order to allow a higher number of discrete volumes in the interface region, without the use of unnecessary number of volumes close to the bulk regions, an exponential mesh was used. Figure 3.7 illustrates this type of mesh. Equation 3.153 shows how to calculate the distance, $\eta(n)$ of the point n from the origin in an exponential mesh, when the total size of the film is δ. In this equation, β is an arbitrary constant, which would give a satisfactory profile. In this model, β was fixed in 3.

Table 3.8: Summary of main equations used in the discrete two-film model

Region	Equation name	Equation number
Bulk gas phase	Mass balance	3.127
	Energy balance	3.137
Gas film	Mass balance	3.128
	Internal mole fluxes	3.129
	Energy balance	3.139
	Internal energy fluxes	3.140
Liquid film	Mass balance	3.134
	Internal mole fluxes	3.135
	Energy balance	3.142
	Internal energy fluxes	3.143
Bulk liquid phase	Mass balance	3.132
	Energy balance	3.138
Gas/liquid interface	Fugacity equality	3.145
	Mole flux equality	3.146
	Temperature equality	3.147
	Energy flux equality	3.148
Bulk phase/film boundary	Bulk gas/film mole flux	3.149
	Bulk gas/film energy flux	3.150
	Bulk liquid/film mole flux	3.151
	Bulk liquid/film energy flux	3.152

$$\eta_G(n) = \frac{\delta_G}{\exp(k_G/\beta) - 1}\left[\exp(n/\beta) - 1\right]$$
$$\eta_L(n) = \frac{\delta_L}{\exp(k_L/\beta) - 1}\left[\exp(n/\beta) - 1\right] \tag{3.153}$$

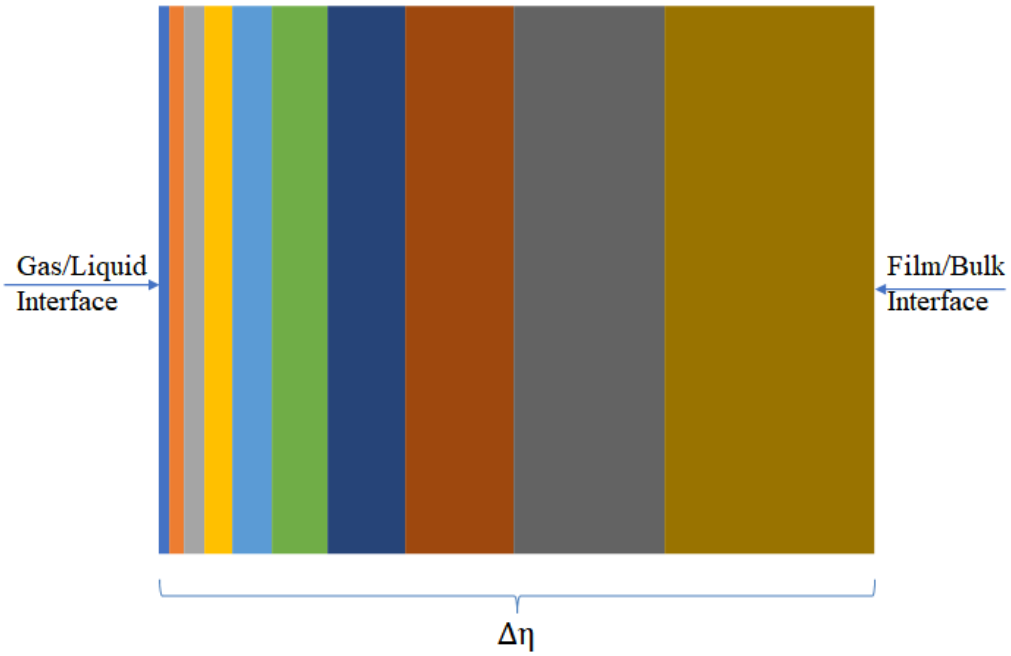

Figure 3.7: Schematic showing an exponential finite volume mesh.

3.2.2 Convergence strategy

The system of differential-algebraic equations resultant from one stage of an absorption column is large and of complex solution. Therefore, to find a coherent steady-state solution, without the concern of giving good initial guesses, the problem was formulated as a non-steady problem, whose initial convergence is easier. The final state of the non-steady problem is then used as guess for steady-state resolution. This procedure is illustrated in Figure 3.8

As mentioned before, an external subroutine was employed in order to calculate physical and thermodynamic properties of gas phase, using Soave-Redlich-Kwong equation of state. This created a drawback, since EMSO is not able to process high order derivatives of external routines, meaning that the structural differential index of the system had to be kept at one.

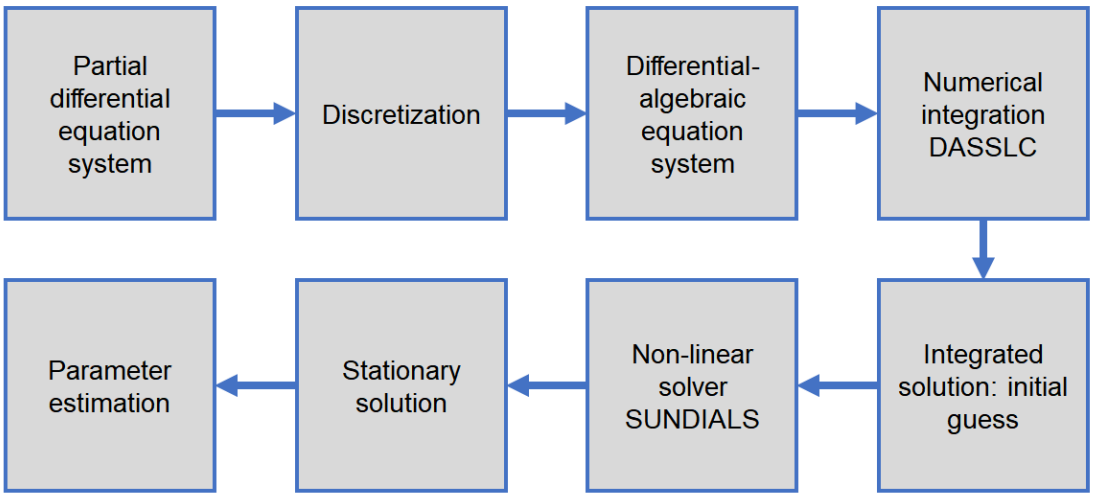

Figure 3.8: Schematic of solution convergence strategy methodology.

For every condition that would generate a second order differential index in the system, a control loop was defined to overcome the index problem. In order to exemplify this consider the boundary condition of the gas/liquid interface in the energy balance, Equation 3.147, which states that gas and liquid temperature must be equal. This boundary condition is an algebraic equation, and the heat flux in the interface, q_G^1 does not appear explicitly in any equation. This means, that two temporal derivatives of the algebraic equation would be necessary to obtain the derivative of the heat flux, as shown in Equation 3.154.

$$\begin{aligned} T_G^{EQ} &= T_L^{EQ} \\ &\rightarrow \frac{dT_G^{EQ}}{dt} = \frac{T_L^{EQ}}{dt} \\ &\rightarrow \frac{1}{C_{p,G}^1 C_{t,G}^1} \frac{q_G^1 - q_G^2}{\Delta\eta_G} = T_L^{EQ} \\ &\rightarrow q_G^1 = C_{p,G}^1 C_{t,G}^1 \Delta\eta_G \frac{T_L^{EQ}}{dt} + q_G^2 \\ &\rightarrow \frac{dq_G^1}{dt} = C_{p,G}^1 C_{t,G}^1 \Delta\eta_G \frac{d^2 T_L^{EQ}}{dt^2} + \frac{dq_G^2}{dt} \end{aligned} \tag{3.154}$$

Therefore, the strategy adopted was to control the interface temperature by changing the heat flux through the interface, by means of a proportional/integral controller, as shown in Equation 3.155, in which $\mathcal{K}_p$ and $\mathcal{K}_i$ are tuning parameters.

$$q_G^1 = \mathcal{K}_p \left(\frac{T_G^{EQ} - T_L^{EQ}}{T_G^{EQ}} \right) + \mathcal{K}_i \int \left(\frac{T_G^{EQ} - T_L^{EQ}}{T_G^{EQ}} \right) dt \tag{3.155}$$

This strategy was used to all equations that would generate a second order structural differential index. This includes the solution of all four chemical equilibrium equations that were presented in Equation 3.48. Equation 3.132 is repeated here To better explain the procedure adopted in these cases. It describes the mass balance of the bulk liquid phase. Two reaction terms were presented, the first referring to the kinetically controlled reaction and the second to the equilibrium reaction degree of advancements - ξ_j.

$$\frac{d\left(x_i^b M_L^b\right)}{dt} = N_L^0 x_i^0 - N_L x_i^b + A^I J_{i,L}^{k_L+1} + V_L \sum_{j=1}^{N_r} \vartheta_{ij} r_j^b + \sum_{j=1}^{N_{req}} \vartheta_{ij} \xi_j^b \tag{3.132}$$

The degree of advancement should be solved to generate equilibrium conditions. However, in order to reduce the structural differential index, an explicit equation must be written for this degree of advancement. To do that, and also to avoid the risk of a degree of advancement which would generate negative values of concentration, an Equation similar to the kinetic law of velocity was implemented, shown in equation 3.156. In that equation, the unknown parameter is now $\hat{k}_j$. In this equation, if one concentration approaches zero, the whole equation also goes to zero and, therefore, no negative concentration will take place.

$$\xi_j^b = V_L \left[\hat{k}_j \prod_e \left(x_e \gamma_e\right)^{\vartheta_{e,j}} - K_j \hat{k}_j \prod_p \left(x_p \gamma_p\right)^{\vartheta_{p,j}} \right] \tag{3.156}$$

Finally, the control loop is possible modifying $k_{j,for}$ as shown in equation

$$\hat{k}_j^b = \mathcal{K}_p \left(K_j - \prod_i \left(x_i^b \gamma_i^b\right)^{\vartheta_{ij}} \right) + \mathcal{K}_i \int \left(K_j - \prod_i \left(x_i^b \gamma_i^b\right)^{\vartheta_{ij}} \right) dt \tag{3.157}$$

These control must also be implemented for each discrete volume. Table 3.9 shows all control loops implemented so that the resulting differential-algebraic system have a first order structural differential index.

Besides implementing the control loops described, the dynamic model was also further simplified, so that integration would progress swiftly. The activity coefficients that are calculated using the e-NRTL model described in Section 3.1.1 were considered constants, and the gas-phase multi-component mass transfer, calculated with Maxwell-Stefan equations - Equation 3.6 - were also simplified to a Fick's law model. This model - which hereafter is referred to as Model 1 - was robust enough to start integration with

initial guess equals to the inlet conditions and could, therefore, generate an initial guess to a steady-state simplified model.

The steady-state simplified model - which is hereafter called Model 2 - has only two simplifications when compared to the full model: all temporal differentials are removed, and the liquid phase activity coefficients are considered constants. It can be solved with a non-linear solver, as long as it has a good initial guess, which was generated by integration of Model 1.

Finally solution of Model 2 is used as an initial guess to solve Model 3 - which is the complete model, only without the temporal derivatives, since in this work only the steady-state solution is being pursued. Table 3.10 summarizes these three models.

Table 3.9: Control loops used to reduce structural differential index

Equation	**Equation**	**Control loop**
$P_G = P_G^0$	3.3	$F_G = \mathcal{K}_p \left(\frac{P_G - P_G^0}{P_G^0}\right) + \mathcal{K}_i \int \left(\frac{P_G - P_G^0}{P_G^0}\right) dt$
$\sum_{i=1}^{N} x_i^b = 1$	3.22	$F_L = \mathcal{K}_p \left(1 - \sum_{i=1}^{N} x_i^b\right) + \mathcal{K}_i \int \left(1 - \sum_{i=1}^{N} x_i^b\right) dt$
$\hat{f}_{i,G}^{EQ} = \hat{f}_{i,L}^{EQ}$	3.145	$J_G^1 = \mathcal{K}_p \left(\frac{\hat{f}_{i,G}^{Bound.} - \hat{f}_{i,G}^{EQ}}{\hat{f}_{i,G}^{EQ}}\right) + \mathcal{K}_i \int \left(\frac{\hat{f}_{i,G}^{Bound.} - \hat{f}_{i,G}^{EQ}}{\hat{f}_{i,G}^{EQ}}\right) dt$
$T_G^{EQ} = T_L^{EQ}$	3.147	$q_G^1 = \mathcal{K}_p \left(\frac{T_G^{\text{Bound.}} - T_G^{EQ}}{T_G^{EQ}}\right) + \mathcal{K}_i \int \left(\frac{T_G^{\text{Bound.}} - T_G^{EQ}}{T_G^{EQ}}\right) dt$
$P_G^k = P_G$	3.10	$J_{4,G}^k = \mathcal{K}_p \left(\frac{P_G^k - P_G}{P^k}\right) + \mathcal{K}_i \int \left(\frac{P_G^k - P_G}{P^k}\right) dt$
$K_j^b = \prod_i \left(x_i^b \gamma_i^b\right)^{\vartheta_{ij}}$	3.133	$\hat{k}_j^b = \mathcal{K}_p \left(K_j - \prod_i \left(x_i^b \gamma_i^b\right)^{\vartheta_{ij}}\right) + \mathcal{K}_i \int \left(K_j - \prod_i \left(x_i^b \gamma_i^b\right)^{\vartheta_{ij}}\right) dt$
$K_j^k = \prod_i \left(x_i^k \gamma_i^k\right)^{\vartheta_{ij}}$	3.136	$\hat{k}_j^k = \mathcal{K}_p \left(K_j - \prod_i \left(x_i^k \gamma_i^k\right)^{\vartheta_{ij}}\right) + \mathcal{K}_i \int \left(K_j - \prod_i \left(x_i^k \gamma_i^k\right)^{\vartheta_{ij}}\right) dt$

Figure 3.8 is then enhanced and expanded in Figure 3.9, which intents to clarify the whole convergence strategy used in this work. Numerical integration was performed using the DASSLC method with relative accuracy of 10^{-3} and absolute accuracy of 10^{-5}. Non-linear solver utilized was SUNDIALS with the same relative accuracy and absolute accuracy of 10^{-6}.

Table 3.10: Main differences between models.

Simplification	Model 1	Model 2	Model 3
Temporal derivatives	Dynamic	Steady	Steady
Control loops	Yes	No	No
Gas-phase mass transfer	Fick's Law	Maxwell-Stefan	Maxwell-Stefan
Activity coefficient in liquid phase	Constant	Constant	Calculated with e-NRTL model
Initial guess	Inlet streams conditions	Model 1 solution	Model 2 solution

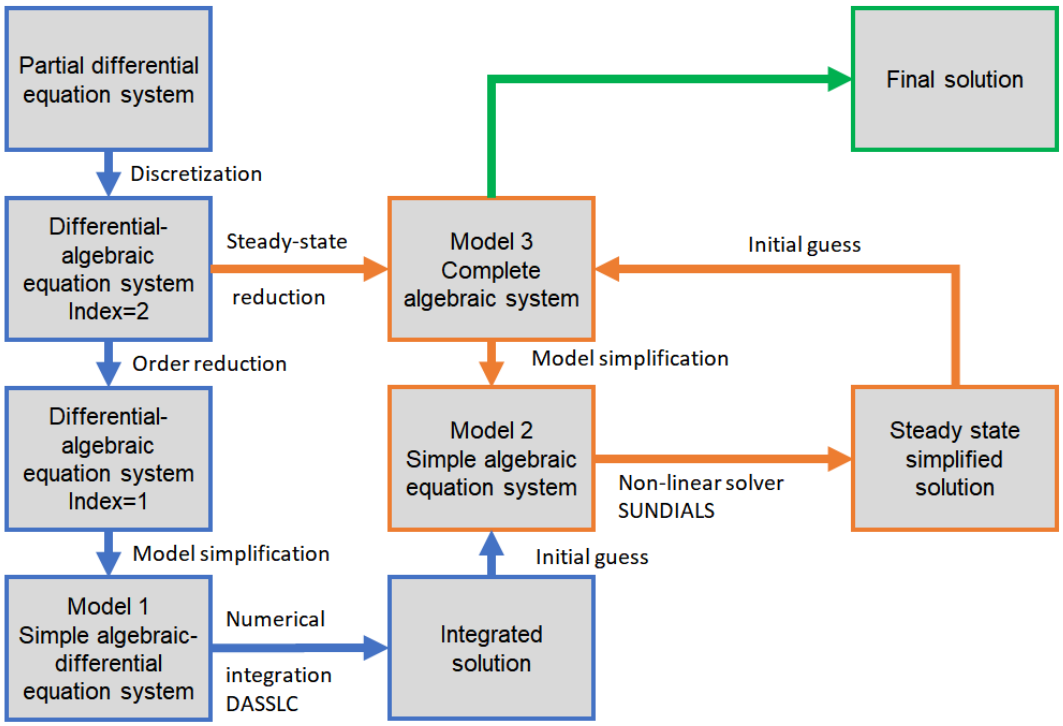

Figure 3.9: Schematic of solution convergence strategy methodology

3.3 Model Parameter Estimation

As previously stated, this model contains one adjustable parameter to account for the uncertainties in the empirical correlations that describe mainly the transport properties. The parameter chosen - α - is a modifier in the interfacial area that would calculate the effective mass transfer area of the column packing. Equation 3.126 is repeated here for better understanding.

$$A_{I,\text{eff}} = \frac{A_I}{\alpha} \tag{3.126}$$

In order to adjust this parameter, it is necessary to have experimental data of the desired simulated gas absorption column. Gas phase CO_2 content is the most important variable, since the column is made for its removal. Therefore, this should be used to adjust the interfacial area modifier. If the effective interfacial area is higher, than more mass is transferred from the gas to the liquid phase and, therefore, lower is the CO_2 concentration. With a set of experimental data, the objective function can be defined as shown in Equation 3.158.

$$OF = \sum_{i=1}^{N_{stages}} \left(y_{1,\text{experimental}}^{\text{stage}=i} - y_{1,\text{calculated}}^{\text{stage}=i} \right)^2 \tag{3.158}$$

This method of adjustment known as Least Squares is but a particular case of the maximum likelihood method when it is considered that all variances of the response variables are equal, and that, according to ALBERTON (2010) it is mostly used, since few works have a rigorous treatment of the measured variances in experiments.

Parameter α must be than adjusted so that the objective function is minimized. Ideally, experimental data contain the outlet CO_2 content of every stage, so that the column profile can be altogether adjusted.

$$\begin{aligned} &\min OF \\ &\text{s.t. } \alpha > 0 \text{ and Model Equations} \end{aligned} \tag{3.159}$$

Since there is only one parameter to adjust, a bisection method was utilized to minimize the objective function, with relative tolerance of 1% on the objective function. To account for parameter uncertainties a confidence interval was used as shown in Equation 3.160.

$$\alpha^{\text{estimated}} - \epsilon_\alpha < \alpha^{\text{true}} < \alpha^{\text{estimated}} + \epsilon_\alpha \tag{3.160}$$

In this equation, the unknown true value of the α parameter is contained in an confidence interval delimited by the parameter error ϵ. If it is assumed that both the parameter and the experimental data are normally distributed, the parametric distribution is assumed to follow a t-student distribution as shown in Equation 3.161.

$$\epsilon_\alpha = t_{\beta,Ngl}\sqrt{V_\alpha} \tag{3.161}$$

In this equation, $t_{\beta,Ngl}$ is the t-student distribution with confidence of β and Ngl degrees of freedom. υ is the corresponding value from the covariance matrix, which is calculated following BOGGS and ROGERS (1990), as shown in Equation 3.162.

$$\boldsymbol{V} = \sigma^2 \left[\boldsymbol{R'}^T \boldsymbol{P} \boldsymbol{R'}\right]^{-1} \tag{3.162}$$

In which R is the experimental residue, which means the difference between measured and calculated values, and σ is estimated by Equation 3.163 (BOGGS and ROGERS, 1990).

$$\sigma^2 = \frac{\boldsymbol{R}^T \boldsymbol{R}}{n-p} \tag{3.163}$$

Experimental data also normally include temperature measurements between stages and, since this model has no extra parameters to do that adjustment, this temperature can be utilized as validation for the model.

Chapter 4

Results and Discussion

4.1 Mesh Analysis

The first step to simulate a full absorption column in this model is to define the number of finite volumes that will be used in the discretization of both gas and liquid films. A simulation of just one stage of absorption was performed to find the appropriate mesh size, and the number of finite volumes was varied. Both temperature and composition profiles were than compared. The objective is to use the minimum amount of discretization points, without losing accuracy in calculation.

Since an exponential grid was adopted, in which Equation 3.153 was utilized to generate the discretization points, when the total number of discrete volumes is changed, all the spacial position of those points also change, what would make a direct comparison between different grids difficult. For that reason, to perform this comparison, the numerical integral of each profile was calculated. Convergence criteria was to stop duplicating the number of discretization points when no change in this integral above a tolerance in respect ot the thinner mesh was observed. For the gas film, this tolerance was 5%, whereas for the liquid film, in which convergence was more difficult, this value was 8%.

Gas film

Figure 4.1 shows the concentration profiles of all gas species and Figure 4.2 shows the temperature profile. It is noticeable that profiles are converging, but quantification of the profiles integral is shown in Table 4.1. It was found that with 4 discrete volumes, gas film is already well described.

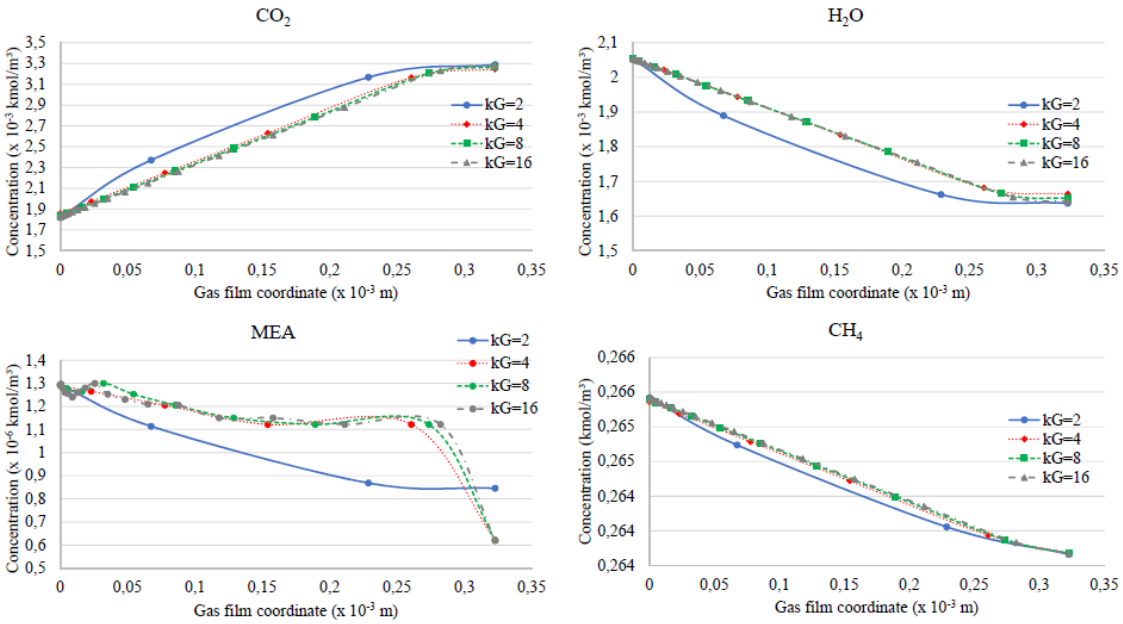

Figure 4.1: Gas film concentration profiles for grid convergence.

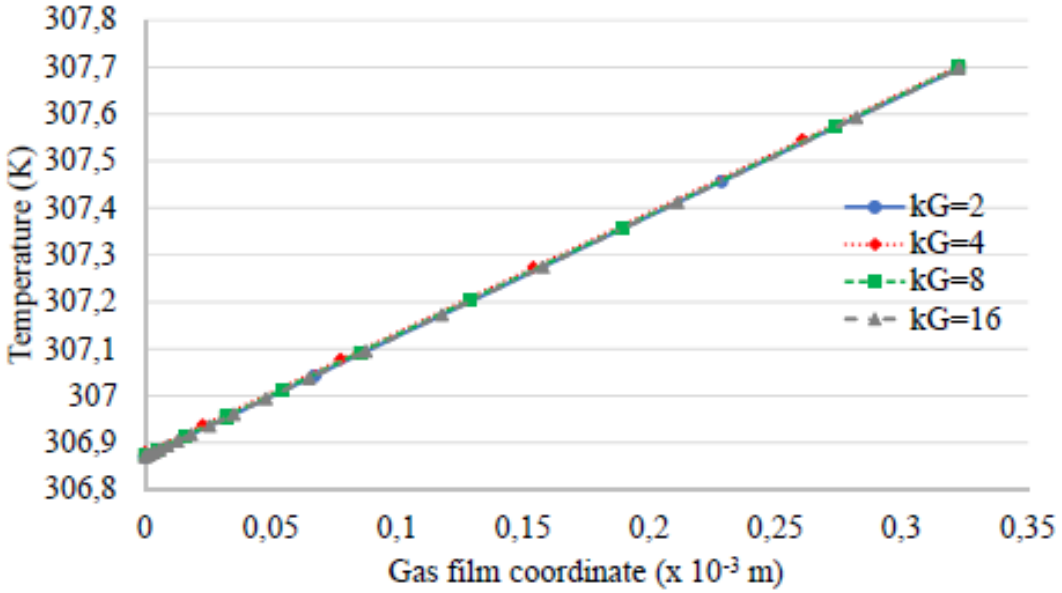

Figure 4.2: Gas film temperature profiles for grid convergence.

Table 4.1: Numerical comparison between gas film grids. Integration units are $\mathrm{kmol/m^2}$ or $\mathrm{K\,m}$ and relative deviations are in respect to the thinner mesh.

Profile		$k_G = 2$	$k_G = 4$	$k_G = 8$	$k_G = 16$
CO_2	Integration	8.9154	8.5377	8.4909	8.4546
	Deviation	5.45%	0.98%	0.43%	-
H_2O	Integration	5.7445	5.9081	5.9025	5.9002
	Deviation	-2.64%	0.13%	0.04%	-
MEA	Integration	0.0032	0.0036	0.0036	0.0037
	Deviation	-12.1%	-1.75%	-0.29%	-
CH_4	Integration	853.619	853.813	853.878	853.923
	Deviation	-0.04%	-0.01%	-0.01%	-
Temperature	Integration	0.0992	0.0992	0.0992	0.0992
	Deviation	0%	0%	0%	-

Liquid film

Figure 4.3 shows the concentration profiles of all molecular species in liquid phase, Figure 4.4 shows the anionic species, Figure 4.5 shows the cationic species, and Figure 4.6 shows the temperature profile. Again, it is noticeable that profiles are converging, and quantification of the profiles integral is shown in Table 4.2. It was decided that 12 discrete volumes are sufficient to accurately describe the liquid film, although two deviations were slightly higher than 5%, which was the tolerance considered in the gas film. This compromise was made in order to significantly reduce computational effort to simulate a full column.

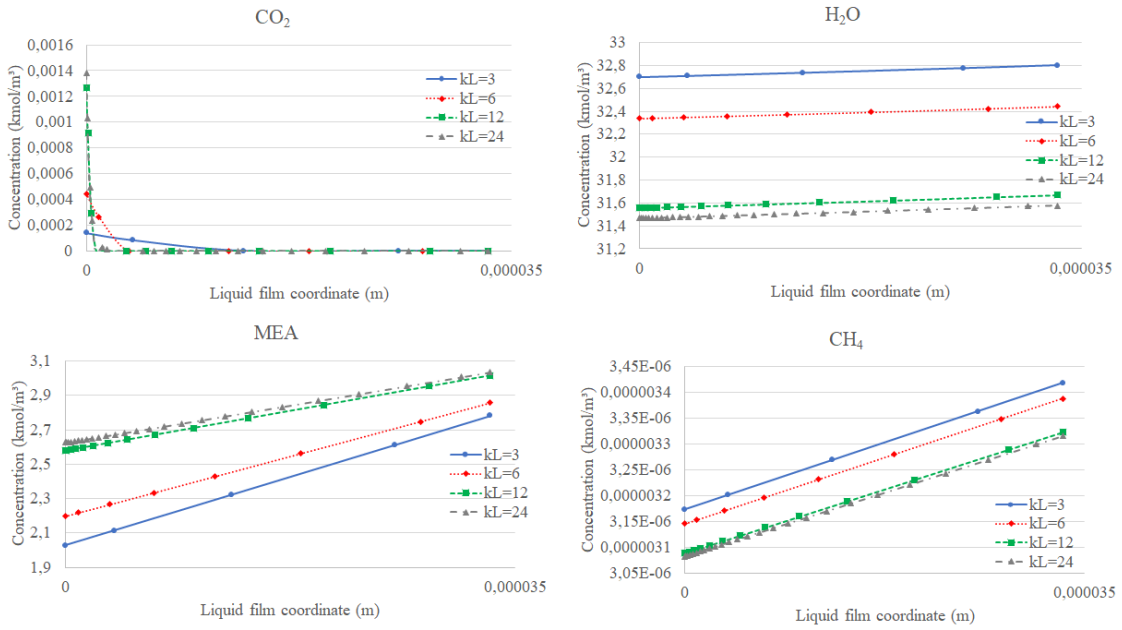

Figure 4.3: Liquid film molar concentration profiles for grid convergence.

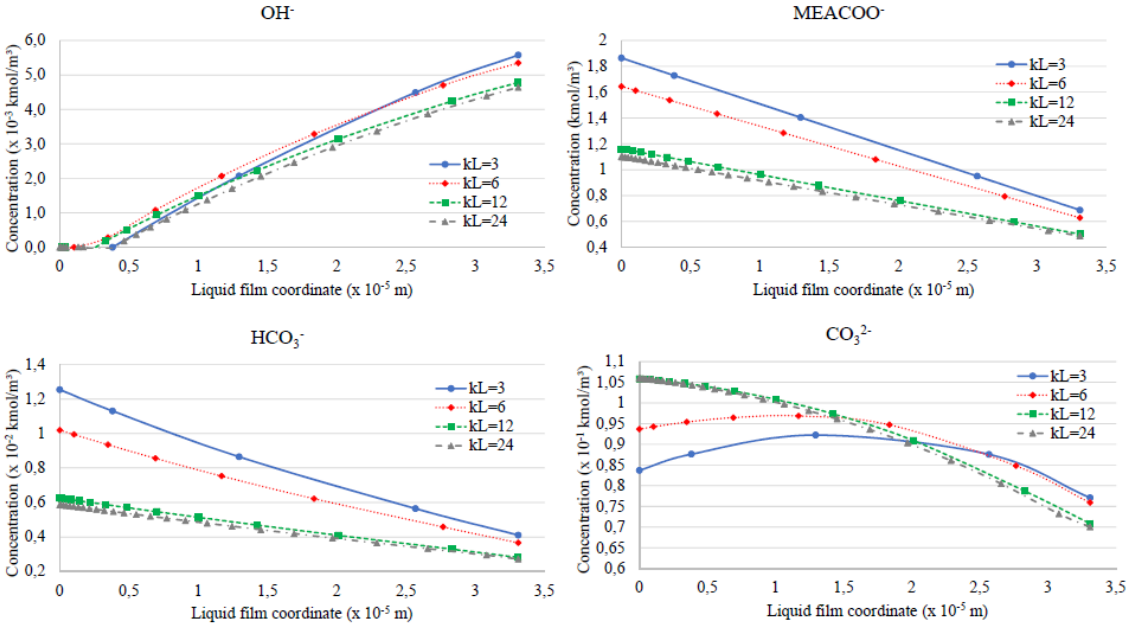

Figure 4.4: Liquid film anionic concentration profiles for grid convergence.

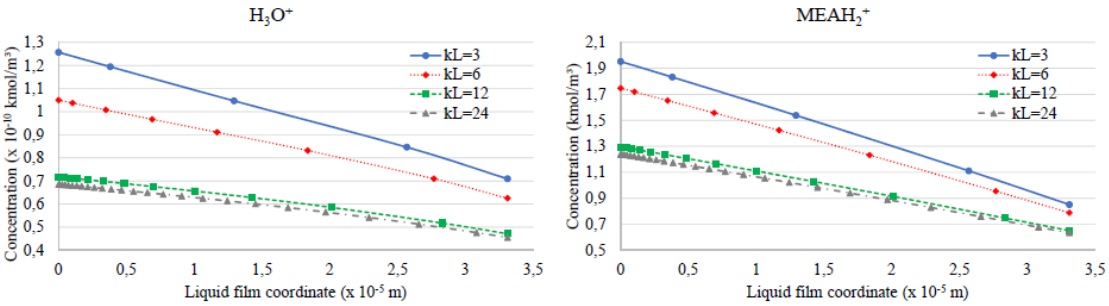

Figure 4.5: Liquid film cationic concentration profiles for grid convergence.

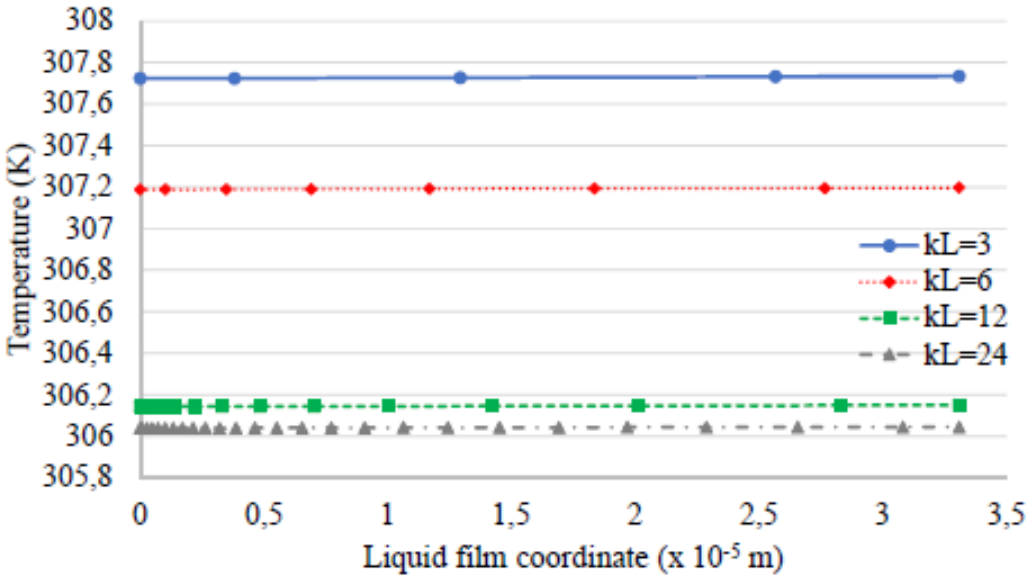

Figure 4.6: Liquid film temperature profiles for grid convergence.

Table 4.2: Numerical comparison between liquid film grids. Integration units are $\mathrm{kmol/m^2}$ or $\mathrm{K\,m}$ and relative deviations are in respect to the thinner mesh.

Profile		$k_L = 3$	$k_L = 6$	$k_L = 12$	$k_L = 24$
CO_2	Integration	8.2458e-10	6.9817e-10	3.7203e-10	3.5624e-10
	Deviation	131.5%	95.9%	4.43%	-
H_2O	Integration	1.0838e-03	1.0718e-03	1.0461e-03	1.0431e-03
	Deviation	3.89%	2.75%	0.29%	-
MEA	Integration	7.9569e-05	8.3612e-05	9.2564e-05	9.3638e-05
	Deviation	15.0%	-10.7%	-1.15%	-
CH_4	Integration	1.0908e-10	1.0813e-10	1.0609e-10	1.0587e-10
	Deviation	-3.03%	2.13%	0.22%	-
OH^-	Integration	8.6785e-08	9.2428e-08	8.0832e-08	7.5300e-08
	Deviation	15.3%	22.7%	7.35%	-
$MEACOO^-$	Integration	4.2218e-05	3.7581e-05	2.7509e-05	2.6285e-05
	Deviation	60.6%	43.7%	4.66%	-
HCO_3^-	Integration	2.6380e-07	2.2163e-07	1.4842e-07	1.4087e-07
	Deviation	87.3%	57.3%	5.36%	-
CO_3^{2-}	Integration	2.9033e-06	3.0306e-06	3.0637e-06	3.0388e-06
	Deviation	-4.45%	-0.27%	0.82%	-
H_3O^+	Integration	3.2728e-15	2.8063e-15	2.0050e-15	1.9249e-15
	Deviation	70.0%	45.8%	4.17%	-
$MEAH_2^+$	Integration	4.6761e-05	4.2304e-05	3.2453e-05	3.1232e-05
	Deviation	49.7%	35.4%	3.91%	-
Temperature	Integration	0.0102	0.0102	0.0101	0.0101
	Deviation	0.2%	0.3%	0%	-

4.2 First Model Solution

This section will present the results of the first attempt to solve a hypothetical column in order to test the methodology presented in this work. The column has the following parameters:

- Internal diameter: 1.9 m
- Packing height: 1.0 m
- Number of stages: 6
- Column pressure: 6.8 atm
- Packing type: Pall ring (50mm)
- Gas molar flow: 1,100 $\mathrm{kmol/h}$
- Gas phase CO_2 molar fraction: 2.53%
- Liquid molar flow: 1,800 $\mathrm{kmol/h}$
- Liquid MEA molar fraction: 10%

As described in the methodology section, in order to solve the model proposed in this work, two auxiliary models had to be solved to generate the initial guess for the final solution. The results of each model will be described next.

Model 1

Model 1 is a dynamic model with structural differential index 1, having some algebraic equations substituted by control equations, and two simplifications: liquid-phase activity coefficient were constants, and gas-phase mass transfer was described with Fick's law.

For a six-stage column Model 1 had:

- 17,957 variables
- 17,034 equations
- 923 specifications
- 1,542 dynamic degrees of freedom

To generate a good initial condition to solve Model 2, Model 1 had to be integrated for a simulation time equal to 100,000 seconds. EMSO was capable of solve this system using the DASSLC solver with relative accuracy of 10^{-3} and absolute accuracy of 10^{-5}. Total CPU time was 55.72 s using a Intel® Core™ i7 7500U processor with 2.7 GHz and 4 MB L3 Cache.

One important result of Model 1 is the tuning parameters of the controllers that were used to reduce the system's structural differential index. Table 4.3 shows the tuning parameters used in this model, after trial and error method.

Table 4.3: Tuning parameters used in the solution of Model 1

Control loop	$\mathcal{K}_p$	$\mathcal{K}_i$	**Obs.**
$F_G = \mathcal{K}_p \left(\frac{P_G - P_G^0}{P_G^0}\right) + \mathcal{K}_i \int \left(\frac{P_G - P_G^0}{P_G^0}\right) dt$	10^4	10^4	-
$F_L = \mathcal{K}_p \left(1 - \sum_{i=1}^{N} x_i^b\right) + \mathcal{K}_i \int \left(1 - \sum_{i=1}^{N} x_i^b\right) dt$	-5×10^3	-10^3	-
$J_G^1 = \mathcal{K}_p \left(\frac{\hat{f}_{i,G}^{Bound.} - \hat{f}_{i,G}^{EQ}}{\hat{f}_{i,G}^{EQ}}\right) + \mathcal{K}_i \int \left(\frac{\hat{f}_{i,G}^{Bound.} - \hat{f}_{i,G}^{EQ}}{\hat{f}_{i,G}^{EQ}}\right) dt$	5.0	10^2	For CO_2
	-5.0	-10	For H_2O
	-5.0	-10	For MEA
	5.0	10^2	For CH_4
$q_G^1 = \mathcal{K}_p \left(\frac{T_G^{\text{Bound.}} - T_G^{EQ}}{T_G^{EQ}}\right) + \mathcal{K}_i \int \left(\frac{T_G^{\text{Bound.}} - T_G^{EQ}}{T_G^{EQ}}\right) dt$	10^5	10^5	-
$\hat{k}_j^k = \mathcal{K}_p \left(K_j - \prod_i \left(x_i^k \gamma_i^k\right)^{\vartheta_{ij}}\right) + \mathcal{K}_i \int \left(K_j - \prod_i \left(x_i^k \gamma_i^k\right)^{\vartheta_{ij}}\right) dt$	9×10^{-2}	9×10^{-2}	For equilibrium reaction 1
	4.5×10^3	9×10^{-2}	For equilibrium reaction 2
	18	9.0×10^{-2}	For equilibrium reaction 3
	10^2	10^3	For equilibrium reaction 4

Model 2

Model 2 - which is a steady-state version of Model 1, without the Maxwell-Stefan simplification - could be solved using the initial guess provided by the integration of Model 1. Model 2 has, naturally, the same number of variables and equations as Model 1, and it was solved using the non-linear algebraic equation (NLA) solver with relative accuracy of 10^{-3} and absolute accuracy of 10^{-6}. CPU time was 334.21 s, although, most

of that time was only to load the initial guess generated by Model 1. Actual CPU time, after initial guess loading, was 0.98 s.

Model 3

Model 3 is the complete model of this work, and could be solved with the initial guess from the solution of Model 2. It had, for a 6-stage column:

- 17,957 variables
- 17,790 equations
- 167 specifications

With addition of liquid phase activity coefficient calculation via e-NRTL equation, computational effort is greatly increased. The same non-linear solver was utilized, with the same accuracy as Model 2, and solution time was 65.51 s.

Figure 4.7 shows gas-phase CO_2 molar fraction and liquid-phase temperature from the solution of each of the three models, to compare the impact of the approximations of each model in the final solution. Although it may seem that models 2 and 3 have very close solutions, some variables are more affected by the activity coefficient, such as the ionic species concentration. To illustrate that, Figure 4.8 shows the OH^- molar fraction results of the three models, in which difference between models 2 and 3 can get to 25%.

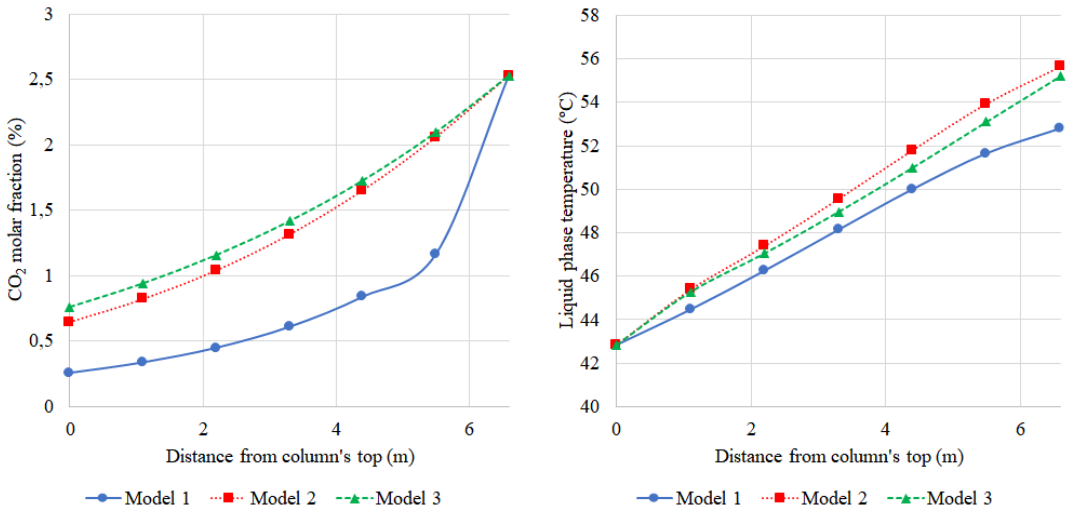

Figure 4.7: Comparison between gas phase CO_2 concentration and liquid phase temperature profiles results of each model.

The methodology was effective, and having a solution of Model 3 already converged allows the user to vary inlet conditions, or tower geometry within a range of approximately 20% of the original converged value. This is useful for the parameter adjustment or to simulate various cases, without having to solve models 1 and 2.

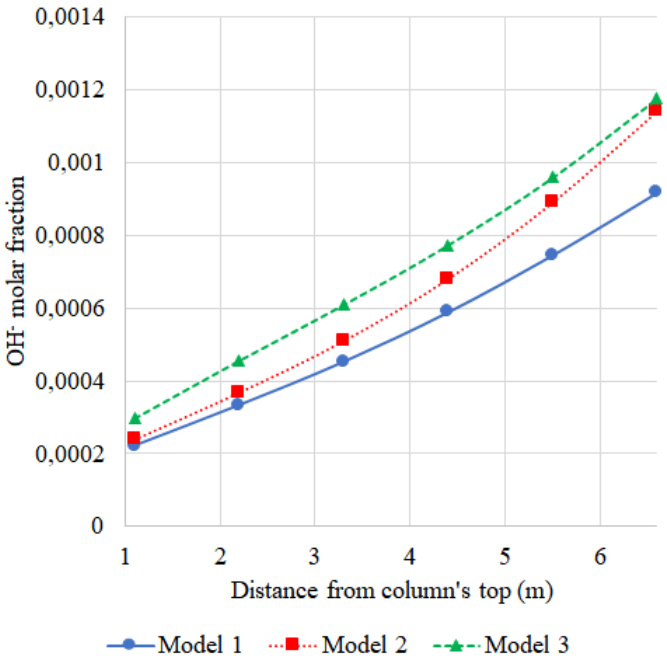

Figure 4.8: Comparison between OH^- concentration profiles results of each model.

4.3 Model Validation

Pilot plant data of absorption of CO_2 with MEA were taken from the published work of TONTIWACHWUTHIKUL *et al.* (1992) to validate Model 3. The column of this publication has the following characteristics:

- Internal diameter: $0.1\mathrm{m}$
- Packing height: $1.2\ \mathrm{m}$
- Number of stages: 6
- Column pressure: $1.01\ \mathrm{bar}$
- Packing type: Ceramic berl saddles (1/2")

Six experiments were performed, in which some inlet characteristics were varied as shown in Table 4.4.

Table 4.4: Inlet condition for the six experiments taken from TONTIWACHWUTHIKUL *et al.* (1992).

Inlet	**Exp.1**	**Exp.2**	**Exp.3**	**Exp.4**	**Exp.5**	**Exp.6**
Liquid molar flow (kmol/h)	5.40	5.40	4.98	5.40	3.80	3.64
MEA molar fraction	0.039	0.040	0.081	0.039	0.039	0.062
Gas molar flow (kmol/h)	0.418	0.418	0.418	0.418	0.314	0.418
CO_2 molar fraction	0.153	0.195	0.156	0.115	0.191	0.191

Each experimental condition was simulated using Model 3, and the effective interfacial area was adjusted for each one. TONTIWACHWUTHIKUL *et al.* (1992) did measurements of CO_2 concentration and liquid phase temperature after each stage. Therefore, the objective function was defined as shown in Equation 4.1.

$$FO = \sum_{i=1}^{6} \left(y_{1,experimental}^{\text{stage}=i} - y_{1,calculated}^{\text{stage}=i} \right)^2 \tag{4.1}$$

This approach of the least squares is a particular case of the maximum likelihood estimation, in which is considered that all variances of the response variables are the

same. This was necessary, since no measurement error was reported by the source.

Table 4.5 shows the results of both the α parameter and the objective function after each adjustment in each experiment. There is also an interval for the estimated parameter with 95% confidence. Figure 4.9 shows a comparison between the experimental and the calculated values for the CO_2 mole fraction in all six experiments.

Table 4.5: Results from parameter adjustment.

Experiment	**Parameter α**	**Confidence interval**	**Objective function**
Exp.1	0.463	0.431-0.497	0.402
Exp.2	0.478	0.460-0.497	0.296
Exp.3	1.244	1.161-1.329	0.577
Exp.4	0.439	0.417-0.463	0.078
Exp.5	0.488	0.468-0.510	0.300
Exp.6	0.633	0.557-0.710	2.242

Liquid-phase temperature data was measured by the authors, and therefore these data was used to validate the model, since no adjustment has been made to fit this variable. Figure 4.10 shows the comparison between measured and calculated liquid-phase temperature in all six experiments. Good agreement can be seen in that property.

The results of the α parameter, which physically correlates to how effective is the mass transfer surface, revelled a significance variance within the same column, being the lower value 0.439, and the higher 1.244. The different properties in the inlet condition for each experiment were analyzed and was found that the MEA concentration in liquid phase fairly correlates to the adjusted value of α, as shown in Figure 4.11. A linear adjustment was made as can be shown in the figure, since there were practically only three different MEA concentration points. The final model - which in previous chapters was called Model 3 - was then modified to include the correlation between the α parameter and the inlet MEA concentration. This slightly different model was called Model 4.

Finally, α parameter was recalculated for each experimental condition using the linear equation presented in Figure 4.11 and the results are shown in Table 4.6 , which compares the new values of the parameter, as well as the new objective functions with the previous values. Graphical comparison between experimental data, calculated data with individual adjustment of α and calculated data with the linear equation for α are shown

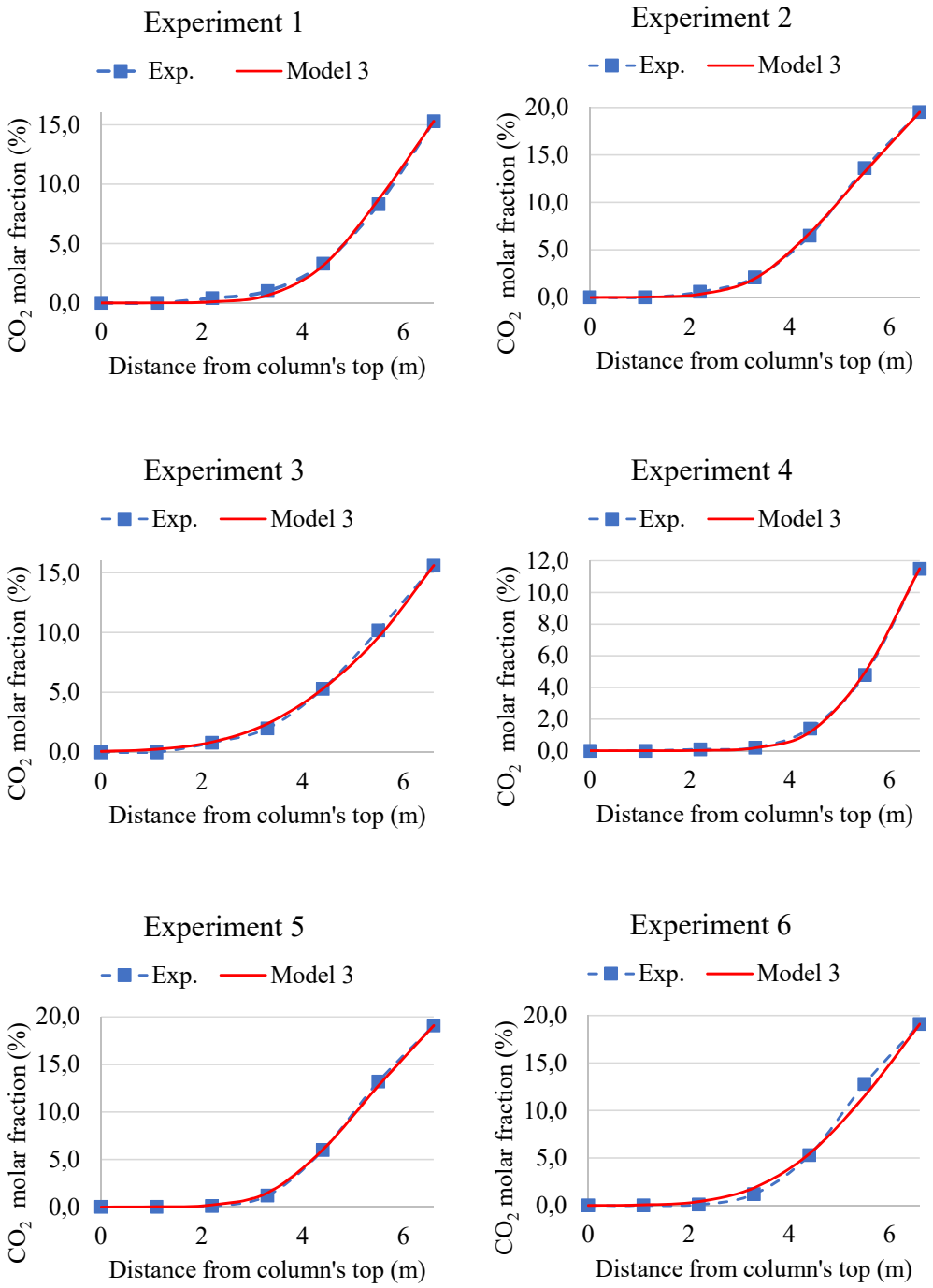

Figure 4.9: Comparison between experimental and calculated values of CO_2 molar fraction in gas-phase after individual parameter adjustment.

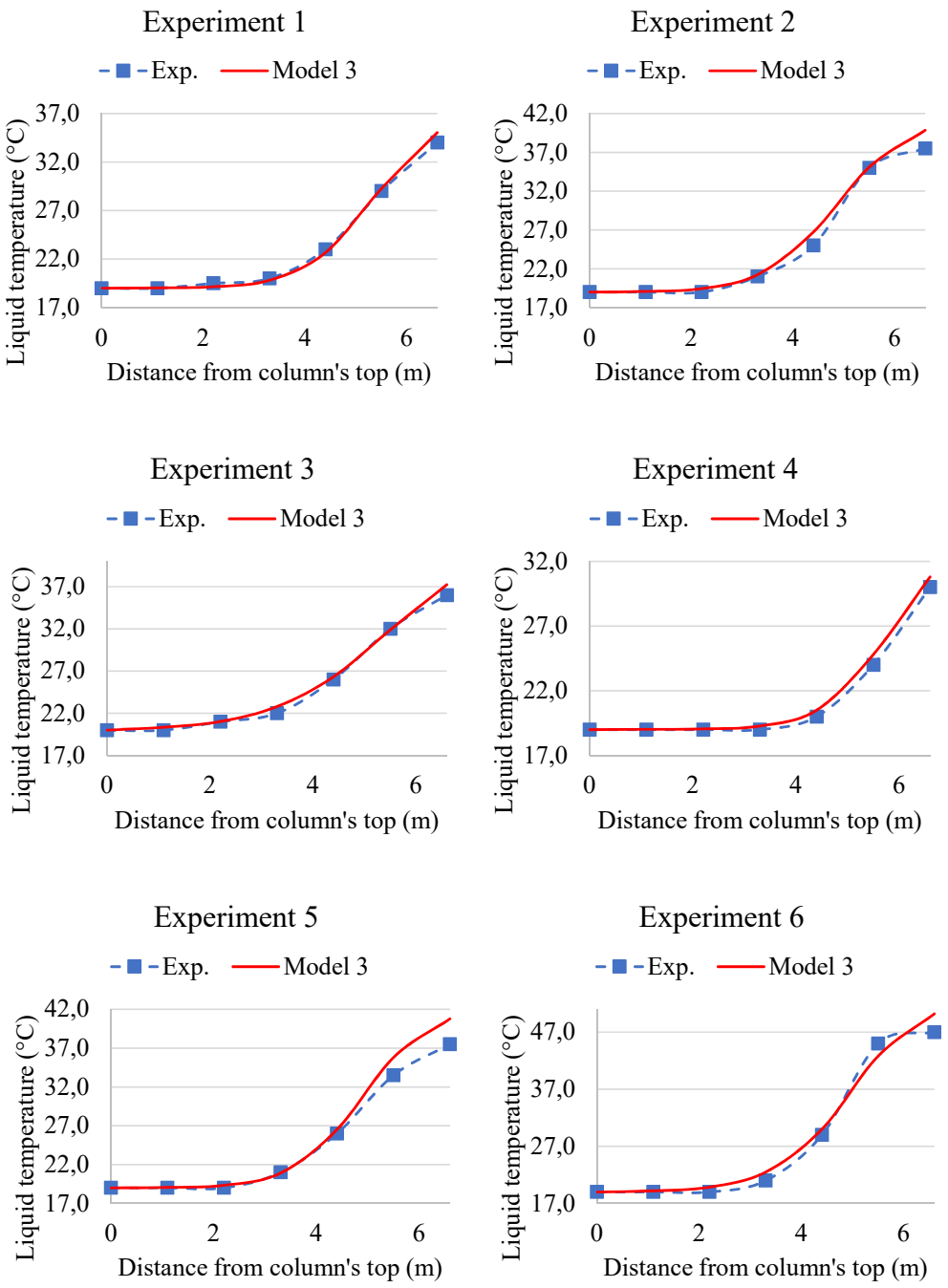

Figure 4.10: Comparison between experimental and calculated values of liquid-phase temperature after individual parameter adjustment.

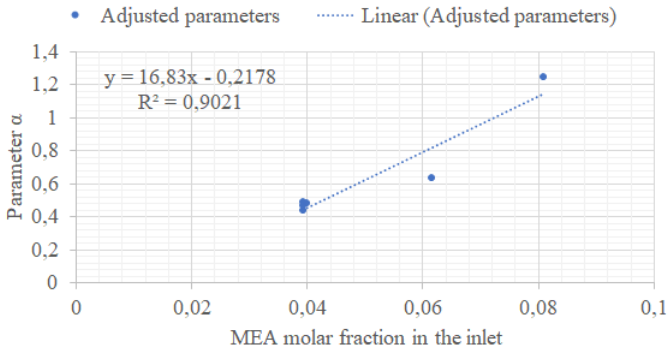

Figure 4.11: Adjusted parameter α as a function of the inlet MEA molar fraction and its linear adjustment.

in Figure 4.12 for the gas-phase CO_2 concentration, and Figure 4.13 for the liquid-phase temperature.

Table 4.6: Results from parameter adjustment.

	Exp.1	**Exp.2**	**Exp.3**	**Exp.4**	**Exp.5**	**Exp.6**
Parameter α (adjusted)	0.463	0.478	1.244	0.439	0.488	0.633
Confidence interval	0.431 - 0.497	0.460 - 0.497	1.161 - 1.329	0.417 - 0.463	0.468 - 0.510	0.557 - 0.710
Parameter α (recalculated)	0.443	0.453	1.145	0.443	0.443	0.818
Objective function ($\times 10^{-4}$) (adjusted)	0.402	0.296	0.577	0.078	0.300	2.242
Objective function ($\times 10^{-4}$) (recalculated)	0.525	0.710	1.300	0.079	1.552	13.025

Experiment 6 was the only one that significantly diverged from the experimental results after using the α parameter given by the linearized model. This can be observed in Figure 4.11, as experiment 6's point (which has a MEA molar fraction of approximately 0.06) is relatively out of the linear fitting.

It is also notable that the new value for the α parameter was inside the confidence interval only in two of the six experiments (Exp.1 and Exp.4). This indicates that the linear adjustment was not good, although a higher number of experiments would be required to

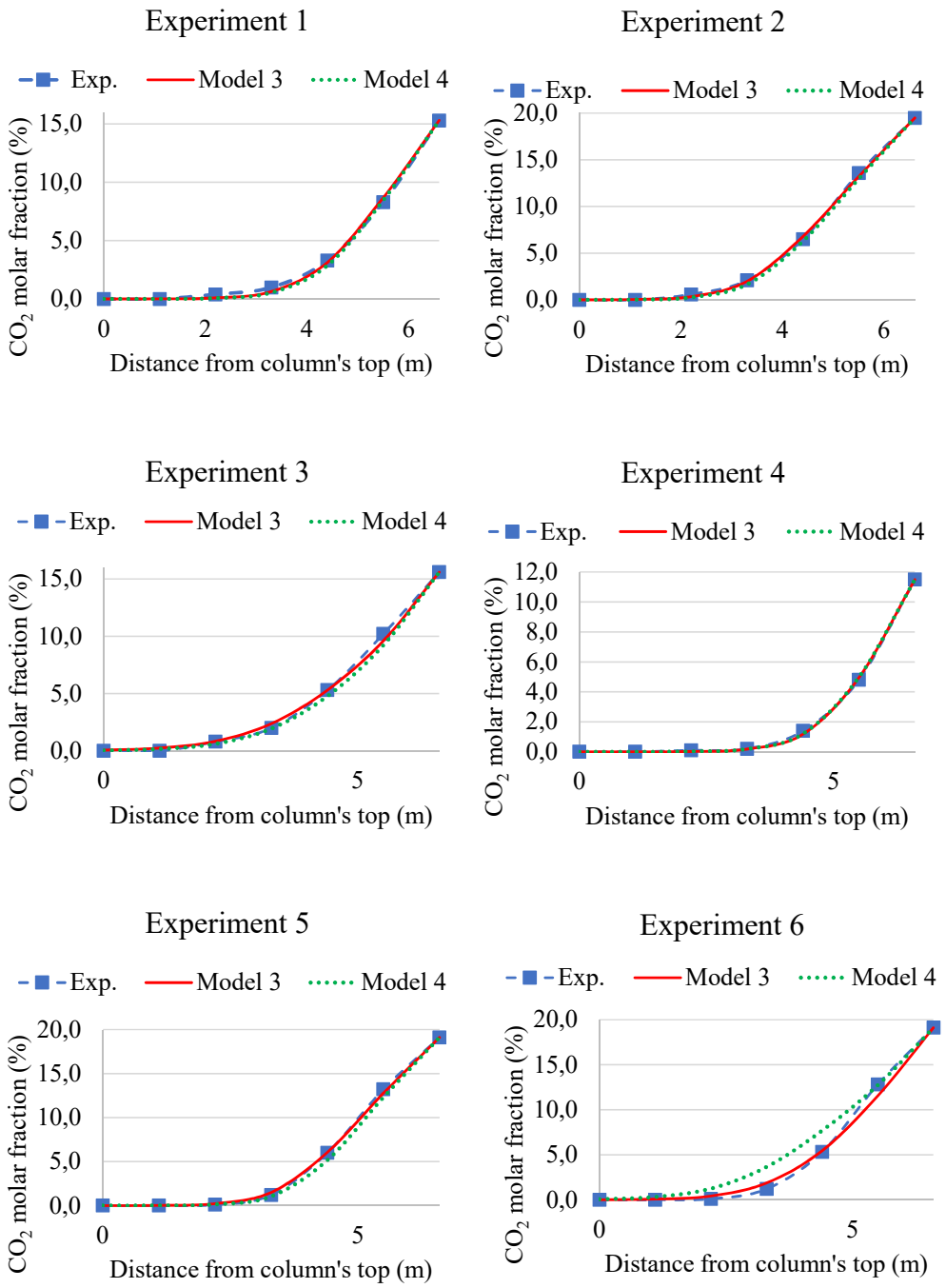

Figure 4.12: Comparison among gas-phase CO_2 molar fraction, experimental and calculated values with Models 3 and 4.

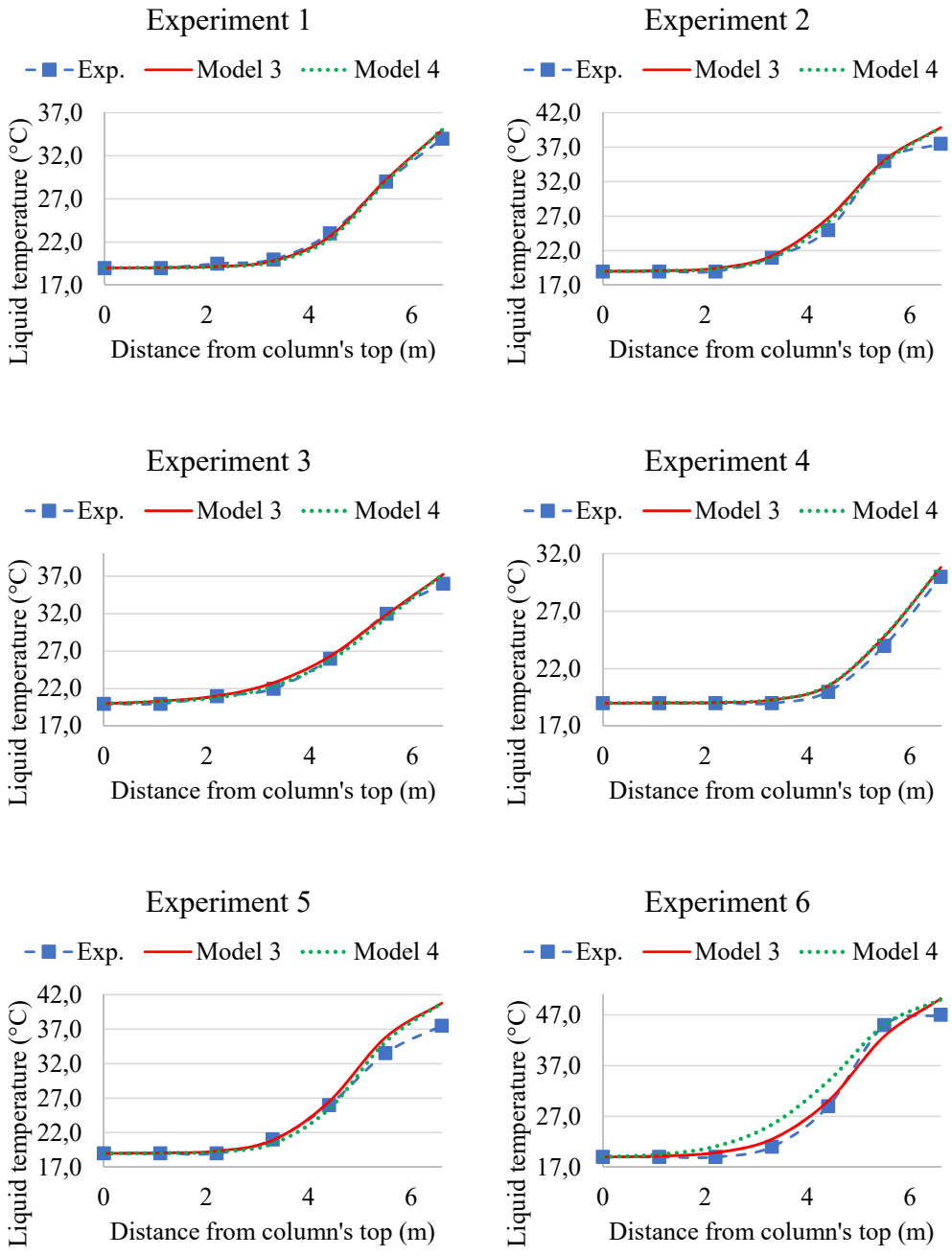

Figure 4.13: Comparison among liquid-phase temperature, experimental and calculated values with Models 3 and 4.

propose a different type of adjustment. It is also worth noting that confidence interval was estimated without knowledge of the measurement errors, because this information was not available. If measurement errors are significant, the confidence interval would be broader.

4.4 Case Studies

In this section, the model used to adjust Experiment 3 in the last section was used as a base case, in which many inputs were varied so that the model responses could be checked whether they are in consonance with what is expected of such processes.

First property analyzed was the column pressure, whose values were varied from 1.5 atm to 6 atm. Results for CO_2 molar fraction profile, and liquid temperature profile are shown in Figure 4.14. As expected, with increase in column pressure, there is also an increase in CO_2 partial pressure, which increases the rate with which CO_2 is consumed in the liquid phase reactions. This causes more CO_2 to be absorbed, and therefore less CO_2 in the column outlet. Also, since the main reaction between CO_2 and MEA is exothermic, in higher pressures a higher liquid-phase temperature is expected, as was shown in the results.

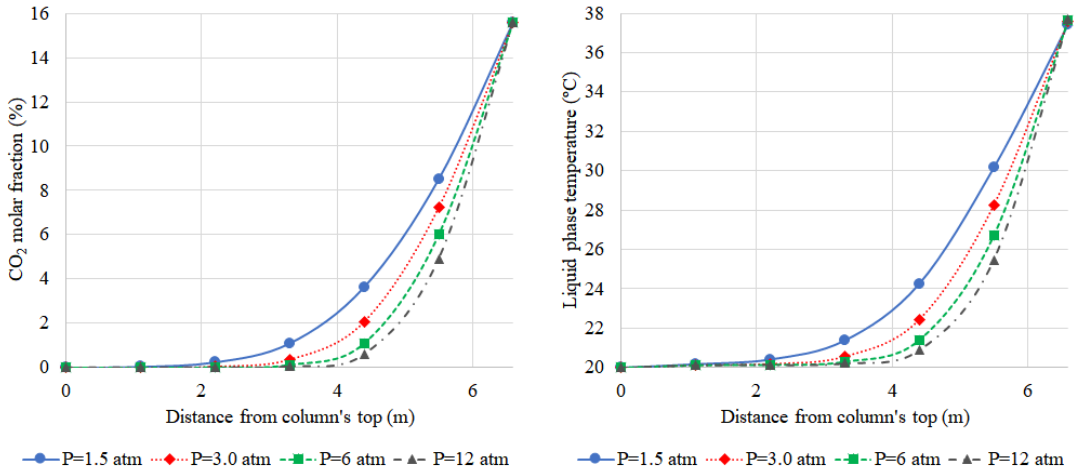

Figure 4.14: Results of gas-phase CO_2 molar fraction and liquid-phase temperature when pressure is varied.

Secondly, gas flow rate to the column was varied from 0.1 to 0.8 $\mathrm{kmol/h}$, and results are shown in Figure 4.15. Since all cases have the same inlet CO_2 concentration, when the gas flow rate is higher there is more CO_2 to be removed, and therefore a lesser drop in CO_2 concentration is observed along the column. The increase on liquid-phase temperature, on the other hand, is dependent on the total amount of CO_2 absorbed, and, since in higher flow rates there is more total CO_2, the temperature increase is more accentuated in those cases.

Next, CO_2 molar fraction in the inlet gas was varied from 4% to 32%, and results are in Figure 4.16. In this case, partial pressure of CO_2 is increased with its content, and therefore will accelerate the main reaction between CO_2 and MEA. As it can be

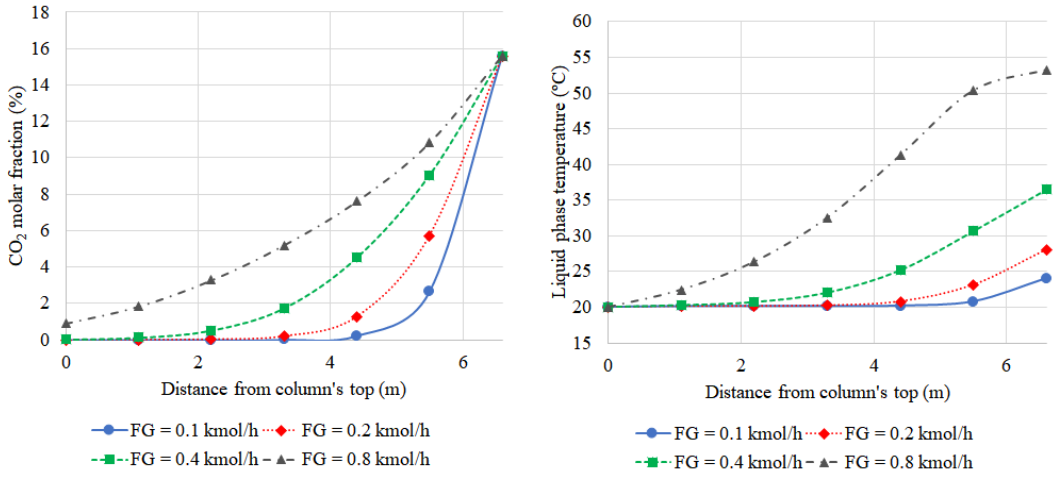

Figure 4.15: Results of gas-phase CO_2 molar fraction and liquid-phase temperature when gas inlet flow rate is varied.

seen, in all cases, CO_2 in the outlet was close to zero, showing the high capacity of MEA to perform the absorption. The stage in which CO_2 is totally absorbed, though, varies, with less inlet CO_2 concentration needing only three stages. Liquid-phase temperature increase, again, is more accentuated in the cases in which more CO_2 is absorbed.

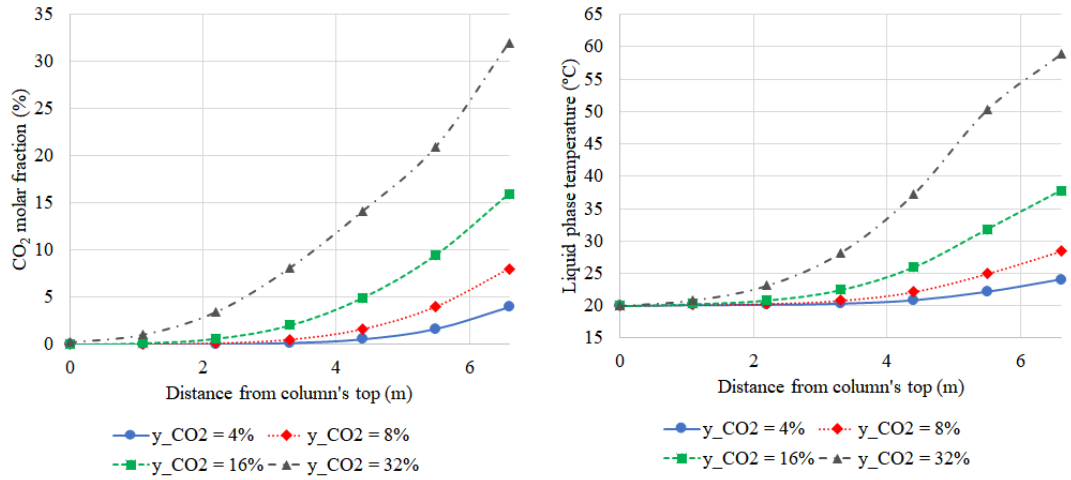

Figure 4.16: Results of gas-phase CO_2 molar fraction and liquid-phase temperature when gas inlet CO_2 molar fraction is varied.

Following to the liquid phase, liquid inlet flow rate was varied from 3 to 9 $\mathrm{kmol/h}$, and results are shown in Figure 4.17. Concerning the CO_2 molar fraction profile, higher liquid flow rates result in more CO_2 absorbed. This has two main reasons: first with more liquid flowing, there is also more MEA and, therefore, its concentration stays higher

as reaction proceeds, what increases reaction rate; second higher flows mean higher velocities, which will enhance mass transfer in the column. Despite the fact that higher liquid flow rates grants higher CO_2 consumption, and therefore generates more heat, the temperature increase in liquid phase is lower, since there is more mass to be heated, and the extra heat does not compensate that, as shown in the results.

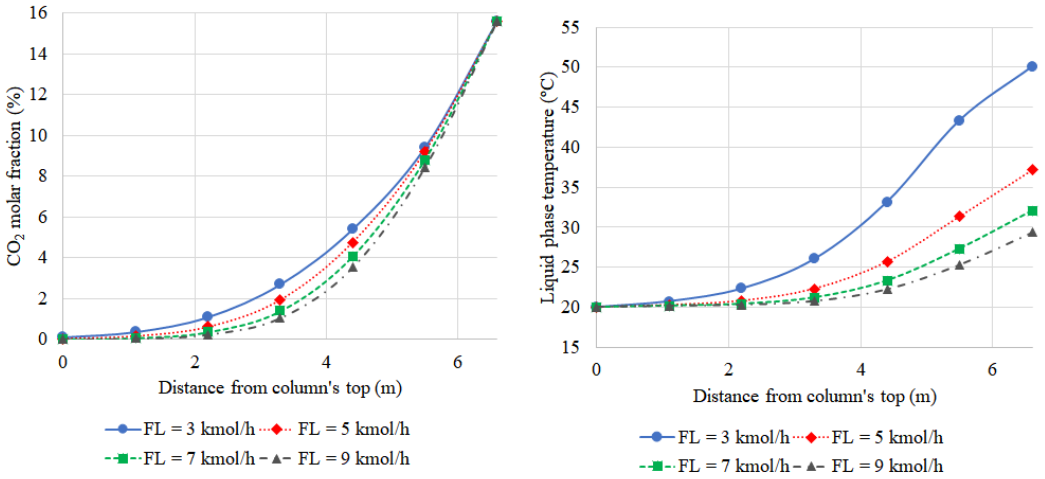

Figure 4.17: Results of gas-phase CO_2 molar fraction and liquid-phase temperature when liquid inlet flow rate is varied.

Next, the MEA molar fraction in the inlet liquid phase was varied from 2% to 16% and results are shown in Figure 4.18. For all cases but that of 2% MEA molar fraction, the column was capable of removing practically all CO_2 from the inlet gas, which means that the amount of heat generated by reaction was similar in those cases, causing an also similar temperature raise in liquid phase. The differences between liquid phase final temperature in those cases lie mainly on the heat capacity difference of distinct concentration solutions. The case which had 2% MEA molar fraction could not remove all CO_2, although there was no stoichiometric restraint, what indicates an kinetic limitation on this condition.

Following, liquid phase inlet temperature was varied from 10 to 40 °C and results are shown in Figure 4.19. The main reaction between CO_2 and MEA - Equation 3.42 - is exothermic and, therefore, an increase in temperature should move equilibrium state towards the reactants. However, as was stated, this reaction is kinetically controlled, and does not reach equilibrium and, for this reason, an increase in temperature also provoked and increase in CO_2 removal, as observed in the results, mainly due to an increase in the reaction rate.

Different than the previously analyzed variables, which are operational variables, or disturbances, the type of internal was also varied. This is defined during the project of

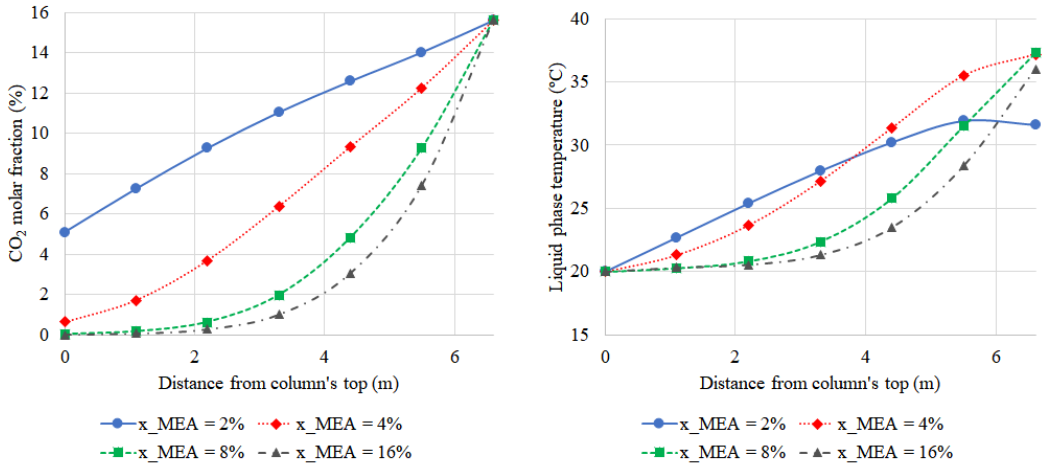

Figure 4.18: Results of gas-phase CO_2 molar fraction and liquid-phase temperature when liquid inlet MEA molar fraction is varied.

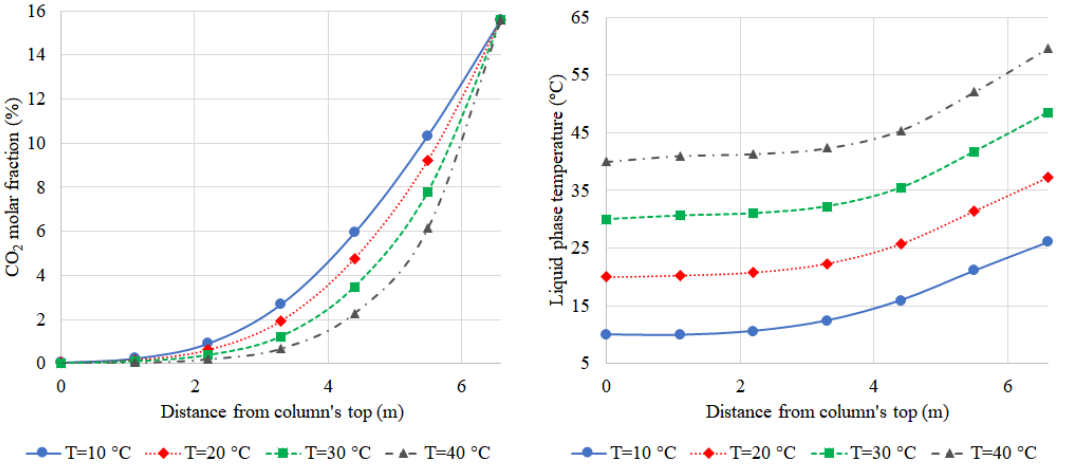

Figure 4.19: Results of gas-phase CO_2 molar fraction and liquid-phase temperature when liquid inlet temperature is varied.

the unit, but can also be modified in case of REVAMPs. Three internals were tested: Ceramic berl saddles, as the original experimental data, Raschig rings and Raschig super rings. Interfacial area calculated for each of the internals is shown in Table 4.7. Results are shown in Figure 4.20. As can be seen, Raschig super rings have a better performance when compared to the other two.

Table 4.7: Parameter of the internals tested in this work

Parameter	**Berl saddle**	**Raschig super ring**	**Raschig ring**
First stage A_I (m^2)	0.5660	0.6879	0.6397

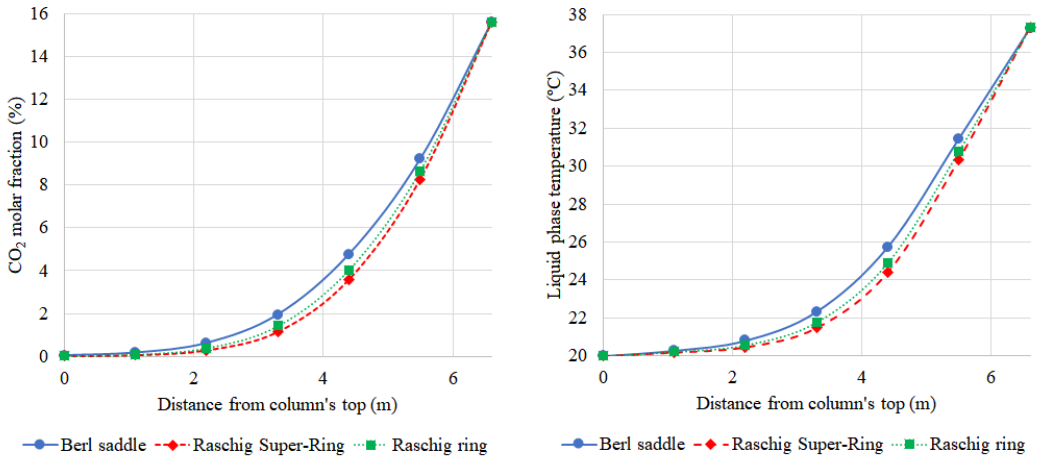

Figure 4.20: Results of gas-phase CO_2 molar fraction and liquid-phase temperature when packing type is varied.

Next, the diameter of the column was varied. Naturally, this is a variable that can only be changed in the project phase. Figure 4.21 shows the results. Column diameter influences a lot of variables, however, as shown in the results, when all other inlets are kept constant, smaller diameters led to less CO_2 removed from the gas stream in each stage, although all but the 0.06 m case were able to remove all CO_2 along the whole column. The explanation for this lies in the fact that the main reaction between CO_2 and MEA are kinetically controlled, as already stated. Therefore, when the diameter is increased, so does the total volume in which reaction takes place, as well as the interfacial area between gas and liquid phases. Both variables would increase the amount of CO_2 that reacts in each stage. One drawback of increasing the diameter would be the lower velocity, which also hinders mass transfer. This effect was less evident though.

Finally, the column number of stages was varied, using the same inlet conditions. Results are shown in Figure 4.22. As expected, when total number of stages is reduced, the

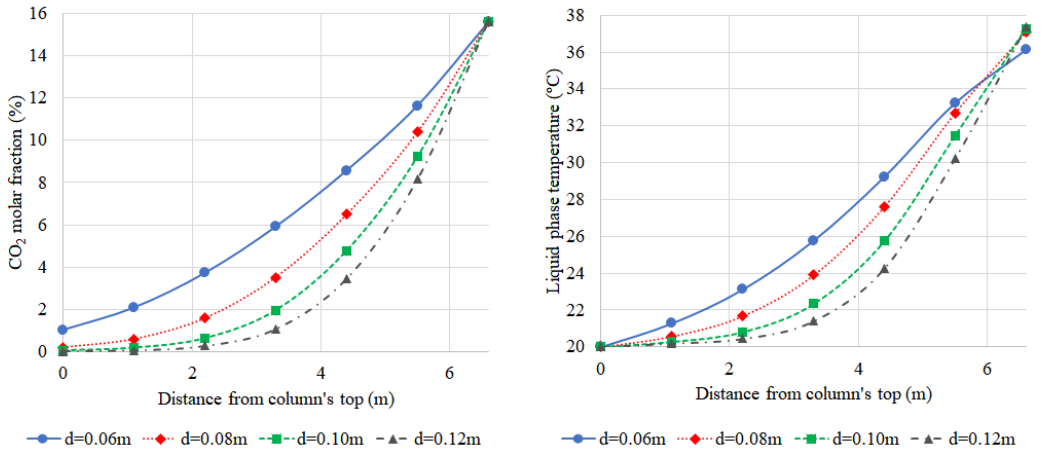

Figure 4.21: Results of gas-phase CO_2 molar fraction and liquid-phase temperature when column diameter is varied.

less capacity to remove CO_2 the column has.

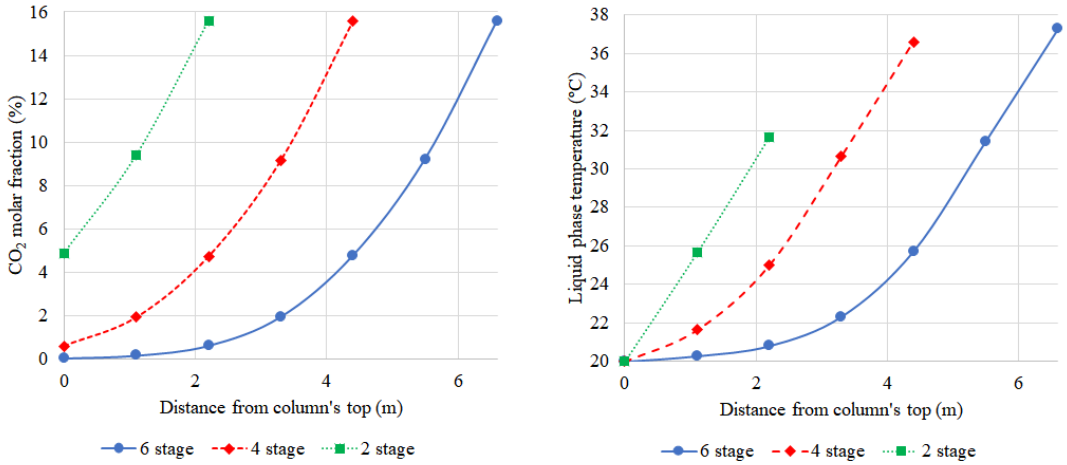

Figure 4.22: Results of gas-phase CO_2 molar fraction and liquid-phase temperature when column number os stages is varied.

Chapter 5

Conclusion and Suggestions for Future Works

Chemical absorption of CO_2 with monoethanolamine was simulated using a rate-based approach and two film theory model with one parameter for adjustment. To cope with the numerical difficulties inherent to this approach, a methodology was proposed in order to achieve convergence without the need of good initial guesses.

The complete model was simplified to remove two of the most numerically complex equations: the Maxwell-Stefan equations which describe mass transfer in the gas phase; and activity coefficient calculation in liquid phase using the e-NRTL equation of state. Also, algebraic equations which would generate structural differential indexes of 2 were replaced by control equations so that a dynamic model was numerically feasible. This was called Model 1, and its numerical integration generated the initial guess for the next model.

Model 2 is a stationary model which removes the Maxwell-Stefan simplification, but keeps the activity coefficient constant. It is an intermediate step to the complete model - Model 3.

The strategy proposed succeeded and the final model was validated using published pilot plant data. The only model parameter, the factor of effective mass transfer area, was then adjusted and showed to be dependent on MEA inlet concentration. A linear dependence was utilized and the final Model agreed fairly with the experimental data, although the newly calculated parameters were not within their confidence interval.

Finally, a number of process variables were varied and the model response was analyzed and showed to be as expected for this process.

As suggestions for future works:

- Implement pressure drop calculation along the column
- Validate the model considering columns of different sizes and packings
- Perform a bigger set of experimental data in order to better model the α parameter as a function o MEA molar fraction, and in the experiments utilize statistical rigour in order to determine measurement errors
- Extend the model to other amines and mixture of amines
- Include other acid gases removals, such as H_2S

Bibliography

ABOUDHEIR, A., TONTIWACHWUTHIKUL, P., IDEM, R., 2006, "Rigorous model for predicting the behavior of CO2 absorption into AMP in packed-bed absorption columns", *Industrial and Engineering Chemistry Research*, v. 45, pp. 2553–2557.

ADDICKS, J., OWREN, G. A., FREDHEIM, A. O., TANGVIK, K., 2002, "Solubility of carbon dioxide and methane in aqueous methyldiethanolamine solutions", *Journal of Chemical and Engineering Data*, v. 47, n. 4, pp. 855–860.

AL-BAGHLI, N. A., PRUESS, S. A., YESAVAGE, V. F., et al., 2001, "A rate-based model for the design of gas absorbers for the removal of CO2 and H2S using aqueous solutions of MEA and DEA", *Fluid Phase Equilibria*, v. 185, n. 1-2, pp. 31–43.

ALBERTON, A. L., 2010, *Estimação de Parâmetros e Planejamento de Experimentos: Estudo de Incertezas e Funções de Informação*. Ph.D. Thesis, Universidade Federal do Rio de Janeiro.

AMUNDSEN, T. G., ØI, L. E., EIMER, D. A., 2009, "Density and viscosity of monoethanolamine + water + carbon dioxide from (25 to 80)C", *Journal of Chemical and Engineering Data*, v. 54, pp. 3096–3100.

ARCHER, D. G., WANG, P., 1989, "The dielectric constant of water and Debye-Hückel lew slopes", *Journal of Physical Chem.*, v. 19, n. 2, pp. 1990.

AROONWILAS, A., CHAKMA, A., TONTIWACHWUTHIKUL, P., et al., 2003, "Mathematical modelling of mass-transfer and hydrodynamics in CO2absorbers packed with structured packings", *Chemical Engineering Science*, v. 58, pp. 4037–4053.

AROUA, M., HAJI-SULAIMAN, M., RAMASAMY, K., 2002, "Modelling of carbon dioxide absorption in aqueous solutions of AMP and MDEA and their blends using Aspenplus", *Separation and Purification Technology*, v. 20, pp. 153–162.

AUSTGEN, D. M., ROCHELLE, G. T., CHEN, C. C., 1991, "Model of Vapor-Liquid Equilibria for Aqueous Acid Gas-Alkanolamine Systems. 2. Representation of H2S and CO2Solubility in Aqueous MDEA and CO2Solubility in Aqueous Mixtures of MDEA with MEA or DEA", *Industrial and Engineering Chemistry Research*, v. 30, n. 3, pp. 543–555.

AUSTGEN, D., ROCHELLE, G., PENG, X., CHEN, C., 1989, "Model of vapor?liquid equilibria for aqueous acid gas-alkanolamine systems-2", *Ind Eng Chem Res,*, v. 28, n. 1967, pp. 1060–1073.

BAKER, R. W., LOKHANDWALA, K., 2008, "Natural gas processing with membranes: An overview", *Industrial and Engineering Chemistry Research*, v. 47, n. 7, pp. 2109–2121.

BARREAU, A., BLANCHON LE BOUHELEC, E., HABCHI TOUNSI, K., MOUGIN, P., LECOMTE, F., 2006, "Absorption of H_2S and CO_2 in Alkanolamine Aqueous Solution: Experimental Data and Modelling with the Electrolyte-NRTL Model", *Oil & Gas Science and Technology - Revue de l'IFP*, v. 61, n. 3, pp. 345–361. .

BERNHARDSEN, I. M., KNUUTILA, H. K., 2017, "A review of potential amine solvents for CO_2 absorption process: Absorption capacity, cyclic capacity and pKa", *International Journal of Greenhouse Gas Control*, v. 61, pp. 27–48.

BILLET, R., SCHULTES, M., 1999, "Prediction of Mass Transfer Columns with Dumped and Arranged Packings", *Trans IChemE*, v. 77.

BISHNOI, S., ROCHELLE, G. T., 2002, "Thermodynamics of piperazine/methyldiethanolamine/water/carbon dioxide", *Industrial and Engineering Chemistry Research*, v. 41, n. 3, pp. 604–612.

BOGGS, P. T., ROGERS, J. E., 1990, "The Computation and Use of the Asymptotic Covariance Matrix for Measurement Error Models The Computation and Use of the Asymptotic Covariance Matrix for Measurement Error Models *", *Applied Computational Mathematics Division*.

BOLHÀR-NORDENKAMPF, M., FRIEDL, A., KOSS, U., TORK, T., 2004, "Modelling selective H2S absorption and desorption in an aqueous MDEA-solution using a rate-based non-equilibrium approach", *Chemical Engineering and Processing: Process Intensification*, v. 43, pp. 701–715.

BUTTON, J., GUBBINS, K. E., 1999, "SAFT prediction of vapour-liquid equilibria of mixtures containing carbon dioxide and aqueous monoethanolamine or diethanolamine", *Fluid Phase Equilibria*, v. 158-160, pp. 175–181.

CHEN, C. C., EVANS, L. B., 1986, "A local composition model for the excess Gibbs energy of aqueous electrolyte systems", *AIChE Journal*, v. 32, n. 3, pp. 444–454.

CHEN, C. C., BRITT, H. I., BOSTON, J. F., EVANS, L. B., 1982, "A local composition model for the excess Gibbs energy of aqueous electrolyte systems - Part I: Single solvent", *AIChE Journal*, v. 28, n. 4, pp. 588–596.

CHEN, C. C., BOKIS, C. P., MATHIAS, P., 2001, "Segment-based excess Gibbs energy model for aqueous organic electrolytes", *AIChE Journal*, v. 47, n. 11, pp. 2593–2602.

CHIU, L. F., LI, M. H., 1999, "Heat capacity of alkanolamine aqueous solutions", *Journal of Chemical and Engineering Data*, v. 44, n. 6 (nov), pp. 1396–1401.

CHUNXI, L., FÜRST, W., 2000, "Representation of CO_2 and H_2S solubility in aqueous MDEA solutions using an electrolyte equation of state", *Chemical Engineering Science*, v. 55, n. 15, pp. 2975–2988.

CULLINANE, J. T., ROCHELLE, G. T., 2005, "Thermodynamics of aqueous potassium carbonate, piperazine, and carbon dioxide", *Fluid Phase Equilibria*, v. 227, n. 2, pp. 197–213.

DEMONTIGNY, D., TONTIWACHWUTHIKUL, P., CHAKMA, A., 2001, "Parametric Studies of Carbon Dioxide Absorption into Highly Concentrated Monoethanolamine Solutions", *The Canadian Journal of Chemical Engineering*, v. 79, pp. 137–142.

DUGAS, R. E., ROCHELLE, G. T., 2011, "Modeling CO_2 absorption into concentrated aqueous monoethanolamine and piperazine", *Chemical Engineering Science*, v. 66, pp. 5212–5218.

EDWARD FULLER, B. N., ENSLEY, K., CALVIN GIDDINGS, J.,, 1969, *Diffusion of Halogenated Hydrocarbons in Helium*. Technical Report.

FARAMARZI, L., KONTOGEORGIS, G. M., THOMSEN, K., STENBY, E. H., 2009, "Extended UNIQUAC model for thermodynamic modeling of CO_2 absorption in aqueous alkanolamine solutions", *Fluid Phase Equilibria*, v. 282, n. 2, pp. 121–132.

GABRIELSEN, J., MICHELSEN, M. L., STENBY, E. H., KONTOGEORGIS, G. M., 2006, "Modeling of CO2 absorber using an AMP solution", *AIChE Journal*, v. 52, n. 10, pp. 3443–3451.

GARCÍA, A. V., THOMSEN, K., STENBY, E. H., 2006, "Prediction of mineral scale formation in geothermal and oilfield operations using the Extended UNIQUAC model. Part II. Carbonate-scaling minerals", *Geothermics*, v. 35, n. 3, pp. 239–284.

GASPAR, J., CORMOS, A.-M., 2012, "Dynamic modeling and absorption capacity assessment of CO_2 capture process", *International Journal of Greenhouse Gas Control*, v. 8, pp. 45–55.

GHAEMI, A., SHAHHOSSEINI, S., MARAGHEH, M. G., 2009, "Nonequilibrium dynamic modeling of carbon dioxide absorption by partially carbonated ammonia solutions", *Chemical Engineering Journal*, v. 149, pp. 110–117.

HARUN, N., DOUGLAS, P. L., RICARDEZ-SANDOVAL, L., CROISET, E., 2011, "Dynamic simulation of MEA absorption processes for CO_2 capture from fossil fuel power plant". In: *Energy Procedia*, pp. 1478–1485.

HAYDUK, W., MINHAS, B. S., 1982, "Correlations for Prediction of Molecular Diffusivities in Liquids", *The Canadian Journal of Chemical Engineering*, v. 60, pp. 295–299.

HIGBIE, R., 1935, *The rate of absorption of a pure gas into still liquid during short periods of exposure*, *Doctor Thesis from University of Michigan*.

HUTTENHUIS, P., AGRAWAL, N., SOLBRAA, E., VERSTEEG, G.F., 2008, "The solubility of carbon dioxide in aqueous N-methyldiethanolamine solutions", *Fluid Phase Equilibria*, v. 264, n. 1-2, pp. 99–112.

IKADA, E., YOSHINORI, H., OKAMOTO, H., HAGINO, J., KOIZUMI, N., 1969, "Dielectric Properties of Ethanolamines", *Bulletin of the Institute for Chemical Research, Kyoto University*, v. 46, n. 5, pp. 239–247.

JAYARATHNA, S. A., LIE, B., MELAAEN, M. C., 2013, "Amine based CO 2 capture plant: Dynamic modeling and simulations", *International Journal of Greenhouse Gas Control*, v. 14, pp. 282–290.

KAEWSICHAN, L., AL-BOFERSEN, O., YESAVAGE, V. F., SELIM, M. S., 2001, "Predictions of the solubility of acid gases in monoethanolamine (MEA) and methyldiethanolamine (MDEA) solutions using the electrolyte-UNIQUAC model", *Fluid Phase Equilibria*, v. 183-184, pp. 159–171.

KAMPS, Á. P.-S., BALABAN, A., JÖDECKE, M., KURANOV, G., SMIRNOVA, N. A., MAURER, G., 2001, "Solubility of Single Gases Carbon Dioxide and Hydrogen Sulfide in Aqueous Solutions of N -Methyldiethanolamine in the Temper-

ature Range 313?413 K at Pressures up to 5 MPa", *Industrial & Engineering Chemistry Research*, v. 40, pp. 696–706.

KENIG, E. Y., SCHNEIDER, R., GÓRAK, A., 1999, "Rigorous Dynamic Modelling of Complex Reactive Adsorption Processes", *Chem. Eng. Sci.*, v. 54, pp. 5195–5203.

KENIG, E. Y., SCHNEIDER, R., GÓRAK, A., 2001, "Reactive absorption: Optimal process design via optimal modelling", *Chemical Engineering Science*, v. 56, n. 2, pp. 343–350.

KENIG, E. Y., KUCKA, L., GÓRAK, A., 2002, "Rigorose modellierung von reaktivabsorptionsprozessen", *Chemie-Ingenieur-Technik*, v. 74, n. 6, pp. 745–764.

KENIG, E., SEFERLIS, P., 2009, "Modeling Reactive Absorption", *Chemical Engineering Progress*.

KENT, R., EISENBERG, B., 1976, "Better data for amine treating", *Hydrocarbon Process.*, v. 2, pp. 87–96.

KHAN, F. M., KRISHNAMOORTHI, V., MAHMUD, T., 2011, "Modelling reactive absorption of CO2in packed columns for post-combustion carbon capture applications", *Chemical Engineering Research and Design*, v. 89, pp. 1600–1608.

KOLEV, N., 1976, *Wirkungsweise von Füllkörperschüttungen*. Technical Report.

KONTOGEORGIS, G. M., FOLAS, G. K., 2010, *Thermodynamic Models for Industrial Applications*. Wiley Inc. ISBN: 9780470747537.

KORONAKI, I. P., PRENTZA, L., PAPAEFTHIMIOU, V., 2015, "Modeling of CO_2 capture via chemical absorption processes - An extensive literature review", *Renewable and Sustainable Energy Reviews*, v. 50, pp. 547–566.

KUCKA, L., RICHTER, J., KENIG, E. Y., GÓRAK, A., 2003a, "Determination of gas-liquid reaction kinetics with a stirred cell reactor", *Separation and Purification Technology*, v. 31, n. 2, pp. 163–175.

KUCKA, L., MÜLLER, I., KENIG, E. Y., GÓRAK, A., 2003b, "On the modelling and simulation of sour gas absorption by aqueous amine solutions", *Chemical Engineering Science*, v. 58, n. 16, pp. 3571–3578.

KVAMSDAL, H. M., JAKOBSEN, J. P., HOFF, K. A., 2009, "Dynamic modeling and simulation of a CO2 absorber column for post-combustion CO_2 capture", *Chemical Engineering and Processing: Process Intensification*, v. 48, pp. 135–144.

LAWAL, A., WANG, M., STEPHENSON, P., KOUMPOURAS, G., YEUNG, H., 2010, "Dynamic modelling and analysis of post-combustion CO_2 chemical absorption process for coal-fired power plants", *Fuel*, v. 89, pp. 2791–2801.

LEWIS, W. K., WHITMAN, W. G., 1924, "Principles of Gas Absorption", *Industrial and Engineering Chemistry*, v. 16, n. 12, pp. 1215–1220.

LIU, Y., ZHANG, L., WATANASIRI, S., 1999, "Representing Vapor?Liquid Equilibrium for an Aqueous MEA?CO_2 System Using the Electrolyte Nonrandom-Two-Liquid Model", *Industrial & Engineering Chemistry Research*, v. 38, n. 5, pp. 2080–2090.

MAC DOWELL, N., SAMSATLI, N. J., SHAH, N., 2013, "Dynamic modelling and analysis of an amine-based post-combustion CO2 capture absorption column", *International Journal of Greenhouse Gas Control*, v. 12, pp. 247–258.

MOCK, B., EVANS, L. B., CHEN, C., 1986, "Thermodynamic representation of phase equilibria of mixed?solvent electrolyte systems", *AIChE Journal*, v. 32, n. 10, pp. 1655–1664.

MOIOLI, S., GIUFFRIDA, A., GAMBA, S., ROMANO, M. C., PELLEGRINI, L., LOZZA, G., 2014, "Pre-combustion CO_2 capture by MDEA process in IGCC based on air-blown gasification". In: *Energy Procedia*, pp. 2045–2053.

MORES, P., SCENNA, N., MUSSATI, S., 2011, "Post-combustion CO2 capture process: Equilibrium stage mathematical model of the chemical absorption of CO_2 into monoethanolamine (MEA) aqueous solution", *Chemical Engineering Research and Design*, v. 89, pp. 1587–1599.

NITTAYA, T., DOUGLAS, P. L., CROISET, E., RICARDEZ-SANDOVAL, L. A., 2014, "Dynamic modelling and control of MEA absorption processes for CO_2 capture from power plants", *Fuel*, v. 116, pp. 672–691.

NOERES, C., KENIG, E. Y., GÓRAK, A., 2003, "Modelling of reactive separation processes: Reactive absorption and reactive distillation", *Chemical Engineering and Processing*, v. 42, n. 3, pp. 157–178.

OLAJIRE, A. A., 2010, "CO 2 capture and separation technologies for end-of-pipe applications e A review", *Energy*, v. 35, pp. 2610–2628.

PINTOLA, T., TONTIWACHWUTHIKUL, P., MEISEN, A., 1993, "Simulation of pilot plant and industrial CO_2-MEA absorbers", *Gas Separation and Purification*, v. 7, n. 1, pp. 47–52.

PITZER, K. S., 1980, "Electrolytes. From Dilute Solutions to Fused Salts", *Journal of the American Chemical Society*, v. 102, n. 9, pp. 2902–2906.

PLAZA, J. M., 2012, *Modeling of Carbon Dioxide Absorption using Aqueous Monoethanolamine, Piperazine and Promoted Potassium Carbonate Committee*. Ph.D. Thesis, University of Texas at Austin.

POLING, B. E., PRAUSNITZ, J. M., O'CONNEL, J. P., 2001, *The Properties of Gases and Liquids*, v. 123. McGraw-Hill. ISBN: 0071499997.

POSEY, M. L., ROCHELLE, G. T., 1997, "A Thermodynamic Model Of Methyldiethanolamine-CO_2-H_2S-Water", *Industrial & engineering chemistry research*, v. 36, n. 9, pp. 3944–3953.

PUXTY, G., ROWLAND, R., ATTALLA, M., 2011, "Describing CO2mass transfer in amine/ammonia mixtures - No shuttle mechanism required". In: *Energy Procedia*, pp. 1369–1376.

RENON, H., PRUASNITZ, J. M., 1968, "Local compositions in thermodynamics excess functions for liquids mixtures", *AIChE J.*, v. 14, n. 1, pp. 116–128.

RUFFORD, T. E., SMART, S., WATSON, G. C., et al., 2012, "The removal of CO2and N2from natural gas: A review of conventional and emerging process technologies", *Journal of Petroleum Science and Engineering*, v. 94-95, pp. 123–154.

SADA, E., KUMAZAWA, H., BUTT, M. A., 1976, "Gas absorption with consecutive chemical reaction: Absorption of carbon dioxide into aqueous amine solutions", *The Canadian Journal of Chemical Engineering*, v. 54, pp. 421–424.

SAIMPERT, M., PUXTY, G., QURESHI, S., et al., 2013, "A new rate based absorber and desorber modelling tool", *Chemical Engineering Science*, v. 96, pp. 10–25.

SECCHI, A. R., 2012. "Differential-Algebraic System Solver in C - v. 3.9". Available at: <http://www.enq.ufrgs.br/enqlib/numeric/>.

SEMA, T., NAAMI, A., LIANG, Z., IDEM, R., TONTIWACHWUTHIKUL, P., SHI, H., WATTANAPHAN, P., HENNI, A., 2012, "Analysis of reaction kinetics of CO_2 absorption into a novel reactive 4-diethylamino-2-butanol solvent", *Chemical Engineering Science*, v. 81, pp. 251–259.

SHI, H., LIANG, Z., SEMA, T., NAAMI, A., USUBHARATANA, P., IDEM, R., SAIWAN, C., TONTIWACHWUTHIKUL, P., 2012, "Part 5a: Solvent chemistry: NMR analysis and studies for amine-CO_2-H_2O systems with vapor-liquid equilibrium modeling for CO_2 capture processes", *Carbon Management*, v. 3, pp. 185–200.

SILKENBA, D., RUMPF, B., LICHTENTHALER, D. N., 1998, "Solubility of Carbon Dioxide in Aqueous Solutions of 2-Amino-2-methyl-1-propanol and N-Methyldiethanolamine and Their Mixtures in the Temperature Range from 313 to 353 K and Pressures up to 2.7 MPa", *Ind Eng Chem Res,*, v. 37, pp. 3133–3141.

SOARES R. P., SECCHI, A. R., , 2003, "EMSO: A New Environment for Modelling, Simulation and Optimisation". In: *European Symposium on Computer Aided Process Engineering*,v.13, pp. 947–952.

SOLBRAA, E., 2002, *Measurement and modelling of absorption of carbon dioxide into methyldiethanolamine solutions at high pressure*. Phd thesis, Norwegian University of Science and Technology.

TAYLOR, R., KRISHNA, R., 1993, *Multicomponent Mass Transfer*. John Wiley and Sons ISBN: 0471574171.

THOMSEN, K., 2005, "Modeling electrolyte solutions with the extended universal quasichemical (UNIQUAC) model", *Pure and Applied Chemistry*, v. 77, n. 3, pp. 531–542.

THOMSEN, K., RASMUSSEN, P., 1999, "Modeling of VLS equilibrium in gas-aqueous electrolyte systems", *Chemical Engineering Science*, v. 54, pp. 1787–1802.

TOBIESEN, F. A., JULIUSSEN, O., SVENDSEN, H. F., 2008, "Experimental validation of a rigorous desorber model for CO_2 post-combustion capture", *Chemical Engineering Science*, v. 63, pp. 2641–2656.

TONTIWACHWUTHIKUL, P., MEISEN, A., LIM, C. J., 1992, "CO2 absorption by NaOH, monoethanolamine and 2-amino-2-methyl-1-propanol solutions in a packed column", *Chemical Engineering Science*, v. 47, n. 2, pp. 381–390.

VALLÉE, G., MOUGIN, P., JULLIAN, S., FÜRST, W., 1999, "Representation of CO_2 and H_2S Absorption by Aqueous Solutions of Diethanolamine Using an Electrolyte Equation of State", *Industrial & Engineering Chemistry Research*, v. 38, n. 9, pp. 3473–3480.

VERSTEEG, G. F., VAN SWAAIJ, W. P. M., 1988, "On the kinetics between CO_2 and alkanolamines both in aqueous and non-aqueous solutions-I. Primary and secondary amines", *Chemical Enginewing Science*, v. 43, n. 3, pp. 573–585.

VRACHNOS, A., VOUTSAS, E., MAGOULAS, K., LYGEROS, A., 2004, "Thermodynamics of Acid Gas?MDEA?Water Systems", *Industrial & Engineering Chemistry Research*, v. 43, n. 11, pp. 2798–2804.

VRACHNOS, A., KONTOGEORGIS, G., VOUTSAS, E., 2006, "Thermodynamic modeling of acidic gas solubility in aqueous solutions of MEA, MDEA and MEA-MDEA blends", *Industrial and Engineering Chemistry Research*, v. 45, n. 14, pp. 5148–5154.

YU, C. H., HUANG, C. H., TAN, C. S., 2012, "A review of CO2 capture by absorption and adsorption", *Aerosol and Air Quality Research*, v. 12, n. 5, pp. 745–769.

Appendix A

Polynomial fits for liquid physical properties

A third degree polynomial adjustment was made to fit data from each A_k from the AMUNDSEN *et al.* (2009) model shown in Table 3.5 in order to utilize the empirical Equation 3.113, repeated here:

$$v_L = x_3 v_3 + (1 - x_3)v_2 + x_3(1 - x_3)\sum_{k=0}^{3} A_k(2x_3 - 1)^k \tag{3.113}$$

Results for this fit are shown in Figure A.1.

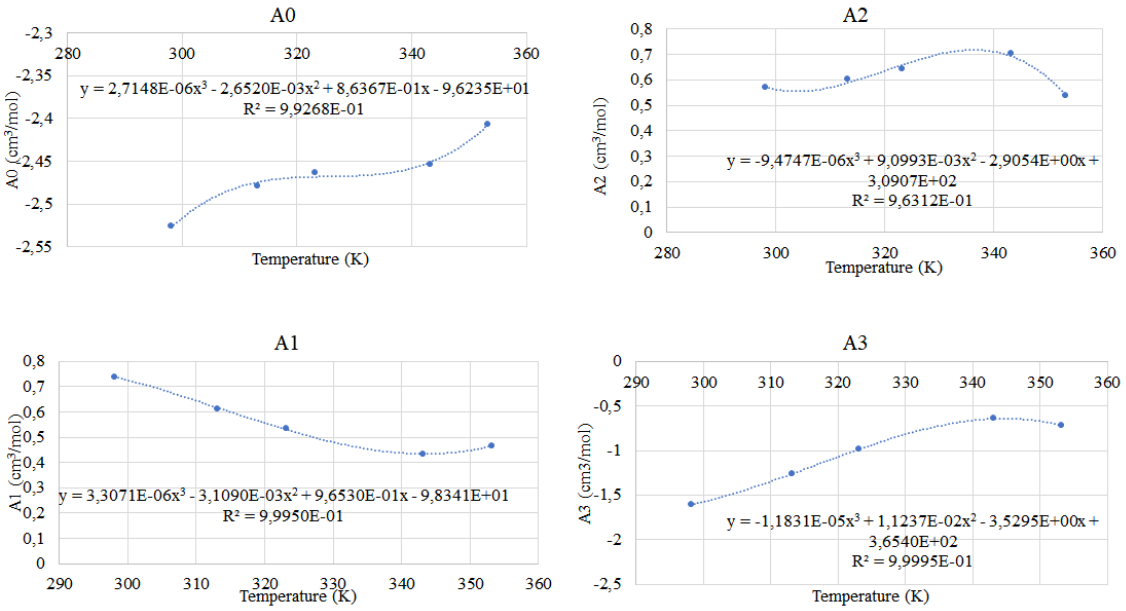

Figure A.1: Polynomial fits for the parameters for liquid-phase volume calculation.

Similarly, the dynamic viscosity of water and monoethanolamine were fitted into exponential models as a function of temperature. Original data is shown in Table 3.6 and results are shown in Figure

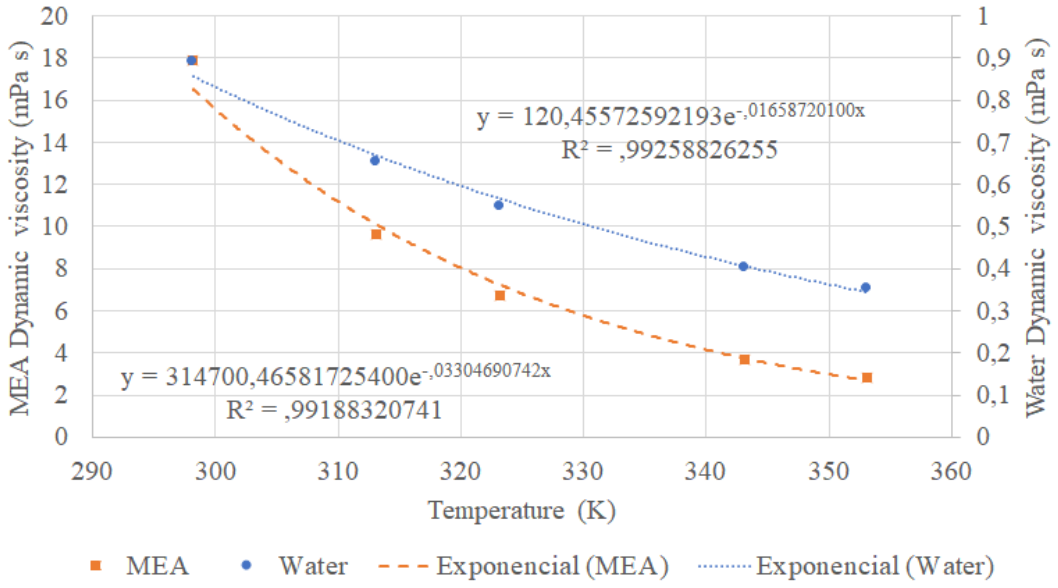

Figure A.2: Exponential fits for MEA and water dynamic viscosity.